

VALIDATING SIMULATION PIPELINES WITH POTENTIAL RECORDINGS

by

Jess David Tate

A dissertation submitted to the faculty of
The University of Utah
in partial fulfillment of the requirements for the degree of

Doctor of Philosophy

Department of Biomedical Engineering
The University of Utah
December 2018

Copyright © Jess David Tate 2018

All Rights Reserved

The University of Utah Graduate School

STATEMENT OF DISSERTATION APPROVAL

The dissertation of

Jess David Tate

has been approved by the following supervisory committee members:

<u>Robert S. MacLeod</u> ,	Chair(s)	<u>7 September 2018</u>
Date Approved		
<u>Christopher R. Johnson</u> ,	Member	<u>7 September 2018</u>
Date Approved		
<u>Frank B. Sachse</u> ,	Member	<u>7 September 2018</u>
Date Approved		
<u>Edward W. Hsu</u> ,	Member	<u>7 September 2018</u>
Date Approved		
<u>Thomas A. Pilcher</u> ,	Member	<u>7 September 2018</u>
Date Approved		

by David W. Grainger, Chair/Dean of
the Department/College/School of Engineering
and by David B. Kieda, Dean of The Graduate School.

ABSTRACT

Computer models of the heart can provide a greater understanding of the mechanisms of arrhythmias as well as tools to develop treatment strategies, yet adoption of computation modeling in biomedical sciences lags behind that in other fields. One of the reasons for the slow adoption of computational models in medicine is the lack of robust validation studies. The goal of this dissertation was to develop and apply validation approaches to two types of computer heart modeling pipelines, electrocardiographic (ECG) forward simulation and a defibrillation simulation, by comparing measured and predicted potential fields.

Previous validation studies have shown that ECG forward simulations produce greater error than expected, which could be caused by insufficient sampling of the cardiac sources. Various sampling strategies over the atrial region were tested to determine the effect of spatial sampling on the forward simulation. Including atrial samples reduced the error in predicted body-surface potentials, with some strategies more effective than others. These findings could help improve measurement protocols when validating the ECG forward simulation and provide more insight into ways to improve ECG imaging techniques.

Simulations of defibrillators have previously been developed to provide patient-specific guidance for improving treatment of fatal arrhythmias. To demonstrate the accuracy of one of these simulations, torso-tank experiments and clinical studies were used to record the potential fields generated by a defibrillator and compared to predicted values. Measurements within the torso-tank, including within the myocardium, and body-surface recordings from patients agreed with corresponding simulated potentials. Predicted defibrillation thresholds (DFTs) also agreed with values observed clinically and experimentally. The simulation's accuracy in predicting potential fields and DFTs supports its use in guiding defibrillation treatment.

For my boys. May you always love to learn.

CONTENTS

ABSTRACT	iii
LIST OF TABLES	vii
ACKNOWLEDGEMENTS	viii
CHAPTERS	
1. INTRODUCTION	1
1.1 Specific Aims	2
1.2 References	4
2. BACKGROUND	8
2.1 Cardiac Arrhythmias	8
2.2 Measuring Bioelectric Fields	9
2.3 Treatment of Arrhythmias	13
2.3.1 Treatment of Arrhythmias Through Defibrillation	14
2.4 Simulation Pipelines for Cardiac Bioelectricity	15
2.4.1 ECG Forward Model	16
2.4.2 Defibrillation Simulation	16
2.5 Validating Computer Models	17
2.5.1 ECG Forward Model Validation	19
2.5.2 Defibrillation Simulation Validation	21
2.6 References	24
3. REDUCING ERROR IN ECG FORWARD SIMULATIONS WITH IMPROVED SOURCE SAMPLING	33
3.1 Abstract	34
3.2 Introduction	34
3.3 Methods	35
3.3.1 Datasets	35
3.3.2 Sampling Strategies	36
3.3.3 ECG Forward Simulation Pipeline	36
3.3.4 Validation Experiments	37
3.3.5 Ethics	38
3.3.6 Data Availability	38
3.4 Results	38
3.5 Discussion	44
3.6 Author Contributions	48
3.7 Acknowledgements	48

4. VALIDATING DEFIBRILLATION SIMULATION IN A HUMAN-SHAPED PHANTOM	50
4.1 Abstract	50
4.2 Introduction	51
4.3 Methods.....	52
4.3.1 Tank Experiments	53
4.3.2 Signal Processing	54
4.3.3 Geometric Registration	55
4.3.4 Simulation Pipeline	55
4.3.5 Potential Comparisons	57
4.3.6 Ethics	58
4.4 Results	58
4.4.1 Potential Field Comparison.....	58
4.4.2 Electric Field Comparison	64
4.5 Discussion	65
4.6 Conclusions	68
4.7 Acknowledgements	69
4.8 References	69
5. MEASURING DEFIBRILLATOR SURFACE POTENTIALS: THE VALIDATION OF A PREDICTIVE DEFIBRILLATION COMPUTER MODEL	72
5.1 Abstract	73
5.2 Introduction	73
5.3 Methods.....	74
5.3.1 Body Surface Potential Estimation of ICD Shocks	74
5.3.2 Recording Surface Potentials	74
5.3.3 Patient-Specific Simulation	75
5.3.4 Collecting Patient Data	76
5.4 Results	76
5.4.1 Reconstruction of Simulated Surface Potentials	76
5.4.2 Surface Potential Comparison.....	76
5.4.3 DFT Comparison	77
5.5 Discussion	77
5.6 Acknowledgements	80
6. CONCLUSIONS	82
6.1 ECG Forward Simulation.....	82
6.1.1 Future Work	84
6.2 Defibrillation Simulation	86
6.2.1 Future Work	87
6.3 References	89

LIST OF TABLES

4.1	Statistical comparisons of the simulated and measured peak potential fields	59
5.1	List of patients in the study with the ICD device manufacturer and geometric information	75
5.2	Metrics of comparison of the limited lead recordings and the simulated potentials at the corresponding location	77
5.3	Metrics relating the simulated potential maps to the maps generated from the surface recordings	79
5.4	Comparison of the DFTs found during clinical testing and predicted by simulation via the critical mass hypothesis	79

ACKNOWLEDGEMENTS

The work in this dissertation was made possible with the input, help, guidance, and support of several people. This research and dissertation would not have been possible without the excellent mentorship, training, teaching, and support of my advisor, Rob MacLeod, and to him I offer my sincere thanks. Thanks to the students and post docs I have worked with, including: Jeroen Stinstra, Darrell Swenson, Josh Blauer, Kedar Aras, Brett Burton, Moritz Dannhauer, Wilson Good, Karli Gillette, and Brian Zenger and our close collaborators Dana Brooks and Jaume Coll-Font, who shared so much of their time and provided crucial advise throughout this work. Thanks also to my committee, Chris Johnson, Ed Hsu, Frank Sachse, and Tom Pilcher, for their support, guidance, and feedback while working on and presenting this research.

I also need to acknowledge the help and support of the staff at the SCI Institute, CVRTI, and Primary Children's Medical Center in facilitating this research. This work was made possible with the computational tools and software developed at the SCI Institute and the CIBC. Thanks to the developer staff (Ayla Khan, Dan White, Jonathan Bronson, Ally Warner, and Mark Dewey) for the technical training they provided. Animal experiments and measurement tools were all performed with the help of the staff (Jayne Davis, Nancy Allen, Alicja Booth, Bruce Steadman, and Phil Ershler) and facilities at CVTRI. The clinical studies were made possible with the help of Primary Children's Medical Center and their staff.

I would also like to thank my family, especially my wife, Sariah, and sons, Hyrum, Winston, and Emrys, for their support, encouragement, patience, and inspiration.

CHAPTER 1

INTRODUCTION

Heart disease, a term used to describe many cardiac conditions, is still the leading cause of death in the United States [1]. Although the main function of the heart is mechanical, i.e., to pump blood throughout the body, cardiac conditions are frequently caused by disruptions in the electrical activity of the heart, called arrhythmias. Arrhythmias account for a large subset of conditions included in heart disease [1], and thus improvements in their diagnosis and treatment are necessary to reduce their impact and to improve individual and public health. The challenge in achieving this goal arises, in part, because their underlying mechanisms are incompletely understood. The understanding is improving, in part driven by the use of well-established animal experiments and clinical studies, but many recent breakthroughs have depended extensively on computer models of the heart.

Computer models of cardiac structure and function can test mechanisms and reveal behaviors inaccessible with experiments and thus improve the understanding of arrhythmias and provide tools for treatment strategies. These models allow unparalleled interrogations of the heart and cardiovascular systems that are otherwise unethical and impractical. Furthermore, patient-specific modeling can provide highly personalized guidance for diagnostics and therapy in the clinical setting. Despite the promising progress in this field and the efforts of regulatory bodies to encourage the use of such models [2], adoption of computational modeling in biomedical sciences lags behind that in other fields.

One of the reasons for the slow adoption of computational models in medicine is the challenge of performing robust validation studies. The main obstacles lie in the complexity of the systems that are being modeled and measured and the difficulty gaining access to measured data, sometimes from within the body. As a result, validation studies have not kept pace with recent advances in the complexity of computer models of the heart [3]–[6]. In our area of cardiac electrocardiology, validating simulations of cardiac defibrillation

and, more generally, simulations of body-surface potentials from cardiac sources, has been specifically challenging in large part because they require measurements within the body.

The goal of this dissertation was to develop and apply validation approaches to two types of computer heart modeling pipelines: electrocardiographic (ECG) forward simulation and a defibrillation simulation. We compared measured potential values from these studies to predicted values to quantify the accuracy of the simulation pipeline. The results of these studies will establish experimental procedures and shared gold standard datasets that can guide further pipeline development and validation studies and provide more confidence in their use to guide diagnoses and treatment of cardiac arrhythmias.

1.1 Specific Aims

A persistent unexplained finding in previous validation studies of ECG forward models has been higher than expected differences between simulated and measured body-surface potentials from known cardiac sources. The ECG forward problem consists of computing the propagation of the electrical field from the cardiac sources to the torso surface. The cardiac sources can be characterized in many ways, but most often as cardiac surface potentials [7]–[11]. The potentials on the torso surface are calculated using numerical approaches such as the boundary or finite element methods (BEM or FEM, respectively) [3]–[5], [12]. The ECG forward problem is well behaved, with substantial confidence in both the numerical and measurement approaches, yet previous validation studies have consistently shown differences that were greater than might be expected between simulated and measured body-surface potentials [13], [14]. Possible origins of error include registration of geometry, deformations of the heart and some of the electrode arrays, inaccurate conductivities, and insufficient spatial sampling of the heart with measurement electrodes. Because of the practical challenges, most studies attempting to validate the ECG forward simulation record only on the ventricles, leaving the atrial surface unsampled. Ignoring these sources could have a significant impact on the forward simulation. Experiments that separate and quantify the effect of sampling of the cardiac surface, especially on the atrial surface, are needed to separate its effect from other origins of error.

A similar paucity of data exists for simulations of defibrillation. Although tools sim-

ulating the effectiveness of defibrillation have shown some promise in improving device use, the limited amount of high-quality validation studies is an impediment to the widespread adoption of this technology. Validation studies have compared the potentials recorded during defibrillator shocks in animals, but the potential fields are either sparsely sampled or only within the heart [15]–[18]. High spatial sampling of the defibrillation potentials, especially if close to and within the myocardium, can improve the precision of the potential field validation and also allow validation of the electric field strength through the myocardium. This validation is important because the critical mass hypothesis relies on the predicted electric field strength [19], [20]. Additionally, we know of no published reports of potential field validation studies with human geometries combined with clinically determined defibrillation threshold (DFT) values. Such studies can show the accurate prediction of the potential field in patients, and combining measured and predicted potential fields with predicted and measured DFT values will allow for a unique analysis of the ability of the critical mass hypothesis to predict DFTs.

The two modeling pipelines we have developed for this research are similar in their structure and implementation in both the simulation and in recording the potential field. The conduction of electrical signals through tissue is fundamentally the same, whether the source of the signals is the heart or a defibrillator. Therefore, the mathematical formulation to calculate the potential field is identical with either pipeline, and the implementation varies only to accommodate the different source signals and geometry. Similarly, recording the potential field from each of these sources requires closely related experimental preparations and equipment to recreate and record potential fields. Validating pipelines requires a well-characterized torso and source geometry and electrical properties to record and to recreate in silico.

In this dissertation, we performed validation studies on the ECG forward and defibrillation simulation pipelines. We used data recorded from torso-tank experiments, clinically recorded surface potentials, and other simulations to compare against the simulation pipelines and develop strategies to improve validation techniques, addressed in three aims:

- 1) Evaluate the error in ECG forward simulations due to incomplete sampling of the atria and develop sampling strategies to reduce it.

- 2) Record defibrillator potentials in torso-tank experiments to validate a defibrillation simulation pipeline.
- 3) Record human body-surface shock potentials during clinical procedures to validate a defibrillation simulation pipeline.

The findings of the studies performed for this dissertation help to validate the defibrillation simulation pipeline and provide some strategies to reduce error in electrocardiographic forward simulation. The studies presented in Chapters 4 and 5 show that simulated and measured potential fields agree in both the torso-tank and patient body-surface mapping studies. We also found that DFTs predicted by the simulation agree with the DFTs determined during device testing Chapter 5. These two findings support the use of the simulation to test device efficiency for a given defibrillator position. They also provide valuable validation for the findings of previous studies using our pipeline, which provides device placement strategies for abnormal geometries [21], [22]. Chapter 3 addresses a related but different problem, shows that atrial sampling is needed to accurately compute the body-surface potential from the heart, and provides some sampling strategies to help reduce the error when the complete surface cannot be sampled. Chapter 3 also shows that missing ventricular sources can increase the error more than missing only atrial sources. We were able to replicate the results of previous studies [13], [14] only when we combined a lack of atrial sampling with incomplete ventricular sampling. These findings have implications in the setting of electrocardiographic imaging (ECGI) studies that use ECG forward solutions as their basis [23]–[26]. The dissertation findings support the use of simulation pipelines to answer clinical and research questions and encourage their use to help understand and treat cardiac arrhythmias.

1.2 References

- [1] E. J. Benjamin, S. S. Virani, C. W. Callaway, A. R. Chang, S. Cheng, S. E. Chiuve, M. Cushman, F. N. Delling, R. Deo, S. D. de Ferranti, J. F. Ferguson, M. Fornage, C. Gillespie, C. R. Isasi, M. C. Jiménez, L. C. Jordan, S. E. Judd, D. Lackland, J. H. Lichtman, L. Lisabeth, S. Liu, C. T. Longenecker, P. L. Lutsey, D. B. Matchar, K. Matsushita, M. E. Mussolino, K. Nasir, M. O’Flaherty, L. P. Palaniappan, D. K. Pandey, M. J. Reeves, M. D. Ritchey, C. J. Rodriguez, G. A. Roth, W. D. Rosamond, U. K. Sampson, G. M. Satou, S. H. Shah, N. L. Spartano, D. L. Tirschwell, C. W. Tsao, J. H. Voeks, J. Z. Willey, J. T. Wilkins, J. H. Wu, H. M.

- Alger, S. S. Wong, and P. Muntner, "Heart disease and stroke statistics—2018 update: A report from the American Heart Association," *Circ.*, 2018. [Online]. Available: <http://circ.ahajournals.org/content/early/2018/01/30/CIR.0000000000000558>
- [2] Food and Drug Administration Center for Devices and Radiological Health, *Reporting of Computational Modeling Studies in Medical Device Submissions—Guidance for Industry and Food and Drug Administration Staff*. Rockville, MD, USA: Food and Drug Administration, 2016.
 - [3] C. Johnson, *Computational Methods and Software for Bioelectric Field Problems*, 4th ed. Boca Raton, FL, USA: CRC Press, 2015, vol. 1, ch. 43, pp. 1–28. [Online]. Available: <http://www.sci.utah.edu/publications/Joh2015c/ComputationalMethodsandSoftwareforBioelectricFieldProblems.pdf>
 - [4] C. Johnson, "Computational and numerical methods for bioelectric field problems," *Crit. Rev. in BioMed. Eng.*, vol. 25, no. 1, pp. 1–81, 1997. [Online]. Available: <http://www.sci.utah.edu/publications/crj97/Crit-Rev-BE-Johnson97.pdf>
 - [5] C. Johnson, R. MacLeod, and M. Matheson, "Computational medicine: Bioelectric field problems," *IEEE Computer*, vol. 26, no. 26, pp. 59–67, Oct. 1993.
 - [6] N. Trayanova, T. O'Hara, J. Bayer, P. Boyle, K. McDowell, J. Constantino, H. Arevalo, Y. Hu, and F. Vadakkumpadan, "Computational cardiology: How computer simulations could be used to develop new therapies and advance existing ones," *Europace*, vol. 14 Suppl 5, pp. v82–v89, Nov. 2012.
 - [7] R. Barr, M. Ramsey, and M. Spach, "Relating epicardial to body surface potential distributions by means of transfer coefficients based on geometry measurements," *IEEE Trans. Biomed. Eng.*, vol. 24, pp. 1–11, Jan. 1977.
 - [8] R. Gulrajani, "The forward and inverse problems of electrocardiography," *EMBS Mag.*, vol. 17, no. 5, pp. 84–101, Sep./Oct. 1998.
 - [9] R. Plonsey and A. van Oosterom, "Implications of macroscopic source strength on cardiac cellular activation models," *J. Electrocardiol.*, vol. 24, pp. 99–112, Apr. 1991.
 - [10] R. Plonsey and R. Barr, "Mathematical modeling of electrical activity of the heart," *J. Electrocardiol.*, vol. 20, pp. 219–226, Jul. 1987.
 - [11] B. Messinger-Rapport and Y. Rudy, "The inverse problem in electrocardiography: A model study of the effects of geometry and conductivity parameters on the reconstruction of epicardial potentials," *IEEE Trans. Biomed. Eng.*, vol. 33, pp. 667–676, Jul. 1986.
 - [12] R. MacLeod and M. Buist, "The forward problem of electrocardiography," in *Comprehensive Electrocardiology*, P. Macfarlane, A. van Oosterom, O. Pahlm, P. Kligfield, M. Janse, and J. Camm, Eds. London, UK: Springer Verlag, 2010, pp. 247–298.
 - [13] M. Ramsey, R. C. Barr, and M. S. Spach, "Comparison of measured torso potentials with those simulated from epicardial potentials for ventricular depolarization and repolarization in the intact dog," *Circ. Res.*, vol. 41, no. 5, pp. 660–672, Nov. 1977.

- [14] L. R. Bear, L. K. Cheng, I. J. LeGrice, G. B. Sands, N. A. Lever, D. J. Paterson, and B. H. Smaill, "The forward problem of electrocardiography: Is it solved?" *Circ. Arrhythm. Electrophysiol.*, vol. 8, no. 3, pp. 677–684, Jun. 2015. [Online]. Available: <https://www.ahajournals.org/doi/10.1161/CIRCEP.114.001573>
- [15] D. B. Jorgenson, P. H. Schimpf, I. Shen, G. Johnson, G. H. Bardy, D. R. Haynor, and Y. Kim, "Predicting cardiothoracic voltages during high energy shocks: Methodology and comparison of experimental to finite element model data," *IEEE Trans. Biomed. Eng.*, vol. 42, no. 6, p. 559, Jun. 1995.
- [16] F. Claydon, T. Pilkington, A. Tang, M. Morrow, and R. Ideker, "A volume conductor model of the thorax for the study of defibrillation fields," *IEEE Trans. Biomed. Eng.*, vol. 35, pp. 981–992, Nov. 1988.
- [17] F. Claydon, T. Pilkington, A. Tang, M. Morrow, and R. Ideker, "Comparison of measured and calculated epicardial potentials during transthoracic stimulation," in *IEEE EMBS 10th Ann. Intl. Conf.* New Orleans, Louisiana, USA: IEEE Press, 1988, pp. 206–207.
- [18] J. P. Rosborough, D. C. Deno, R. G. Walker, and J. T. Niemann, "A percutaneous catheter-based system for the measurement of potential gradients applicable to the study of transthoracic defibrillation," *PACE*, vol. 30, no. 2, pp. 166–174, Feb. 2007. [Online]. Available: <http://dx.doi.org/10.1111/j.1540-8159.2007.00645.x>
- [19] P. Chen, P. Wolf, F. Claydon, E. Dixon, H. Vidaillet, N. Danieley, T. Pilkington, and R. Ideker, "The potential gradient field created by epicardial defibrillation electrodes in dogs," *Circ.*, vol. 74, pp. 626–636, Sep. 1986.
- [20] R. E. Ideker, P. D. Wolf, C. Alferness, W. Krassowska, and W. M. Smith, "Current concepts for selecting the location, size and shape of defibrillation electrodes," *PACE*, vol. 14, no. 2 Pt 1, p. 227, Feb. 1991.
- [21] M. Jolley, J. Stinstra, S. Pieper, R. MacLeod, D. Brooks, F. Cecchin, and J. Triedman, "A computer modeling tool for comparing novel ICD electrode orientations in children and adults," *Heart Rhythm J.*, vol. 5, no. 4, pp. 565–572, Apr. 2008.
- [22] M. Jolley, J. Stinstra, J. Tate, S. Pieper, R. MacLeod, L. Chu, P. Wang, and J. Triedman, "Finite element modeling of subcutaneous implantable defibrillator electrodes in an adult torso," *Heart Rhythm J.*, vol. 7, no. 5, pp. 692–698, May 2010.
- [23] J. Burnes, B. Taccardi, R. MacLeod, and Y. Rudy, "Noninvasive electrocardiographic imaging of electrophysiologically abnormal substrates in infarcted hearts: A model study," *Circ.*, vol. 101, pp. 533–540, Feb. 2000.
- [24] J. Burnes, B. Taccardi, and Y. Rudy, "A noninvasive imaging modality for cardiac arrhythmias," *Circ.*, vol. 102, pp. 2152–2158, Oct. 2000.
- [25] B. Erem, A. Ghodrati, G. Tadmor, R. MacLeod, and D. Brooks, "Combining initialization and solution inverse methods for inverse electrocardiography," *J. Electrocardiol.*, vol. 44, no. 2, p. e21, Apr. 2011.

- [26] D. Wang, R. Kirby, and C. Johnson, "Finite-element-based discretization and regularization strategies for 3-D inverse electrocardiography," *IEEE Trans. Biomed. Eng.*, vol. 58, no. 6, pp. 1827–1838, Jun. 2011.

CHAPTER 2

BACKGROUND

2.1 Cardiac Arrhythmias

Arrhythmias of the heart are deviations from normal rhythm and function that are caused by changes in the electrical properties of the myocardium. The myocardial tissue consists of networks of electrically coupled cells that normally receive an electrical signal from an adjacent cell and propagate it to other neighboring cells, resulting in a propagating electrical wave that activates the cells and initiates contraction of the tissue [1]. Many arrhythmogenic properties may arise from local changes in the electrical properties of the cells and tissues. Two examples of such changes are spontaneous self-excitation, or “ectopic focal activity,” and slow or inhomogeneous propagation. These behaviors can cause what is known as “reentrant” propagation, i.e., propagation that circles back upon itself and becomes self-sustaining, thus disrupting the normal activity of the heart. The severity of an arrhythmia depends on the persistence of the reentry; a few cycles of arrhythmia are common even in healthy individuals. Arrhythmias become potentially fatal as the normal spread of electrical activation degrades into a set of multiple, sustained reentrant circuits [2], called ventricular fibrillation (VF). VF eliminates effective contraction of the heart, causing rapid death if left untreated [3]. Persistent but less directly deadly arrhythmias, such as ventricular tachycardia (VT) and atrial fibrillation (AF), may only partially disrupt the function of the heart, yet they also impact the health of the individual. Additionally, many initially benign arrhythmias also carry a high risk of developing into VF [4] or may cause other serious side effects such as stroke, as in AF [5], [6]. Therefore, prompt and effective detection of all arrhythmias is critical to achieve effective treatment [7], [8].

In order to understand, detect, and treat arrhythmias, clinicians must be able to effectively record the bioelectric fields generated by the heart [9], [10]. Such fields arise in the heart but also throughout the torso and on the body surface. Recordings taken in or

near the heart are called electrograms, and recordings taken on the body surface are called electrocardiograms (ECGs).

Clinicians often use a combination of ECG and electrogram recordings to first diagnose arrhythmias and then to identify the regions of tissue that cause the arrhythmia and become the targets of treatment. Due to the ease of acquisition, ECGs can often be used to quickly determine the nature of an arrhythmia and can sometimes provide a general location of arrhythmogenic tissue. Electrograms are often required to provide a more precise description and location of the arrhythmogenic tissue. One of the goals of this research was to explore the relationship between cardiac electrograms and ECGs in the setting of arrhythmia detection.

2.2 Measuring Bioelectric Fields

When electrical sources, from the heart or from an external source like a defibrillation pulse, are located in the body, the resulting electric field permeates the torso and generates electrical currents. The current flow through the torso depends on the electrical properties of the various tissues and the distance from the source, meaning that recordings near the sources will have a higher amplitude than those farther away, and the current through poorly conducting tissue will be lower than through tissues that conduct well. The electric potential generated by such currents flowing through the torso can be measured at various positions to obtain information regarding the electrical sources [11].

There is an inherent trade off between measurements from the torso surface and those obtained through invasive procedures. As the heart is activated, the transmembrane currents driving the action potentials create extracellular currents, which are electrical sources that conduct through the torso. Each of these small electrical sources superimposes through the torso, so that the resulting measured potentials contain a summation of all the cardiac sources within the torso, weighted by the distance from the source. This combination of the attenuation with distance and spatial summation causes signals near the heart to be not only larger but also more sensitive to the local cardiac activity than signals located farther away [12]. The dichotomy between signal sensitivity and access is an ongoing challenge in the evaluation and understanding of arrhythmias. Signals on the body surface, i.e., far from the heart, are far easier to record than signals near the heart, but they are lower in

amplitude and contain less localized information.

Electrograms, recordings taken in or near the heart, are signals that characterize the activity of the region within a few centimeters of the heart and can be used to infer directly the properties of the tissue, such as local activation time and duration [13] (Fig. 2.1). When acquired as a set of multiple, simultaneously sampled recordings from known electrode locations, electrograms can provide a spatially detailed representation of the electrical activity of the heart and can reconstruct reentrant pathways characteristic of arrhythmias [14]–[16]. Well-developed commercial systems and instrumentation based on electrodes housed within vascular catheters are used to obtain electrograms in patients [17]–[20]. However, obtaining electrograms is invasive, expensive, time consuming, and not without risk, thus reducing the utility of such recordings in the clinical detection and diagnoses of arrhythmia.

ECGs, recordings of the activity of the heart from the body surface, are a noninvasive method of observing the activity of the heart [9], [10]. Because ECG recordings are obtained farther from the heart than electrograms, the relative distance to each point in the heart is more uniform, and therefore they contain signals that represent the sum of all the sources in the heart. A normal ECG, shown in Fig. 2.2, contains five distinct waveforms,

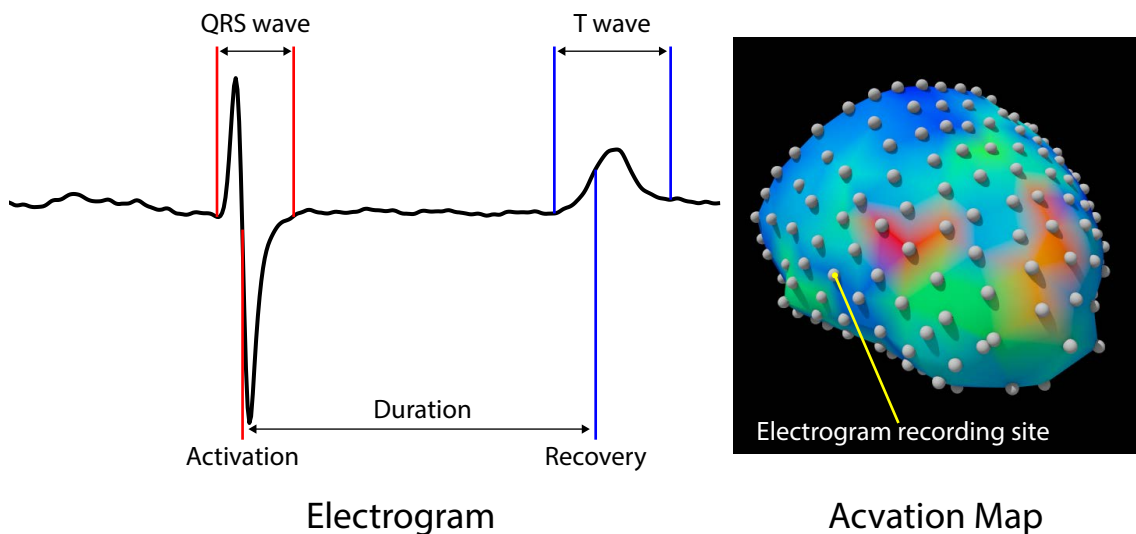


Fig. 2.1. Example electrogram and activation map. Local tissue activity, such as the activation and recovery time, can be inferred from the morphology of the signal and spatially analyzed for arrhythmia diagnosis and treatment.

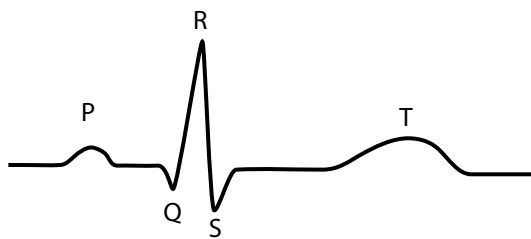


Fig. 2.2. Cartoon ECG to show each of the waveforms.

labeled the P, Q, R, S, and T waves, and each wave reflects activity from various regions of the heart. The P wave is caused by atrial activation, the Q, R, and S waves (or the QRS complex) are caused by ventricular activation, and the T wave is caused by ventricular repolarization. The global information of ECG signals and the ease and low cost of recording have made the ECG vital to the early detection and diagnosis of arrhythmias, which can occur based only on changes in heart rate and the coarse morphology of the ECG.

Body-surface potential mapping (BSPM) requires a much higher spatial sampling of the same signals as the standard ECG recordings to characterize the cardiac potential field on the full surface of the torso [21], [22]. By using up to 200 electrodes, distributed in carefully considered (but not universally agreed upon) patterns over the body, BSPM methods can capture the subtle spatial variation of the surface bioelectric fields. The resulting surface bioelectric field activity can be used to infer the underlying cardiac activity [23] either through direct observation of the BSPM patterns [24], [25] or by using them as input signals for an electrocardiographic imaging (ECGI) method that predicts cardiac activity quantitatively [26].

ECGI is an emerging technology that involves estimating the cardiac activity from BSPM recordings and known thoracic geometry and electrical conductivities [26], [27] (Fig. 2.3). Although this technology is still in the academic and commercial research phase, studies have shown promise in predicting areas of ectopic activity [28]–[31] and poor conduction [32]. ECGI requires accurate knowledge of the torso volume conductor shape and properties together with concise, quantitative descriptions of cardiac electric sources. These elements are then combined into a predictive model known as an “ECG forward model,” which predicts torso potentials from known heart sources. The forward model

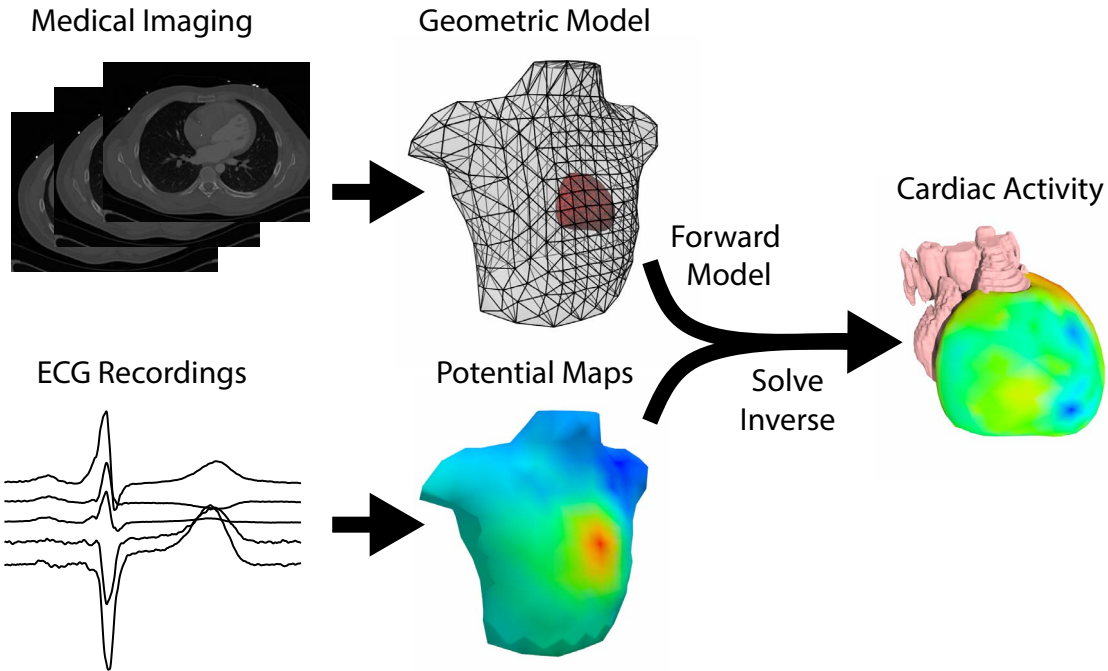


Fig. 2.3. ECG imaging (ECGI) pipeline. ECGI is dependent on the accuracy of the ECG forward simulation.

must then be mathematically or numerically inverted to solve an associated “inverse problem” to predict cardiac sources from body-surface potentials, ECGI. We cover both topics in more detail because a major focus of the research presented in this dissertation is to evaluate aspects of the ECG forward model.

Clinicians often use a combination of ECG and electrogram recordings to first diagnose arrhythmias and then to identify regions of tissue that cause the arrhythmia and direct treatment. Due to the ease of implementation, ECGs can often be used to quickly determine the nature of an arrhythmia and can sometimes provide a general location of arrhythmogenic tissue. Electrograms are then often required to provide a more precise description and location of the arrhythmogenic tissue. The research in this dissertation seeks to explore the relationship between cardiac electrograms and ECGs in the setting of arrhythmia detection.

In addition to measuring potentials fields generated by cardiac sources, this dissertation contains studies with measurements of potential fields generated by defibrillator pulses. The physics of electrical current flow through the torso and the recording of

the potential field are the same, regardless of the sources [11]. However, some additional considerations are required to record defibrillator potentials in practice. Both the amplitude and frequency of defibrillator pulses are higher than those in signals from cardiac sources, and therefore using the same recording system to measure fields from both types of sources requires some adjustment. However, by recording at higher sampling rates and attenuating the signal, either the pulse generated by the device or the signal acquired in the tissues can be measured with cardiac mapping systems. We carried out such measurements in this study and used them to validate computer simulations.

2.3 Treatment of Arrhythmias

Once an arrhythmia is detected, usually with ECG recordings, it can be treated with three types of methods: pharmacology, ablation, and defibrillation. Each method is designed to target a different aspect of arrhythmogenesis.

Pharmacological treatments are generally used to alter the electrical properties of the tissue to reduce the risk of an arrhythmia occurring. For instance, β blockers or Na^+ channel antagonists will reduce the excitability of the heart and can reduce or eliminate arrhythmogenic activity in the heart [33]–[35].

Ablation is the process of applying thermal energy, typically heat (radio frequency), but also cold, by specialized catheters in order to create scar tissue at carefully identified regions in the heart [36]. Doctors create such scar tissue with the goal of permanently altering the electrical properties of the tissue in a way that interrupts the formation of reentrant pathways and thus eliminates arrhythmias. Clinicians may also use ablation to destroy arrhythmogenic stimuli or modify tissue substrates in order to reduce the possibility of initiating an arrhythmia. However, in order to target the appropriate region for ablation, clinicians need to know the locations of arrhythmogenic tissue.

Identifying arrhythmogenic tissue or tissue substrates requires acquiring electrograms and mapping the electrical activity of the heart. To acquire the signals, catheters are typically introduced via the vasculature to access the endocardium or through small incisions in the chest wall for access to the epicardium. These procedures are thus semi-invasive, at least marginally risky, and time consuming [18], [37]–[39]. ECG imaging (ECGI) provides a noninvasive means to acquire this information (Fig. 2.3).

2.3.1 Treatment of Arrhythmias Through Defibrillation

Short-term, emergency treatment of life-threatening arrhythmias involves terminating reentrant circuits and the resulting fibrillation with an electrical shock, known as defibrillation [40]. Conventional defibrillation involves applying a large electric field through the heart to forcibly drive a large portion of the heart into the electrically activated or depolarized state. All the cells in the heart will then return to their electrical resting potential, allowing normal rhythm to resume [41].

Three main defibrillator device types automatically detect and treat fibrillation: automatic external defibrillators (AEDs), wearable cardioverter defibrillators (WCDs), and implantable cardioverter defibrillators (ICDs). AEDs are designed as a tool for bystanders to quickly administer defibrillation to a subject with life-threatening arrhythmias. WCDs are external devices that patients wear on their bodies, and ICDs are devices that are implanted into the body of the patient to deliver therapy to the heart. Although the details of these defibrillators are significantly different, the behavior of each is fairly similar: detect fibrillation from measured electrograms or electrocardiograms and apply large, carefully timed electric fields to defibrillate the heart. These devices are widely used and save many lives [7].

We can quantify the effectiveness of a defibrillator configuration by means of the DFT, which is the lowest energy the system (device plus electrodes) needs to deliver for effective defibrillation. Reducing the DFT of defibrillators maximizes the efficiency while the reduced energy usage also preserves device battery life, which reduces the frequency of replacement for implantable devices. Lower energy defibrillation also reduces the excess current delivered to the myocardium and surrounding tissue, which in turn reduces both pain and damage to the tissue [42].

Although the mechanisms for defibrillation are not fully understood, the critical mass hypothesis [43] is one approach that seeks to quantify the shock that successfully restores normal sinus rhythm and is a valuable tool for use in simulation approaches. The critical mass hypothesis stems from the assumption that a large enough electric field will activate adequate proportions of cardiac tissue to achieve defibrillation [44]–[46]. This hypothesis provides an efficient way to calculate the DFT and therefore the effectiveness of the device. However, critical mass hypothesis does not fully describe the mechanisms of defibrillation,

with documented cases in which 1) defibrillation occurred without reaching critical mass, and conversely, 2) defibrillation shocks achieved critical mass but were not successful [41], [47]. Another mechanistic theory is the virtual electrode hypothesis [48], which states that in the presence of a strong external electric field, e.g., from a defibrillator, regions of tissue experience hyperpolarization or depolarization of the transmembrane potential. These virtual stimulation sites then stimulate or suppress electrical activity of the cells to extinguish fibrillating wavefronts in certain circumstances.

Although defibrillators have been used to save lives for many decades, further optimization could improve their effectiveness. One form of optimization is to determine electrode locations that balance the many device requirements [43], [49]. An example of such a strategy is subcutaneous ICD implantations, which are less invasive with more benign failure modes than the traditional strategy [50].

2.4 Simulation Pipelines for Cardiac Bioelectricity

Modeling electrical conduction through a medium such as the torso can range from overly simple to needlessly complex, and all such models require a description of both the electrical sources and the conduction through the torso. Although electrical sources in the torso may be modeled in many ways, this dissertation will focus on two types of voltage sources: the epicardial surface of the heart and the electrodes from a defibrillator. In both approaches, the voltage sources are assumed to be outside the simulation domain, and the resulting potential distribution through the body can be described with Laplace's equation:

$$\nabla \cdot \sigma \nabla \phi = 0 \quad (2.1)$$

where ∇ is the gradient operator, $\nabla \cdot$ is the divergence operator, σ describes the electrical conductivities of the (possibly heterogeneous and even anisotropic) tissues, and ϕ is the potential field. To compute a unique solution for ϕ , some locations must have known potentials set as known as Dirichlet boundary conditions, or be constrained to have zero normal components of the electric field, the Neumann conditions. Numerical methods such as boundary or finite element methods (BEM or FEM, respectively) are used to approximate the solution to Laplace's equation over a discrete domain described by a

polygonal discretization [23], [51]–[53].

2.4.1 ECG Forward Model

The ECG forward model describes the prediction of the electric potentials throughout a known passive conductive medium from a bioelectric source representing the heart [23]. Three well-characterized ways to represent the cardiac source are 1) as single or multiple current dipoles representing the summation of the cardiac current [54]–[56], 2) as a layer of current dipoles along the activation wavefront [57], [58], or 3) as an enclosed surface of potentials that encompasses the myocardium [59]–[62]. Other common assumptions are that conduction through the passive tissue is linear and that the frequencies of the cardiac sources are low enough that the torso potentials reach steady state almost instantly (the quasistatic assumption) [23]. The predicted potential fields are calculated at desired locations using numerical techniques, e.g., BEM or FEM, as described above [23], [51]–[53].

Using these assumptions and numerical estimation techniques, the ECG forward model can be represented as a linear system, where the potentials at a set of locations away from the sources are equal to a matrix of all the coefficients relating the cardiac sources to the remote locations multiplied by the vector of all the source values [59]–[62] (Fig. 2.4). This formulation is useful because it allows for quickly calculating multiple instances of source values, representing either different candidate sources or a sequence or time series. This formulation also provides a conceptually straightforward means of solving associated inverse problems, i.e., to determine the cardiac source values from the measured remote potentials, as in ECGI [26], [27] (Fig. 2.4).

2.4.2 Defibrillation Simulation

Simulating the effect of defibrillation on the heart requires overcoming two main challenges: calculating the electric field of the defibrillator throughout the medium and predicting how this electric field within the heart will achieve successful defibrillation. The first challenge is mathematically similar to the ECG forward model; the difference is that the source is external to the heart, a set of two or more defibrillator electrodes instead of the intrinsic bioelectricity of cardiac tissue. Both sources are modeled as voltage supplies and the resulting potentials in the torso are computed, typically using the FEM [51], [52]

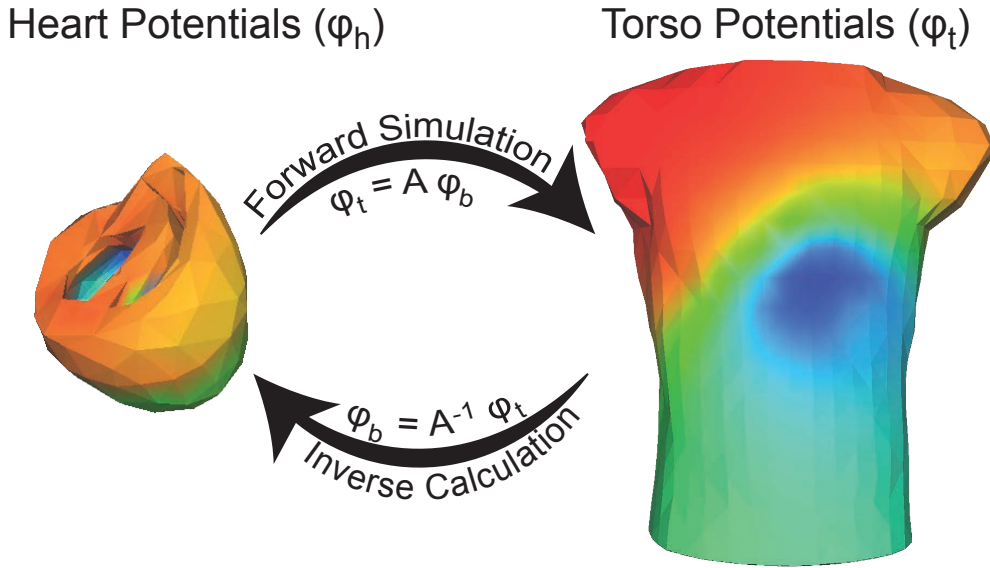


Fig. 2.4. ECG forward and inverse computational pipeline. ECG inverse, also called ECGI, is dependent on the accuracy of the ECG forward simulation.

(Fig. 2.5).

To address the second challenge, once the electric field within the heart is calculated, different strategies can be employed to predict the effect of the defibrillation shock on the heart. One such strategy is to use the previously described critical mass hypothesis [44]–[46]. Critical mass can be used to calculate the DFT by scaling the predicted electric field throughout the heart until the necessary criteria are met (Fig. 2.5). Simulations using the critical mass hypothesis can be fast to compute, so that multiple parameters and configurations of defibrillation can be tested quickly to determine the effect of each on the DFT. Other strategies could be used in this pipeline, such as computing a time-dependent simulation of the fibrillating and defibrillating activity of the tissue and evaluating which shocks produce successful defibrillation [41], [47].

2.5 Validating Computer Models

Validation of any simulation approach is essential, especially in medical applications, before computational predictions can play any role in driving research, device development, or clinical practice. Specific validation of geometry-based computer models, such as the ECG forward simulation and the defibrillation simulation, is challenging because

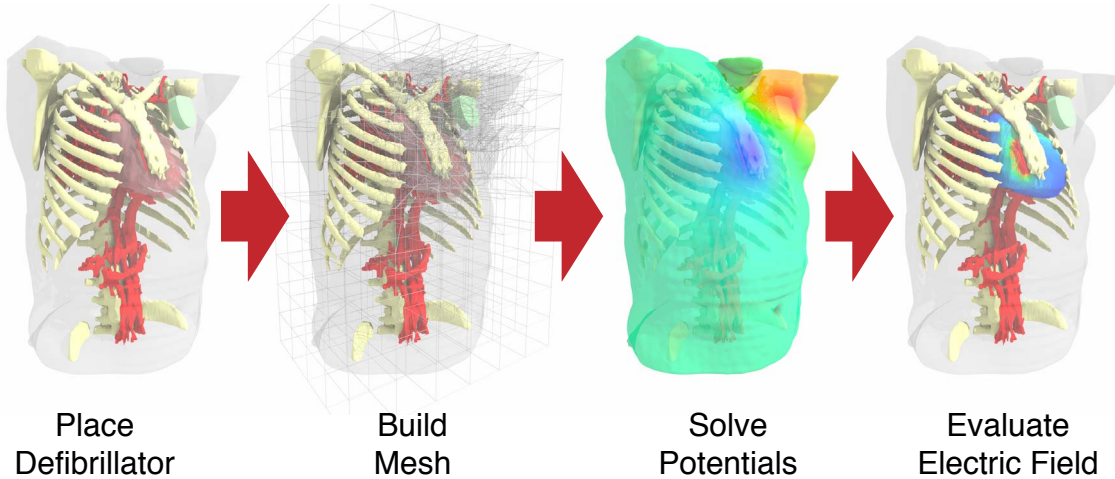


Fig. 2.5. Patient-specific pipeline for simulating defibrillation.

such studies need to capture complex interactions of sources within the irregular and often heterogeneous volume conductors of the body and then place invasive measurement electrodes within living organisms while maintaining the integrity of the volume conductor. Experiments that enable validation need some combination of three types of data: body-surface potential recordings, comprehensive measurements of cardiac sources or an otherwise known extracardiac source, and high-fidelity characterization of the geometry of the volume conductor in which the heart resides.

The three most commonly used types of preparations that address these needs are *in situ* animal experiments, experiments using physical, electrolytical phantoms, e.g., realistically shaped “torso-tank,” and clinical studies. *In situ* animal experiments involve capturing the potential field with electrodes that are placed throughout the animal, most often on the torso and heart surface, while various interventions are performed [45], [63]. Such preparations are physiologically realistic provided the native position and conditions of the heart and surrounding tissues in the torso are maintained [64], [65]. Torso-tank experiments combine an isolated animal heart and an electrolytic tank to represent the torso, allowing recording electrodes to be placed virtually anywhere within the tank and the heart [29], [66]–[74]. Tank experiments allow for greater control of many of the variables involved with the generation of ECGs than *in situ* animal preparations or clinical studies, including the conductivity and geometry of the torso volume conductor, facilitating

replication in silico. However, they are phantoms and not intact torsos, and they represent simplifications of reality. Clinical studies are highly realistic and involve recording the potential field while a medical intervention is applied to the patient [46], [75]. Potential recordings are most often captured on the body surface and on the endocardial surface of the heart by means of catheter-based electrodes. In this dissertation, we utilized torso-tank and clinical studies to validate and improve ECG forward and defibrillation simulations.

When experimental studies disagree with simulations, identifying the aspects of the simulation and experiment setup that differ can be challenging. Both the simulation and experiment have inherent uncertainties associated with them, and analyzing the contribution of each step can be virtually impossible for specific cases. One approach to discovering sources of error is to systematically vary parameters of the simulation or the experimental protocols, either individually [76] or with a statistical approach, such as the Monte-Carlo method [77] or stochastic collocation [78]–[80]. Once the sensitivity of various parameters is established, the simulation or experiment can be modified to reduce the error.

2.5.1 ECG Forward Model Validation

Many studies have used *in situ* animal experiments to validate ECG forward models [63], [81]–[83] but with mixed results due to the many unavoidable technical challenges of placing electrodes and then maintaining an intact physiological volume conductor, usually by re-closing the chest [63], [64]. Hence, although these experiments provide data that are arguably the most physiologically realistic, the conditions of the experiment can be challenging to recreate in silico. Recent studies have shown disappointing levels of accuracy when comparing predicted and measured ECGs (Fig. 2.6) [64], a finding that provoked some of the goals of this research.

Previous studies using torso-tank preparations have focused not only on ECGI validation [29], [84], but also on the characterization of ischemia [72] and the evaluation of the effects of changes in heart position [76], [85] and torso conductivity [86]. Most studies for ECGI validation have not used measured torso potentials but rather forward-computed facsimiles to which noise was added and ECGI performed. Conspicuously missing from published studies are examples using fully measured data from torso-tank studies to validate ECG forward models. One likely reason for this omission is that the agreement

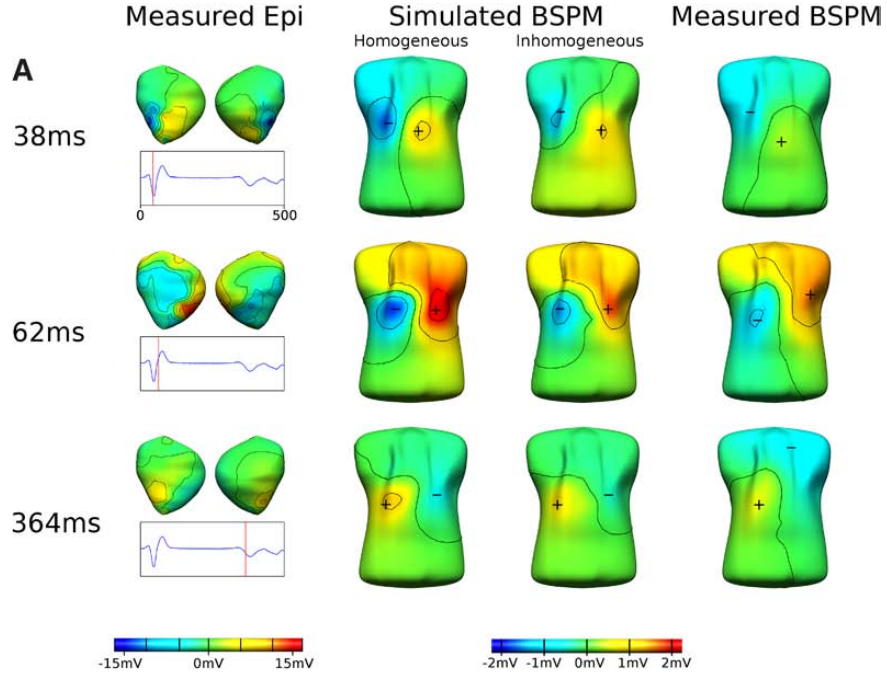


Fig. 2.6. In situ validation of ECG forward simulations. Residual error exists despite mature experimental and simulation techniques. Reprinted with permission from Bear et al. [64].

between these experimental recordings and predicted ECG signals has been lower than expected, a challenge we address in Chapter 3 of this dissertation.

Several studies have recorded body-surface potentials and cardiac sources in clinical settings. These studies are often designed to validate ECGI [75], [87]–[92] and have generally shown that ECGI can accurately calculate specific aspects of the cardiac activity, such as earliest site of activation [75], [89], [90], [93]. However, these studies have less accuracy in calculating total activity of the heart, such as the cardiac-surface potentials [75], [92]. Clinical studies that attempt to validate the ECG forward simulations often record some cardiac source data, such as a stimulus or rotor site, and simulate resulting cardiac activity to produce body-surface potentials [87], [94], [95].

The accuracy of the validation of ECG forward models can also vary depending on the type of electrodes used to record cardiac potentials. The majority of published studies describe configurations of measuring epicardial potentials either by means of contact electrodes [72] or from electrodes placed near the heart in a torso tank [29] (Fig. 2.7). Contact epicardial potentials are more relevant in validation studies because, as discussed

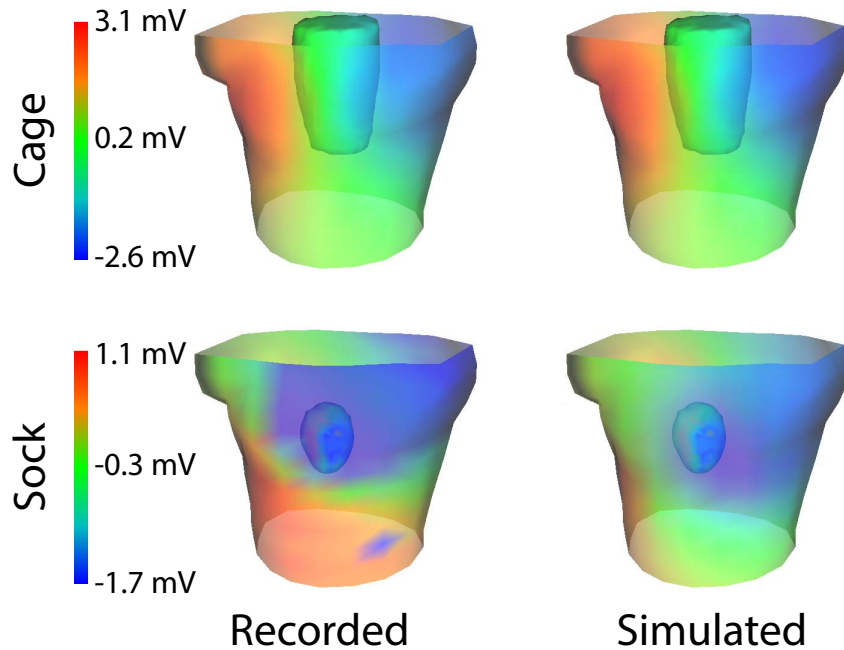


Fig. 2.7. Forward simulations compared to measured values using cardiac sock and cage electrode arrays. The cage shows better agreement between measured and simulated potentials than the sock. The cardiac surface with the sock contains interpolated potentials over the atria where the sock did not cover.

earlier, sensitivity to local features of the cardiac sources decreases with distance and electrograms are spatially smoothed. However, noncontact electrograms are often easier to reproduce in silico specifically because of this spatial smoothing; therefore, they are easier to solve numerically. Noncontact electrograms can be less sensitive to perturbations in heart location and have more accurate registration because the electrodes are often rigidly mounted in the tank. Noncontact electrodes also often surround the heart, providing more complete spatial sampling of the cardiac sources. In Chapter 3, we analyze the effect of removing samples surrounding the heart to develop strategies to improve ECG forward model validation studies.

2.5.2 Defibrillation Simulation Validation

Previous studies have used *in situ* animal experiments to capture potentials generated by defibrillators at recording sites throughout the torso; however, these locations were either sparsely spaced or only in the heart [45], [96]–[98] (Figs. 2.8 and 2.9). A different

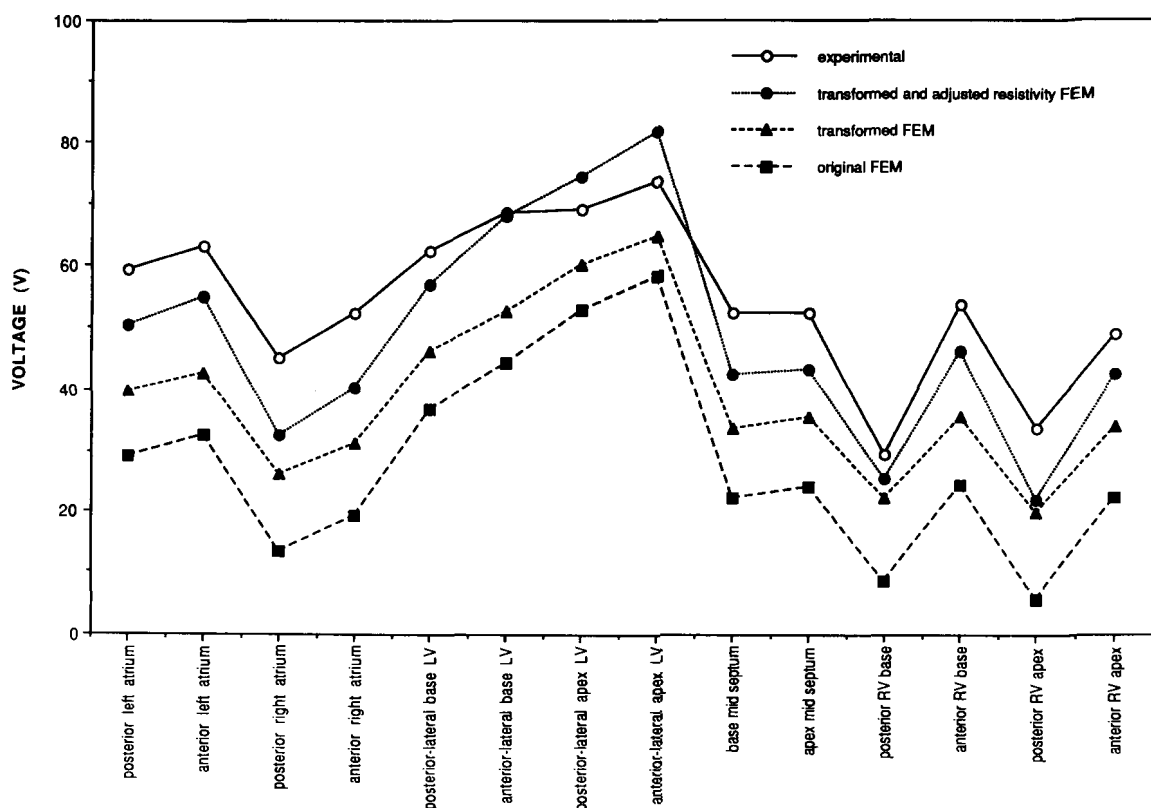


Fig. 2.8. In situ validation of potential fields predicted by defibrillation simulation in the torso. Reprinted with permission from Jorgenson et al. [45]. Copyright ©1995 IEEE.

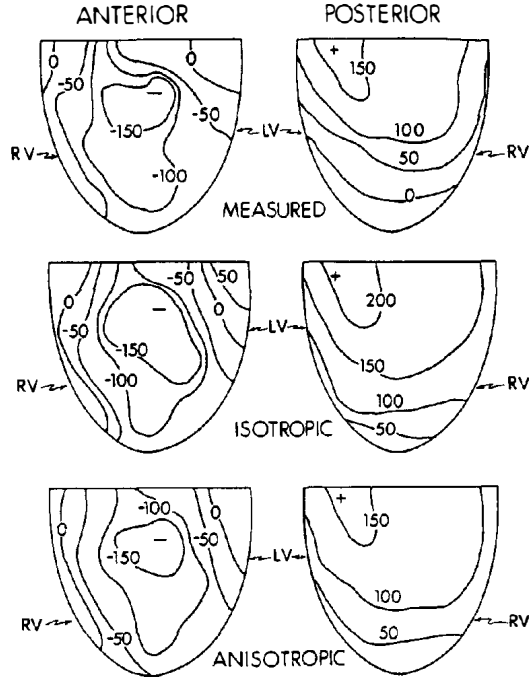


Fig. 2.9. In situ validation of potential fields predicted by defibrillation simulation on the epicardium. Reprinted with permission from Claydon et al. [96]. Copyright ©1988 IEEE.

approach based on physical phantoms, i.e., torso-tank studies, offers the capacity for higher resolution and more consistent sampling of the torso volume than in situ studies. Such torso-tank studies have reported defibrillation potentials [99] but have not compared them to simulated defibrillation fields. Related studies have used optical mapping to record high-resolution cellular potentials [100]–[102] but only to record the subsequent cardiac activity, not the defibrillation shock field. To date, no published tank studies have been used to validate the predicted electric field through a volume conductor, especially within the heart. Chapter 4 will address this omission.

Validation of DFT prediction can be achieved with animal studies and clinical trials, both of which have similar methodologies. VF is induced in a subject, who then receives defibrillation treatments in increasing energy values. The lowest energy to terminate fibrillation is considered the DFT. DFT studies in animals have shown that simulations can replicate the predictions of DFT based on the critical mass hypothesis [45], [103]. Some studies have measured DFTs in humans [104]–[106], and we have used these data to conduct our own validation studies [46]. The major limitation of these studies for validation

of simulations has been the lack of measured potentials; the studies measured only DFT, i.e., the success or failure of defibrillation. This dissertation addresses this shortcoming in Chapter 5 by measuring body-surface potentials during testing of ICDs in patients.

2.6 References

- [1] N. Sperelakis, "Electrogenesis and regulation of the currents underlying the cardiac action potential and propagation mechanisms," in *IEEE EMBS 9th Ann. Intl. Conf.* Boston, MA, USA: IEEE Press, 1987, pp. 887–889.
- [2] C. Antzelevitch, S. Sicouri, S. Litovsky, A. Lukas, S. Krishnan, DiegoDi, G. Gin-tant, and D. Liu, "Heterogeneity within the ventricular wall. Electrophysiology and pharmacology of epicardial, endocardial, and M cells," *Circ. Res.*, vol. 69, no. 6, pp. 1427–49, Dec. 1991.
- [3] A. Schmidt, C. F. Azevedo, A. Cheng, S. N. Gupta, D. A. Bluemke, T. K. Foo, G. Gerstenblith, R. G. Weiss, E. Marban, G. F. Tomaselli, J. A. Lima, and K. C. Wu, "Infarct tissue heterogeneity by magnetic resonance imaging identifies enhanced cardiac arrhythmia susceptibility in patients with left ventricular dysfunction," *Circ.*, vol. 115, no. 15, pp. 2006–14, Apr. 2007.
- [4] S. Pogwizd and P. Corr, "Mechanisms underlying the development of ventricular fibrillation during early myocardial ischemia," *Circ.*, vol. 66, no. 3, pp. 672–95, Mar. 1990.
- [5] P. Wolf, R. Abbott, and W. Kannel, "Atrial fibrillation as an independent risk factor for stroke: The Framingham Study," *Stroke*, vol. 22, pp. 983–988, Aug. 1991.
- [6] W. Lee, G. Lamas, S. Balu, J. Spalding, Q. Wang, and C. Pashos, "Direct treatment cost of atrial fibrillation in the elderly American population: A Medicare perspective," *J. Med. Econ.*, vol. 11, no. 2, pp. 281–298, Feb. 2008.
- [7] D. Mozaffarian, E. J. Benjamin, A. S. Go, D. K. Arnett, M. J. Blaha, M. Cushman, S. R. Das, S. de Ferranti, J.-P. Després, H. J. Fullerton, V. J. Howard, M. D. Huffman, C. R. Isasi, M. C. Jiménez, S. E. Judd, B. M. Kissela, J. H. Lichtman, L. D. Lisabeth, S. Liu, R. H. Mackey, D. J. Magid, D. K. McGuire, E. R. Mohler, C. S. Moy, P. Muntner, M. E. Mussolino, K. Nasir, R. W. Neumar, G. Nichol, L. Palaniappan, D. K. Pandey, M. J. Reeves, C. J. Rodriguez, W. Rosamond, P. D. Sorlie, J. Stein, A. Towfighi, T. N. Turan, S. S. Virani, D. Woo, R. W. Yeh, and M. B. Turner, "Heart disease and stroke statistics—2016 update," *Circ.*, 2015. [Online]. Available: <http://circ.ahajournals.org/content/early/2015/12/16/CIR.0000000000000350>
- [8] E. J. Benjamin, M. J. Blaha, S. E. Chiuve, M. Cushman, S. R. Das, R. Deo, S. D. de Ferranti, J. Floyd, M. Fornage, C. Gillespie, C. R. Isasi, M. C. Jimenez, L. C. Jordan, S. E. Judd, D. Lackland, J. H. Lichtman, L. Lisabeth, S. Liu, C. T. Longenecker, R. H. Mackey, K. Matsushita, D. Mozaffarian, M. E. Mussolino, K. Nasir, R. W. Neumar, L. Palaniappan, D. K. Pandey, R. R. Thiagarajan, M. J. Reeves, M. Ritchey, C. J. Rodriguez, G. A. Roth, W. D. Rosamond, C. Sasson, A. Towfighi, C. W. Tsao, M. B. Turner, S. S. Virani, J. H. Voeks, J. Z. Willey, J. T. Wilkins, J. H. Wu, H. M. Alger, S. S.

- Wong, and P. Muntner, "Heart disease and stroke statistics-2017 update: A report from the American Heart Association," *Circ.*, vol. 135, no. 10, pp. e146–e603, Mar. 2017.
- [9] W. Einthoven, "Nieuwe methoden voor clinisch onderzoek," *Ned. T. Geneesk*, vol. 29, no. II, pp. 263–286, 1893.
 - [10] W. Einthoven, "Le telecardiogramme," *Arch. Int. de Physiol.*, vol. 4, pp. 132–164, 1906.
 - [11] R. Plonsey and R. Barr, *Bioelectricity: A Quantitative Approach*. New York, USA; London, UK: Plenum Publishing, 1988.
 - [12] C. Haws and R. Lux, "Correlation between *in vivo* transmembrane action potentials and activation-recovery intervals from electrograms: Effects of interventions that alter repolarization time," *Circ.*, vol. 81, pp. 281–288, Jan. 1990.
 - [13] T. Fitzgerald and J. Triedman, "Spatial resolution of catheter-based ventricular pace activation mapping using signal-averaged electrograms," in *IEEE Computers in Cardiology*, vol. 25. IEEE Computer Society, 1998, pp. 517–520.
 - [14] G. A. Kaiser, A. L. Waldo, J. Frederick O. Bowman , B. F. Hoffman, and J. R. Malm, "The use of ventricular electrograms in operation for coronary artery disease and its complications," *The Ann. of Thorac. Surg.*, vol. 10, no. 2, pp. 153–162, Aug. 1970. [Online]. Available: [http://dx.doi.org/10.1016/S0003-4975\(10\)65581-6](http://dx.doi.org/10.1016/S0003-4975(10)65581-6)
 - [15] M. Burgess, R. Lux, R. Wyatt, and J. Abildskov, "The relation of localized myocardial warming to changes in cardiac surface electrograms in dogs," *Circ. Res.*, vol. 43, no. 6, pp. 899–907, Dec. 1978.
 - [16] J. Gallagher, J. Kasell, W. Sealy, E. Prichett, and A. Wallace, "Epicardial mapping in the Wolff-Parkinson-White syndrome," *Circ.*, vol. 57, no. 5, pp. 854–866, May 1978.
 - [17] L. Davis, M. Cooper, D. Johnson, J. Uther, D. Richards, and D. Ross, "Simultaneous 60-electrode mapping of ventricular tachycardia using percutaneous catheters," *J. Am. Coll. Cardiol.*, vol. 24, no. 3, pp. 709–719, Sep. 1994.
 - [18] J. Smeets, S. B. Haim, L. Rodriguez, C. Timmermans, and H. Wellens, "New method for nonfluoroscopic endocardial mapping in humans," *Circ.*, vol. 97, pp. 2426–2432, Jun. 1998.
 - [19] J. Dong, T. Dickfeld, D. Dalal, A. Cheema, C. Vasamreddy, C. Henrikson, J. Marine, H. Halperin, R. Berger, J. Lima, D. Bluemke, and H. Calkins, "Initial experience in the use of integrated electroanatomic mapping with three-dimensional MR/CT images to guide catheter ablation of atrial fibrillation," *J. Cardiovasc. Electrophysiol.*, vol. 17, no. 5, pp. 459–466, May 2006.
 - [20] R. Cappato, H. Calkins, S. Chen, W. Davies, Y. Iesaka, J. Kalman, Y. Kim, G. Klein, A. Natale, D. Packer, A. Skanes, F. Ambrogi, and E. Biganzoli, "Up-dated worldwide survey on the methods, efficacy and safety of catheter ablation for human atrial fibrillation," *Circ. Arrhythm. Electrophysiol.*, vol. 3, no. 1, pp. 32–38, Feb. 2009. [Online]. Available: <http://circep.ahajournals.org/cgi/content/abstract/CIRCEP.109.859116v1>

- [21] R. Lux, M. Burgess, R. Wyatt, A. Evans, G. Vincent, and J. Abildskov, "Clinically practical lead systems for improved electrocardiography: Comparison with precordial grids and conventional lead systems," *Circ.*, vol. 59, pp. 356–363, Feb. 1979.
- [22] R. Lux, "Mapping techniques," in *Comprehensive Electrocardiology*, P. Macfarlane and T. Veitch Lawrie, Eds. Oxford, England: Pergamon Press, 1989, vol. 2, ch. 26, pp. 1001–1014.
- [23] R. MacLeod and M. Buist, "The forward problem of electrocardiography," in *Comprehensive Electrocardiology*, P. Macfarlane, A. van Oosterom, O. Pahlm, P. Kligfield, M. Janse, and J. Camm, Eds. London, UK: Springer Verlag, 2010, pp. 247–298.
- [24] L. D. Ambroggi, T. Bertoni, M. Bregghi, M. Marconi, and M. Mosca, "Diagnostic value of body surface potential mapping in old anterior non-Q myocardial infarction," *J. Electrocardiol.*, vol. 21, no. 4, pp. 321–329, Nov. 1988.
- [25] M. Gardner, T. Montague, C. Armstrong, M. Horacek, and E. Smith, "Vulnerability to ventricular arrhythmia: Assessment by mapping of body surface potential," *Circ.*, vol. 73, no. 4, pp. 684–692, Apr. 1986.
- [26] A. Pullan, L.K.Cheng, M. Nash, D. Brooks, A. Ghodrati, and R. MacLeod, "The inverse problem of electrocardiography," in *Comprehensive Electrocardiology*, P. Macfarlane, A. van Oosterom, O. Pahlm, P. Kligfield, M. Janse, and J. Camm, Eds. London, UK: Springer Verlag, 2010, pp. 299–344.
- [27] Y. Rudy and B. Lindsay, "Electrocardiographic imaging of heart rhythm disorders: From bench to bedside," *Card. Electrophysiol. Clin.*, vol. 7, no. 1, pp. 17–35, Mar. 2015.
- [28] C. Penney, J. Clements, M. Gardner, L. Sterns, and B. Horacek, "The inverse problem of electrocardiography: Application to localization of Wolff-Parkinson-White pre-excitation sites," in *Proc. IEEE EMBS 17th Ann. Intl. Conf.* Montreal, Canada: IEEE Press, 1995, pp. 215–216.
- [29] H. Oster, B. Taccardi, R. Lux, P. Ershler, and Y. Rudy, "Noninvasive electrocardiographic imaging: Reconstruction of epicardial potentials, electrograms, and isochrones and localization of single and multiple electrocardiac events," *Circ.*, vol. 96, no. 3, pp. 1012–1024, Aug. 1997.
- [30] R. Modre, B. Tilg, G. Fischer, F. Hanser, B. Messnarz, F. Roithinger, and F. Hintringer, "A clinical pilot study on the accessory pathway localization accuracy applying ECG mapping," in *Proc. IEEE EMBS 24th Ann. Intl. Conf.*, vol. 2, 2002, pp. 1381–1382.
- [31] S. Jamil-Copley, R. Bokan, P. Kojodjojo, N. Qureshi, M. Koa-Wing, S. Hayat, A. Kyriacou, B. Sandler, A. Sohaib, I. Wright, D. Davies, Z. Whinnett, N. S. Peters, P. Kanagaratnam, and P. Lim, "Noninvasive electrocardiographic mapping to guide ablation of outflow tract ventricular arrhythmias," *Heart Rhythm J.*, vol. 11, no. 4, pp. 587–594, Apr. 2014.
- [32] F. Atienza, A. Climent, M. Guillem, and O. Berenfeld, "Frontiers in noninvasive cardiac mapping rotors in atrial fibrillation-body surface frequency-phase mapping," *Card. Electrophysiol. Clin.*, vol. 7, no. 1, pp. 59–69, Mar. 2015.

- [33] D. Mangano, E. Layug, A. Wallace, and I. Tateo, "Effect of atenolol on mortality and cardiovascular morbidity after noncardiac surgery," *New Eng. J. Med.*, vol. 335, no. 23, pp. 1713–1719, May 1996.
- [34] M. Merri, A. Moss, J. Benhorin, E. Locati, M. Alberti, and F. Badilini, "Relation between ventricular repolarization duration and cardiac cycle length during 24-hour holter recordings. Findings in normal patients and patients with long QT syndrome," *Circ.*, vol. 85, no. 5, pp. 1816–21, May 1992.
- [35] I. C. Van Gelder, V. E. Hagens, H. A. Bosker, J. H. Kingma, O. Kamp, T. Kingma, S. A. Said, J. I. Darmanata, A. J. Timmermans, J. G. Tijssen, and H. J. Crijns, "A comparison of rate control and rhythm control in patients with recurrent persistent atrial fibrillation," *New Eng. J. Med.*, vol. 347, no. 23, pp. 1834–1840, Dec. 2002.
- [36] D. Ward and A. Camm, "The current status of ablation of cardiac conduction tissue and ectopic myocardial foci by transvenous electrical discharges," *Clin. Cardiol.*, vol. 9, no. 6, pp. 237–244, Jun. 1986.
- [37] M. Schalij, F. van Ronge, M. Siezenga, and E. van der Velde, "Endocardial activation mapping ventricular tachycardia in patients: First application of a 32-site bipolar mapping electrode catheter," *Circ.*, vol. 98, pp. 2168–2179, Nov. 1998.
- [38] N. Peters, W. Jackman, R. Schilling, and D. Divies, "Human left ventricular endocardial activation mapping using a novel noncontact catheter," *Circ.*, vol. 95, pp. 1658–1660, Mar. 1997.
- [39] Y. Takahashi, M. Hocini, M. D. O'Neill, P. Sanders, M. Rotter, T. Rostock, A. Jonsson, F. Sacher, J. Clementy, P. Jais, and M. Haissaguerre, "Sites of focal atrial activity characterized by endocardial mapping during atrial fibrillation," *J. Am. Coll. Cardiol.*, vol. 47, no. 10, pp. 2005–2012, May 2006.
- [40] R. Ideker, R. Cooper, and K. Walcott, "Comparison of atrial ventricular fibrillation and defibrillation," *Pacing Clin. Electrophysiol.*, vol. 17, no. 5 Pt 2, pp. 1034–42, May 1994.
- [41] N. Trayanova, "Defibrillation of the heart: insights into mechanisms from modelling studies," *Exp. Physiol.*, vol. 91, no. 2, pp. 323–337, Mar. 2006.
- [42] G. Ristagno, T. Wang, W. Tang, S. Sun, C. Castillo, and M. H. Weil, "High-energy defibrillation impairs myocyte contractility and intracellular calcium dynamics," *Crit. Care Med.*, vol. 36, no. 11, pp. S422–S427, Nov. 2008.
- [43] R. E. Ideker, P. D. Wolf, C. Alfernness, W. Krassowska, and W. M. Smith, "Current concepts for selecting the location, size and shape of defibrillation electrodes," *PACE*, vol. 14, no. 2 Pt 1, p. 227, Feb. 1991.
- [44] N. Sepulveda, J. Wikswo, and D. Echt, "Finite element analysis of cardiac defibrillation current distributions," *IEEE Trans. Biomed. Eng.*, vol. 37, pp. 354–365, Apr. 1990.
- [45] D. B. Jorgenson, P. H. Schimpf, I. Shen, G. Johnson, G. H. Bardy, D. R. Haynor, and Y. Kim, "Predicting cardiothoracic voltages during high energy shocks: Methodology and comparison of experimental to finite element model data," *IEEE Trans. Biomed. Eng.*, vol. 42, no. 6, p. 559, Jun. 1995.

- [46] M. Jolley, J. Stinstra, S. Pieper, R. MacLeod, D. Brooks, F. Cecchin, and J. Triedman, "A computer modeling tool for comparing novel ICD electrode orientations in children and adults," *Heart Rhythm J.*, vol. 5, no. 4, pp. 565–572, Apr. 2008.
- [47] L. Rantner, F. Vadakkumpadan, P. Spevak, J. Crosson, and N. Trayanova, "Placement of implantable cardioverter-defibrillators in paediatric and congenital heart defect patients: A pipeline for model generation and simulation prediction of optimal configurations," *J. Physiol.*, vol. 591, no. Pt 17, pp. 4321–4334, Sep. 2013.
- [48] I. Efimov and C. M. Ripplinger, "Virtual electrode hypothesis of defibrillation," *Heart Rhythm J.*, vol. 3, no. 9, pp. 1100–1102, Aug. 2006. [Online]. Available: <https://doi.org/10.1016/j.hrthm.2006.03.005>
- [49] P. A. Guse, K. M. Kavanagh, C. A. Alferness, P. D. Wolf, D. Rollins, J. Hagler, W. M. Smith, and R. E. Ideker, "Defibrillation with low voltage using a left ventricular catheter and four cutaneous patch electrodes in dogs," *Pacing Clin. Electrophysiol.*, vol. 14, no. 3, pp. 443–451, Mar. 1991.
- [50] G. H. Bardy, W. M. Smith, M. A. Hood, I. G. Crozier, I. C. Melton, L. Jordaeans, D. Theuns, R. E. Park, D. J. Wright, D. T. Connelly, S. P. Fynn, F. D. Murgatroyd, J. Sperzel, J. Neuzner, S. G. Spitzer, A. V. Ardashev, A. Oduro, L. Boersma, A. H. Maass, I. C. V. Gelder, A. A. Wilde, P. F. van Dessel, R. E. Knops, C. S. Barr, P. Lupo, R. Cappato, and A. A. Grace, "An entirely subcutaneous implantable cardioverter defibrillator," *New Eng. J. Med.*, vol. 363, no. 1, pp. 36–44, Jul. 2010.
- [51] C. Johnson, *Computational Methods and Software for Bioelectric Field Problems*, 4th ed. Boca Raton, FL, USA: CRC Press, 2015, vol. 1, ch. 43, pp. 1–28. [Online]. Available: <http://www.sci.utah.edu/publications/Joh2015c/ComputationalMethodsandSoftwareforBioelectricFieldProblems.pdf>
- [52] C. Johnson, "Computational and numerical methods for bioelectric field problems," *Crit. Rev. in BioMed. Eng.*, vol. 25, no. 1, pp. 1–81, 1997. [Online]. Available: <http://www.sci.utah.edu/publications/crj97/Crit-Rev-BE-Johnson97.pdf>
- [53] C. Johnson, R. MacLeod, and M. Matheson, "Computational medicine: Bioelectric field problems," *IEEE Computer*, vol. 26, no. 26, pp. 59–67, Oct. 1993.
- [54] R. Barr, T. Pilkington, J. Boineau, and M. Spach, "Determining surface potentials from current dipoles, with application to electrocardiography," *IEEE Trans. Biomed. Eng.*, vol. 13, pp. 88–92, Apr. 1966.
- [55] D. Cohen and L. Chandler, "Measurements and simplified interpretation of magnetocardiograms from humans," *Circ.*, vol. 3, pp. 395–402, Mar. 1969.
- [56] D. Barth, C. Baumgartner, and W. Sutherling, "Neuromagnetic field modeling of multiple brain regions producing interictal spikes in human epilepsy," *Electroencephalogr. Clin. Neurophysiol.*, vol. 73, no. 5, pp. 389–402, Nov. 1989.
- [57] M. Lorange and R. Gulrajani, "A computer heart model incorporating anisotropic propagation," *J. Electrocardiol.*, vol. 26, no. 4, pp. 245–261, Oct. 1993.
- [58] P. Colli Franzone, L. Guerri, and C. Viganotti, "Oblique dipole layer potentials applied to electrocardiology," *J. Math. Biology*, vol. 17, no. 1, pp. 93–124, May 1983.

- [59] R. Barr, M. Ramsey, and M. Spach, "Relating epicardial to body surface potential distributions by means of transfer coefficients based on geometry measurements," *IEEE Trans. Biomed. Eng.*, vol. 24, pp. 1–11, Jan. 1977.
- [60] R. Gulrajani, "The forward and inverse problems of electrocardiography," *EMBS Mag.*, vol. 17, no. 5, pp. 84–101, Sep./Oct. 1998.
- [61] R. Plonsey and A. van Oosterom, "Implications of macroscopic source strength on cardiac cellular activation models," *J. Electrocardiol.*, vol. 24, pp. 99–112, Apr. 1991.
- [62] R. Plonsey and R. Barr, "Mathematical modeling of electrical activity of the heart," *J. Electrocardiol.*, vol. 20, pp. 219–226, Jul. 1987.
- [63] M. Ramsey, R. C. Barr, and M. S. Spach, "Comparison of measured torso potentials with those simulated from epicardial potentials for ventricular depolarization and repolarization in the intact dog," *Circ. Res.*, vol. 41, no. 5, pp. 660–672, Nov. 1977.
- [64] L. R. Bear, L. K. Cheng, I. J. LeGrice, G. B. Sands, N. A. Lever, D. J. Paterson, and B. H. Smaill, "The forward problem of electrocardiography: Is it solved?" *Circ. Arrhythm. Electrophysiol.*, vol. 8, no. 3, pp. 677–684, Jun. 2015. [Online]. Available: <https://www.ahajournals.org/doi/10.1161/CIRCEP.114.001573>
- [65] M. J. Cluitmans, M. M. de Jong, P. G. Volders, R. L. Peeters, and R. L. Westra, "Physiology-based regularization improves noninvasive reconstruction and localization of cardiac electrical activity," in *Comp. in Cardiol. Conf. (CinC)*, 2014, vol. 41, 2014, pp. 1–4.
- [66] H. Burger and J. van Milaan, "Heart-vector and leads. Part III: Geometrical representation," *Br. Heart J.*, vol. 10, pp. 229–33, Oct. 1948.
- [67] Y. Nagata, "The electrocardiographic leads for telemetering as evaluated from the view point of the transfer impedance vector," *Jap. Heart J.*, vol. 11, no. 2, pp. 183–194, Mar. 1970.
- [68] B. Taccardi, R. Lux, P. R. Ershler, R. MacLeod, and Y. Vyhmeister, "Effect of myocardial anisotropy on the body surface potential distributions," in *Proc. of the Intl. Cong. on Electrocardiol., XXth Ann. Meeting*, P. MacFarlane, Ed., 1993, p. abstract.
- [69] R. MacLeod and D. Brooks, "Validation approaches for electrocardiographic inverse problems," in *Computational Inverse Problems in Electrocardiography*, P. Johnston, Ed. Ashurst, UK: WIT Press, 2001, pp. 229–268.
- [70] C. Ramanathan and Y. Rudy, "Electrocardiographic imaging: I. effect of torso inhomogeneities on body surface electrocardiographic potentials," *J. Cardiovasc. Electrophysiol.*, vol. 12, pp. 229–240, Feb. 2001.
- [71] C. Ramanathan and Y. Rudy, "Electrocardiographic imaging: II. effect of torso inhomogeneities on epicardial surface electrocardiographic potentials," *J. Cardiovasc. Electrophysiol.*, vol. 12, pp. 241–252, Feb. 2001.
- [72] S. Shome and R. MacLeod, "Simultaneous high-resolution electrical imaging of endocardial, epicardial and torso-tank surfaces under varying cardiac metabolic load

- and coronary flow," in *Functional Imaging and Modeling of the Heart*, ser. Lecture Notes in Computer Science 4466. Berlin, Heidelberg, Germany: Springer-Verlag, 2007, pp. 320–329.
- [73] B. Soucy, R. Gulrajani, and R. Cardinal, "Inverse epicardial potential solutions with an isolated heart preparation," in *Proc. IEEE EMBS 11th Ann. Intl. Conf.* Seattle, WA, USA: IEEE Press, 1989, pp. 193–194.
 - [74] M. Zabel, S. Portnoy, and M. Franz, "Electrocardiographic indexes of dispersion of ventricular repolarization: An isolated heart validation study," *J. Am. Coll. Cardiol.*, vol. 25, pp. 746–752, Mar. 1995.
 - [75] J. L. Sapp, F. Dawoud, J. C. Clements, and B. M. Horáček, "Inverse solution mapping of epicardial potentials: Quantitative comparison with epicardial contact mapping," *Circ. Arrhythm. Electrophysiol.*, vol. 5, no. 5, pp. 1001–1009, Oct. 2012. [Online]. Available: <http://circep.ahajournals.org/content/5/5/1001>
 - [76] R. MacLeod, Q. Ni, B. Punske, P. Ershler, B. Yilmaz, and B. Taccardi., "Effects of heart position on the body-surface ECG," *J. Electrocardiol.*, vol. 33, no. (supp), pp. 229–238, Feb. 2000.
 - [77] S. Seigneur, T. Teche, R. Roth, and L. Reid, "Sensitivity of complex urban air quality model to input data," *J. of App. Meteorol.*, vol. 20, pp. 157–177, Sep. 1981.
 - [78] D. Swenson, S. Geneser, J. Stinstra, R. Kirby, and R. MacLeod, "Cardiac position sensitivity study in the electrocardiographic forward problem using stochastic collocation and BEM," *Annal. Biomed. Eng.*, vol. 30, no. 12, pp. 2900–2910, Dec. 2011.
 - [79] D. Xiu and J. Hesthaven, "High-order collocation methods for differential equations with random inputs," *SIAM J. on Sci. Comp.*, vol. 27, no. 3, pp. 1118–1139, Jul. 2005.
 - [80] D. Xiu and J. Shen, "An efficient spectral method for acoustic scattering from rough surfaces," *Comm. in Comp.*, vol. 2, no. 1, pp. 54–72, Feb. 2007.
 - [81] M. Spach, R. Barr, C. Lanning, and P. Tucek, "Origin of body surface QRS and T-wave potentials from epicardial potential distributions in the intact chimpanzee," *Circ.*, vol. 55, pp. 268–278, Feb. 1977.
 - [82] M. Spach and R. Barr, "Origin of epicardial ST-T wave potentials in the intact dog," *Adv. Cardiol.*, vol. 21, pp. 15–18, Jun. 1978.
 - [83] P. Stanley, T. Pilkington, and M. Morrow, "The effects of thoracic inhomogeneities on the relationship between epicardial and torso potentials," *IEEE Trans. Biomed. Eng.*, vol. 33, pp. 273–284, Mar. 1986.
 - [84] J. Burnes, B. Taccardi, R. MacLeod, and Y. Rudy, "Noninvasive electrocardiographic imaging of electrophysiologically abnormal substrates in infarcted hearts: A model study," *Circ.*, vol. 101, pp. 533–540, Feb. 2000.
 - [85] R. MacLeod, R. Lux, and B. Taccardi, "A possible mechanism for electrocardiographically silent changes in cardiac repolarization," *J. Electrocardiol.*, vol. 30, no. Suppl, pp. 114–121, Apr. 1997.

- [86] R. MacLeod, Q. Ni, and B. Taccardi, "Modeling cardiac bioelectricity in realistic volumes: How real is real?" in *Einthoven 2002*, M. Schalij, M. Janse, A. van Oosterom, H. Wellens, and E. van der Wall, Eds. Leiden, The Netherlands: Einthoven Society, 2002, pp. 45–56.
- [87] W. H. W. Schulze, D. Potyagaylo, R. Schimpf, T. Papavassiliu, E. Tüluinen, B. Rudic, V. Liebe, C. Doesch, J. Trächtler, M. Borggrefe, and O. Dössel, "A simulation dataset for ECG imaging of paced beats with models for transmural, endo-and epicardial and pericardial source imaging," in *First Meeting of the Consortium for EGI Imaging*, 03 2015, p. 1. [Online]. Available: <http://doi.org/10.13140/RG.2.1.1946.8568>
- [88] J. Zhang, F. Sacher, K. Hoffmayer, T. O'Hara, M. Strom, P. Cuculich, J. Silva, D. Cooper, M. Faddis, M. Hocini, M. Haissaguerre, M. Scheinman, and Y. Rudy, "Cardiac electrophysiologic substrate underlying the ECG phenotype and electrogram abnormalities in Brugada syndrome patients," *Circ.*, vol. 131, no. 22, pp. 1950–9, Jun. 2015.
- [89] P. Cuculich, Y. Wang, B. Lindsay, R. Vijayakumar, and Y. Rudy, "Noninvasive real-time mapping of an incomplete pulmonary vein isolation using electrocardiographic imaging," *Heart Rhythm J.*, vol. 7, no. 9, pp. 1316–1317, Sep. 2010.
- [90] P. Cuculich, Y. Wang, B. Lindsay, M. Faddis, R. Schuessler, J. D. RJ, L. Li, and Y. Rudy, "Noninvasive characterization of epicardial activation in humans with diverse atrial fibrillation patterns," *Circ.*, vol. 122, no. 14, pp. 1364–1372, Oct. 2010.
- [91] R. Ghanem, C. Ramanathan, P. Jia, and Y. Rudy, "Heart-surface reconstruction and ECG electrodes localization using fluoroscopy, epipolar geometry and stereovision: Application to noninvasive imaging of cardiac electrical activity," *j-TMI*, vol. 22, no. 10, pp. 1307–1318, Oct. 2003.
- [92] R. Ghanem, P. Jia, C. Ramanathan, K. Ryu, A. Markowitz, and Y. Rudy, "Noninvasive electrocardiographic imaging (ECGI): Comparison to intraoperative mapping in patients," *Heart Rhythm J.*, vol. 2, no. 4, pp. 339–354, Apr. 2005.
- [93] A. Intini, R. Goldstein, P. Jia, C. Ramanathan, K. Ryu, B. Giannattasio, R. Gilkeson, B. Stambler, P. Brugada, W. Stevenson, Y. Rudy, and A. Waldo, "Electrocardiographic imaging (ECGI), a novel diagnostic modality used for mapping of focal left ventricular tachycardia in a young athlete," *Heart Rhythm J.*, vol. 2, no. 11, pp. 1250–1252, Nov. 2005.
- [94] P. M. Boyle, J. B. Hakim, S. Zahid, W. H. Franceschi, M. J. Murphy, A. Prakosa, K. N. Aronis, T. Zghaib, M. Balouch, E. G. Ipek, J. Chrispin, R. D. Berger, H. Ashikaga, J. E. Marine, H. Calkins, S. Nazarian, D. D. Spragg, and N. A. Trayanova, "The fibrotic substrate in persistent atrial fibrillation patients: Comparison between predictions from computational modeling and measurements from focal impulse and rotor mapping," *Front. Physiol.*, vol. 9, p. 1151, Aug. 2018.
- [95] N. A. Trayanova, P. M. Boyle, and P. P. Nikolov, "Personalized imaging and modeling strategies for arrhythmia prevention and therapy," *Current Opinion in Biomed. Eng.*, vol. 5, pp. 21 – 28, Mar. 2018. [Online]. Available: <http://www.sciencedirect.com/science/article/pii/S2468451117300922>

- [96] F. Claydon, T. Pilkington, A. Tang, M. Morrow, and R. Ideker, "A volume conductor model of the thorax for the study of defibrillation fields," *IEEE Trans. Biomed. Eng.*, vol. 35, pp. 981–992, Nov. 1988.
- [97] F. Claydon, T. Pilkington, A. Tang, M. Morrow, and R. Ideker, "Comparison of measured and calculated epicardial potentials during transthoracic stimulation," in *IEEE EMBS 10th Ann. Intl. Conf.* New Orleans, Louisiana, USA: IEEE Press, 1988, pp. 206–207.
- [98] J. P. Rosborough, D. C. Deno, R. G. Walker, and J. T. Niemann, "A percutaneous catheter-based system for the measurement of potential gradients applicable to the study of transthoracic defibrillation," *PACE*, vol. 30, no. 2, pp. 166–174, Feb. 2007. [Online]. Available: <http://dx.doi.org/10.1111/j.1540-8159.2007.00645.x>
- [99] J. J. Mastrotaoaro, T. C. Pilkington, R. E. Ideker, and H. Z. Massoud, "Thin-film multielectrode arrays for potential gradient measurements in the heart," in *Proc. IEEE EMBS 10th Ann. Intl. Conf.*, 1988, p. 90.
- [100] B. Rodriguez, L. Li, J. Eason, I. Efimov, and N. Trayanova, "Differences between left and right ventricular chamber geometry affect cardiac vulnerability to electric shocks," *Circ. Res.*, vol. 97, no. 2, pp. 168–175, Jul. 2005.
- [101] M. J. Bishop, B. Rodriguez, F. Qu, I. R. Efimov, D. J. Gavaghan, and N. A. Trayanova, "The role of photon scattering in optical signal distortion during arrhythmia and defibrillation," *Biophys. J.*, vol. 93, no. 10, pp. 3714–3726, Nov. 2007. [Online]. Available: <http://www.ncbi.nlm.nih.gov/pmc/articles/PMC2072057/>
- [102] B. J. Boukens, S. R. Gutbrod, and I. R. Efimov, "Imaging of ventricular fibrillation and defibrillation: The virtual electrode hypothesis," *Adv. Exp. Med. Biol.*, vol. 859, pp. 343–365, Jan. 2015.
- [103] P. S. Chen, N. Shibata, E. G. Dixon, R. O. Martin, and R. E. Ideker, "Comparison of the defibrillation threshold and the upper limit of ventricular vulnerability," *Circ.*, vol. 73, no. 5, pp. 1022–1028, May 1986. [Online]. Available: <http://circ.ahajournals.org/content/73/5/1022>
- [104] F. E. Marchlinski, B. Flores, J. M. Miller, C. D. Gottlieb, and W. Hargrove, "Relation of the intraoperative defibrillation threshold to successful postoperative defibrillation with an automatic implantable cardioverter defibrillator," *Am. J. Cardiol.*, vol. 62, no. 7, pp. 393–398, Sep. 1988. [Online]. Available: <http://www.sciencedirect.com/science/article/pii/0002914988909654>
- [105] P. S. Chen, G. K. Feld, J. M. Kriett, M. M. Mower, R. Y. Tarazi, R. P. Fleck, C. D. Swerdlow, E. S. Gang, and R. M. Kass, "Relation between upper limit of vulnerability and defibrillation threshold in humans," *Am. Heart J.*, vol. 88, no. 1, pp. 186–192, Jul. 1993. [Online]. Available: <http://circ.ahajournals.org/content/88/1/186>
- [106] C.-P. Lau and N.-S. Lok, "A comparison of transvenous atrial defibrillation of acute and chronic atrial fibrillation and the effect of intravenous sotalol on human atrial defibrillation threshold," *PACE*, vol. 20, no. 10, pp. 2442–2452, Oct. 1997. [Online]. Available: <http://dx.doi.org/10.1111/j.1540-8159.1997.tb06084.x>

CHAPTER 3

REDUCING ERROR IN ECG FORWARD SIMULATIONS WITH IMPROVED SOURCE SAMPLING

This chapter addresses the unresolved error that exists in Electrocardiographic (ECG) forward simulation validation studies and presents the research for the first aim of this dissertation: evaluate the error in ECG forward simulations due to incomplete sampling of the atria and developing sampling strategies to reduce it. The following manuscript was published in September 2018 in the *Frontiers in Physiology - Cardiac Electrophysiology* journal as part of the Electrocardiographic Imaging research topic (*Front. Physiol.* 9:1304, 2018. DOI link: <https://doi.org/10.3389/fphys.2018.01304>). The published version appears here with permission.



Reducing Error in ECG Forward Simulations With Improved Source Sampling

Jess Tate^{1,2*}, Karli Gillette³, Brett Burton^{1,2}, Wilson Good^{1,2}, Brian Zenger^{1,2}, Jaume Coll-Font⁴, Dana Brooks⁵ and Rob MacLeod^{1,2}

¹ Department of Bioengineering, University of Utah, Salt Lake City, UT, United States, ² Scientific Computing and Imaging Institute, University of Utah, Salt Lake City, UT, United States, ³ Institute of Biophysics, Medical University of Graz, Graz, Austria, ⁴ Computational Radiology Lab, Children's Hospital, Boston, MA, United States, ⁵ SPIRAL Group, Department of Electrical and Computer Engineering, Northeastern University, Boston, MA, United States

OPEN ACCESS

Edited by:

Carlos Figueira,
Universidad Rey Juan Carlos, Spain

Reviewed by:

Rob Gourdie,
Medical University of South Carolina,
United States
Jason D. Bayer,
Université de Bordeaux, France

*Correspondence:

Jess Tate
jess@sci.utah.edu

Specialty section:

This article was submitted to
Cardiac Electrophysiology,
a section of the journal
Frontiers in Physiology

Received: 12 June 2018

Accepted: 29 August 2018

Published: 21 September 2018

Citation:

Tate J, Gillette K, Burton B, Good W, Zenger B, Coll-Font J, Brooks D and MacLeod R (2018) Reducing Error in ECG Forward Simulations With Improved Source Sampling. *Front. Physiol.* 9:1304.
doi: 10.3389/fphys.2018.01304

A continuing challenge in validating electrocardiographic imaging (ECGI) is the persistent error in the associated forward problem observed in experimental studies. One possible cause of this error is insufficient representation of the cardiac sources; cardiac source measurements often sample only the ventricular epicardium, ignoring the endocardium and the atria. We hypothesize that measurements that completely cover the pericardial surface are required for accurate forward solutions. In this study, we used simulated and measured cardiac potentials to test the effect of different levels of spatial source sampling on the forward simulation. Not surprisingly, increasing the source sampling over the atria reduced the average error of the forward simulations, but some sampling strategies were more effective than others. Uniform and random distributions of samples across the atrial surface were the most efficient strategies in terms of lowest error with the fewest sampling locations, whereas “single direction” strategies, *i.e.*, adding to the atrioventricular (AV) plane or atrial roof only, were the least efficient. Complete sampling of the atria is needed to eliminate errors from missing cardiac sources, but while high density sampling that covers the entire atria yields the best results, adding as few as 11 electrodes on the atria can significantly reduce these errors. Future validation studies of the ECG forward simulations should use a cardiac source sampling that takes these considerations into account, which will, in turn, improve validation and understanding of ECGI.

Keywords: ECG imaging, ECG forward simulation, cardiac source sampling, epicardial potentials, body-surface potentials

1. INTRODUCTION

Electrocardiographic Imaging (ECGI) is a promising technology for diagnosing and treating cardiac arrhythmias (Pullan et al., 2010; Rudy and Lindsay, 2015). Its goal is to compute some formulation of cardiac sources from known patient torso geometry (typically extracted from medical imaging) and body-surface potential mapping (BSPM) recordings (Barr et al., 1977; Plonsey and Barr, 1987; Plonsey and van Oosterom, 1991; Gulrajani, 1998). This computation is possible by first establishing a model of the ECG from knowledge of cardiac sources and geometry, known as a numerical forward simulation (MacLeod and Buist, 2010) and then inverting this process to solve the associated inverse problem (Pullan et al., 2010). Establishing well-validated

ECG forward simulations is, therefore, critical to developing ECGI as a technology.

The purpose of an ECG forward simulation is to predict the electric potential response through a passive volume conductor, i.e., the torso, from cardiac sources (MacLeod and Buist, 2010). Cardiac sources are represented in the literature in several ways, but the most common and most readily measured method is a surface of potentials surrounding the myocardium (Barr et al., 1977; Messinger-Rapport and Rudy, 1986; Plonsey and Barr, 1987; Plonsey and van Oosterom, 1991; Gulrajani, 1998). Predicting the resulting ECGs requires solving a partial differential equation using numerical techniques, such as boundary or finite element methods (BEM and FEM, respectively) (Johnson et al., 1993; Johnson, 1997, 2015; MacLeod and Buist, 2010).

Despite the existence of well-established methods of the ECG forward simulation, previous validation studies have consistently shown differences that were higher than might be expected between simulated and measured body-surface potentials, such as higher overall error and changes in extrema location (Ramsey et al., 1977; Bear et al., 2015). The ECG forward problem is well behaved, and we have sufficient confidence in all aspects of the simulation and measurement protocols to expect errors well below those reported. This disparity between confidence in the simulation approaches and persistent errors in experimental validation, along with the sensitivity of ECGI to model errors due to its ill-posed nature (Pullan et al., 2010), provides powerful motivation to explore possible explanations.

One as yet unexplored source of error in these studies is insufficient cardiac source representation, i.e., either inadequate coverage or spatial density of coverage of the cardiac sources. For example, many experimental validation studies use an epicardial sock electrode array to record cardiac surface potentials from the animal heart (Ramsey et al., 1977; Stanley et al., 1986; Shome and MacLeod, 2007; Bear et al., 2015). A common limitation of these epicardial socks is that they position electrodes on the ventricles only, ignoring the atria. Not only does such a set up exclude measurement of atrial sources, but some ventricular sources, such as locations either on the apex or at the base of the heart, lack either adequate spatial coverage or stable mechanical contact by sock electrodes. Such conditions are problematic as the mathematical formulation of the ECG forward simulation with potential sources assumes a complete and closed representative surface that is adequately sampled; the compromises driven by practical limitations in experiments suggest that missing sources exist and they could have a significant impact on the predicted potential values on the torso surface (Barr et al., 1977). Our goal was to examine some aspects of this dilemma, using a combination of experimental and numerical approaches.

In addition to experimental studies, we can also use computer simulation to help answer questions about the effect of cardiac sampling on the forward simulation. Simulation methods such as pseudo-bidomain (Vigmond et al., 2003, 2008) and cellular automaton (Schulze et al., 2015) can predict full pericardial potentials in a way that cannot be measured experimentally due to regions of the epicardium being inaccessible to measurement. Using simulated potentials together

with experimentally recorded values provides a more complete evaluation of the effect of pericardial source sampling.

In this study, we tested the impact of cardiac source representation of the atrial region on ECG forward simulations. We hypothesize that, in the context of forward simulations from epicardial potentials, measurements that completely cover the heart are required for accurate prediction of the body-surface potentials. To test this hypothesis, we used simulated and measured cardiac potentials to determine the effect of different levels of sampling on a typical forward simulation pipeline (Burton et al., 2011). Our results support this hypothesis and encourage us to propose some sampling strategies that may minimize error resulting from incomplete sampling of cardiac sources.

2. METHODS

We analyzed the effect of source representation coverage and density of the atrial region of the heart on ECG forward simulations by sampling the cardiac source with a range of strategies, and then used those sources in our ECG forward simulation pipeline. We tested these sampling strategies on three different geometries and source models: (1) simulated epicardial potentials using the CARP (Vigmond et al., 2003, 2008) cardiac propagation modeling software package, (2) a second set of simulations provided in the EDGAR database (Aras et al., 2015) by the Biomedical Engineering team at the Karlsruhe Institute of Technology, KIT (Schulze et al., 2015), and (3) one experimentally recorded dataset from the CardioVascular Research and Training Institute (CVRITI) at the University of Utah using a unique “cage” electrode (Milanic et al., 2014), also available in the EDGAR database (Aras et al., 2015). We then computed ECG forward simulations from subsampled versions of the original sources, which we compared to FEM simulations from our ground truth cardiac potential sources. We also performed experiments in which we recorded source potentials with a ventricular sock and an electrode plaque placed on the atria and used these recorded potentials in our simulation pipeline to compare the predicted body-surface potentials with and without the additional atrial potential sources.

2.1. Datasets

2.1.0.1. CARP Dataset

The set of cardiac potentials generated using the CARP (Vigmond et al., 2003, 2008) modeling software consisted of simulated extracellular potentials using the pseudo-bidomain method (Bishop and Plank, 2011) in an isolated rabbit ventricle model previously described (Deo et al., 2009). The four pacing profiles were sinus rhythm, left ventricle (LV) free wall pacing, right ventricle (RV) free wall pacing, and apical pacing. The heart geometry was then manually registered and scaled to a human torso geometry of dimensions $\sim 36 \times 22 \times 40$ cm, 771 nodes, and an internodal distance of 24.6 mm (MacLeod et al., 1995; Shome and MacLeod, 2007; Milanic et al., 2014). An ellipsoidal cap was placed on a mesh of the epicardial surface of the ventricles (to replicate a typical sock array) by fitting a precomputed ellipsoid mesh to the points near the base of

the ventricles and clipping it to cover the open region in the sock. The combination of the sock mesh and the ellipsoid cap formed a pericardial mesh of dimensions $\sim 6 \times 6 \times 7$ cm with 498 nodes with an average internodal spacing of 5.3 mm. To compute the potentials on both the cap of the mesh and the torso surface, we used the previously computed ventricular surface extracellular potentials from both the endocardial and epicardial surfaces and the FEM approach in SCIRun (<http://scirun.org>, Parker et al., 1997; MacLeod et al., 2004) with the Forward/Inverse Toolkit (Burton et al., 2011). This calculation consisted of generating a tetrahedral mesh for the region between the heart and torso surface, including the vertex locations for the pericardial mesh with the ellipsoid cap. Then for each time step, the endocardial and epicardial potentials were used to set the Dirichlet boundary conditions along the cardiac surface and Neumann boundary conditions on the torso surface to solve for the potentials distribution throughout the homogeneous torso volume. The potentials were extracted at the torso and pericardial surfaces to use in the subsequent sampling tests described below.

2.1.0.2. KIT Dataset

The KIT geometric model of a single heart and torso geometry was generated from a patient scan (Schulze et al., 2015) and is available on the EDGAR database (<http://edgar.sci.utah.edu>, Aras et al., 2015). The torso surface had the dimensions $\sim 47 \times 30 \times 35$ cm, 2002 nodes, and an internodal distance of 19.0 mm. The cardiac potentials computed from this model, also available from EDGAR, consisted of four activation profiles: septal, RV free wall, LV free wall, and apical pacing. In contrast to the pseudo-bidomain approach using CARP, the KIT investigators computed cardiac potentials using a cellular automaton approach for the activation sequence, and calculated first the transmembrane potentials based on the activation times with a monodomain simulation and the ten Tusscher electrophysiological model (ten Tusscher and Panfilov, 2006; Loewe et al., 2015) and then the extracellular potentials using the bidomain approach (Schulze et al., 2015). As in the CARP dataset, we added an ellipsoidal cap on a mesh of the epicardium to form a pericardial mesh of dimensions $\sim 13 \times 19 \times 10$ cm with 532 nodes with an average spacing of 9.4 mm. We used the ventricular surface extracellular potentials from both the endocardial and epicardial surfaces to simulate the potential values on the ellipsoidal cap and the torso surface using FEM, as described for the CARP dataset.

2.1.0.3. Utah Cage Dataset

The cage dataset available in EDGAR consists of measurements from our group using a perfused, isolated canine heart preparation placed inside a cylindrical cage of dimensions $\sim 10 \times 10 \times 15$ cm (600 electrodes, with average spacing of 10.7 mm) within a human torso-shaped electrolytic tank (dimensions $\sim 36 \times 22 \times 40$ cm) instrumented with 192 surface electrodes (average spacing of 40 mm MacLeod et al., 1995; Shome and MacLeod, 2007; Milanic et al., 2014). For this study, we used recorded signals from three activation profiles: sinus rhythm and left and right ventricular pacing. The geometric model and measured potentials are all available on the EDGAR database. We used the cage electrodes as a pericardial source and compared

forward computed and measured torso-tank surface potentials. We also generated simulated ground truth torso potentials from the recorded cage potentials using FEM, just as for the other two datasets.

2.2. Sampling Strategies

The main goal of the study was to evaluate the effect of source representation in the forward solution by varying coverage and sampling density of the signals representing that source. We used five different incremental sampling strategies with each of the datasets to analyze the specific effect of atrial sampling on the simulated ECG, as shown in **Figure 1**. Sampling locations were added to the atria in an increasing fashion: (1) starting near the atrioventricular (AV) plane (closest to the ventricular sock) and moving toward the atrial roof, (2) from the atrial roof to the AV plane, (3) combining sites from the AV plane and atrial roof, (4) adding sites in a uniformly distributed order, and (5) adding sites in a randomly distributed order. The sampling locations were added in nine iterations for the KIT dataset, seven for the CARP dataset, and seven for the cage dataset.

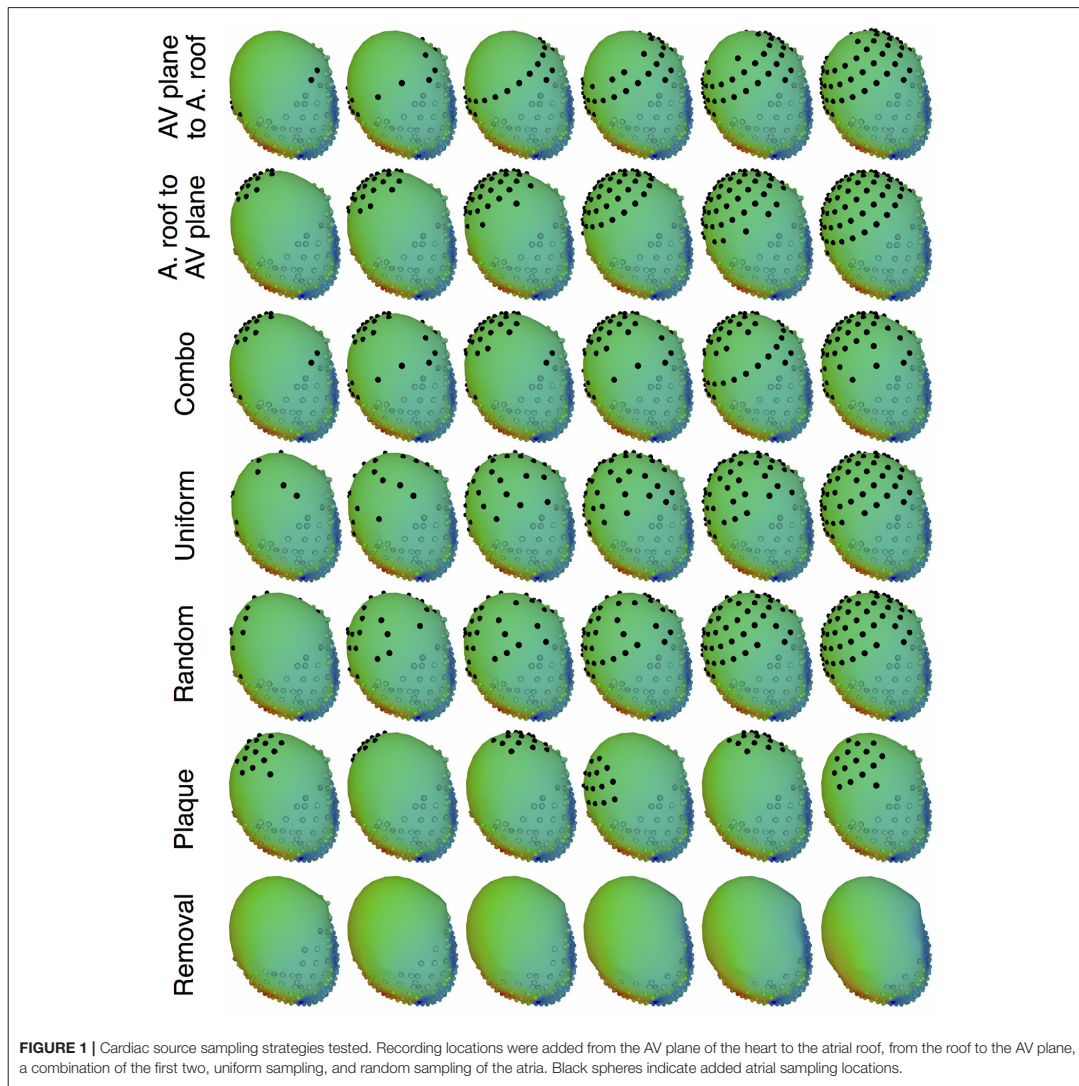
In addition to testing a variable number of added electrodes to the atria, we also tested the effect of adding a cluster of electrodes, similar to a plaque electrode array, in a variety of different locations (**Figure 1**): 22 for the KIT dataset, 34 for the CARP dataset, and 72 for the cage datasets. The simulated plaque was generated by picking the nearest electrodes to each of the central locations. The number of plaque electrodes match the number of electrodes added in each iteration explained above, i.e., 11 for the KIT dataset, 15 for the CARP dataset, and 40 for the cage datasets.

In addition to testing the effect of missing atrial source samples, this study also evaluated the effect of missing ventricular source samples. To test this, source samples were incrementally removed from the basal region of the ventricles (**Figure 1**). Sampling locations were removed in eight iterations for the KIT dataset, six for the CARP dataset, and six for the cage datasets.

2.3. ECG Forward Simulation Pipeline

To simulate the body surface potentials from pericardial surface potentials with various sampling strategies, we first interpolated values from the sampled cardiac surface mesh to the entire cardiac surface and then simulated the torso surface potentials. For the interpolation step, we used Laplacian interpolation (Oostendorp et al., 1989) to estimate the values missing due to undersampling and for the forward simulation we used the BEM, as implemented in SCIRun (Parker et al., 1997; MacLeod et al., 2004) with the Forward/Inverse toolkit (Burton et al., 2011). Similar to the simulations and experiments that provided the ground truth data, the torso was modeled as homogeneous outside the heart.

We compared simulated torso potentials with those from the ground truth data using several standard approaches. We first visually compared potential maps of the results during ventricular activation, identify similarities of the main features of activation. The quantitative comparisons that followed consisted of three standard error metrics, root mean square error (\bar{E}),



relative root mean squared error ($rRMSE$), and correlation (ρ), defined as follows:

$$\bar{E} = \frac{\|\Phi_{gt} - \Phi_s\|}{\sqrt{n}} \quad (1)$$

$$rRMSE = \frac{\|\Phi_{gt} - \Phi_s\|}{\|\Phi_{gt}\|} \quad (2)$$

$$\rho = \frac{\Phi_{gt}^T \Phi_s}{\|\Phi_{gt}\| \|\Phi_s\|}, \quad (3)$$

where Φ_{gt} is a vector of the ground truth BSPM values, Φ_s is a vector of the associated simulated BSPMs, and n is the number of body surface electrodes.

2.4. Validation Experiments

With data acquired in experiments, we tested the sampling strategy of placing a regularly spaced array of electrodes on the atria to validate the prediction of our hypothesis. In an *in situ* open-chest preparation (Aras, 2015; Aras et al., 2016), we placed a cardiac sock with 247 electrodes

around the ventricles and a plaque electrode array with 24 electrodes fixed to the atria on an accessible anterior epicardial region near the AV plane. With the electrodes in place, we recorded electrograms in sinus rhythm and as the heart developed ventricular tachycardia through the duration of the experiments.

Generating datasets for validation required the electrograms from the experiments be placed inside a complete geometric model of the torso. At the end of the experiments, we used a manual digitizer (Microscribe, Solution Technologies, Inc.) to capture the locations of anatomically distinct landmarks. We identified correspondance points from a previously generated geometric model of a human thorax, resulting in two meshes of the heart surfaces with a set of corresponding spatial reference points. These meshes were then registered using a combination of the RANSAC (Fischler and Bolles, 1981), Iterative closest point (ICP) (Besl and McKay, 1992), and thin plate spline techniques, followed by any necessary manual adjustments, implemented in MATLAB and SCIRun. To process the electrogram recordings, we isolated representative beats and performed baseline correction and filtering with the default settings in PFEIFER (<https://www.sci.utah.edu/software/pfeifer.html>; Rodenhauser et al., 2018).

The resulting registered meshes and processed cardiac surface recordings served as the input for our ECG forward simulation pipeline. The forward computations of body surface potentials also required closed surfaces, so we integrated the cardiac sock and atrial plaque meshes into an ellipsoidal cap similar to those described in section 2.1. Laplacian interpolation was then used to estimate the missing potential values on the cap. The resulting complete set of cardiac potentials was used in the ECG forward simulation pipeline, as explained in section 2.3. Torso potentials were simulated from cardiac potentials, with and without the additional plaque recordings, and compared using the metrics explained in section 2.3. We compared the resulting metrics to those from the simulated cardiac potentials described above (Figure 1).

2.5. Ethics

All experiments were performed with approval from the Institutional Animal Care and Use Committee at the University of Utah and conform to the Guide for the Care and Use of Laboratory Animals (National Institutes of Health publication No. 85-23).

2.6. Data Availability

Some of the data used in this study (KIT and cage datasets) are available in the EDGAR database (<http://edgar.sci.utah.edu>), as previously noted. The rabbit model used in the CARP dataset was obtained from a third party, and requests for that data should be directed to the CARP software team (Deo et al., 2009). The raw data collected or generated for this study will be made available by the authors, without undue reservation, to any qualified researcher.

3. RESULTS

Removing potentials from the atrial region of the cardiac surface had a significant impact on the computed forward simulations. For all pacing profiles and data sets, the errors in computed body-surface potentials increased when atrial samples were omitted. Furthermore, the errors grew monotonically with reduced numbers of atrial sample sites. Our experimentally recorded data also produced similar effects on the torso surface to those observed with the simulated data.

Figures 2, 3 show representative tracings of the various metrics over the course of ventricular activation with and without atrial sampling. As shown, the $rRMSE$ tracings of the forward simulation using full pericardial sampling more closely match those of the ground truth. The values of ρ computed from pericardial potentials both with and without atrial sampling were high during most of the time signals, but the minima were reduced or eliminated when we included atrial sampling. The mean ρ without atrial sampling was 0.94 compared to 0.99 with atrial sampling. The $rRMSE$ values showed a similar trend when comparing the forward solution with and without full atrial sampling; the maxima were reduced or eliminated when atrial samples were included. In a few time steps, adding atrial sampling produced a slight increase in $rRMSE$ error, as seen in the KIT (Figure 2) and cage experiment datasets (Figure 3). However, the mean $rRMSE$ was always reduced, with the total mean $rRMSE$ reduced from 0.54 to 0.08. The peak \bar{E} with only ventricular sampling ranged from 0.05 to 0.77 mV, while the peak \bar{E} with full sampling dropped substantially, ranging from 0.01 to 0.19 mV and the peak \bar{E} was reduced for each simulation by a mean of 0.40 mV.

Figure 4 shows the representative cases of the general effect of excluding the potential sources in the atrial region. Comparing the potential maps simulated from only ventricular sources to the ground truth demonstrates qualitative differences, especially in the right anterior region in the CARP and KIT datasets, and over the entire anterior region with the cage datasets. However, there were no qualitative differences in the location of the extrema. The observed differences in the potential maps were reduced when we used full sampling of the atrial surface. The areas with the greatest differences were consistent across all activation profiles, as were the improvements whenever we included atrial sampling.

Increasing the number of recording locations on the atrial surface systematically resulted in reduced error in the forward simulations. Every dataset and activation profile showed a progressive decrease in the peak $rRMSE$, except the apical stimulation of the KIT dataset, which showed an increase in the peak $rRMSE$ from the previous iteration when adding 22 electrodes (from 11) near the AV plane (2.85 from 1.84). The mean peak $rRMSE$ over all datasets and activation profiles decreased from 2.40 to 0.06. The mean $rRMSE$ also progressively decreased as atrial sampling increased in all datasets, with the same exception of the apical stimulation of the KIT dataset, which showed an increase in mean the $rRMSE$ from the previous iteration (0.30 from 0.27) when adding 22 electrodes (from 11). The mean $rRMSE$ decreased from 0.54 to 0.08.

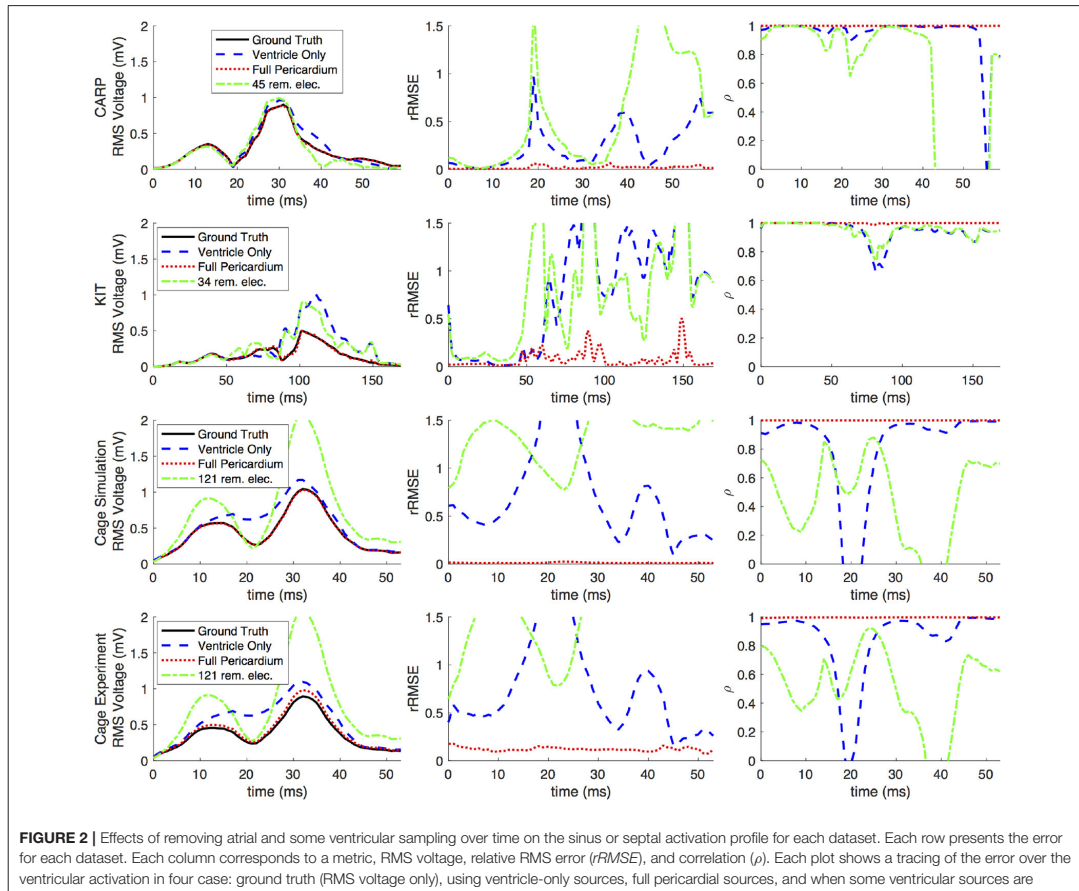
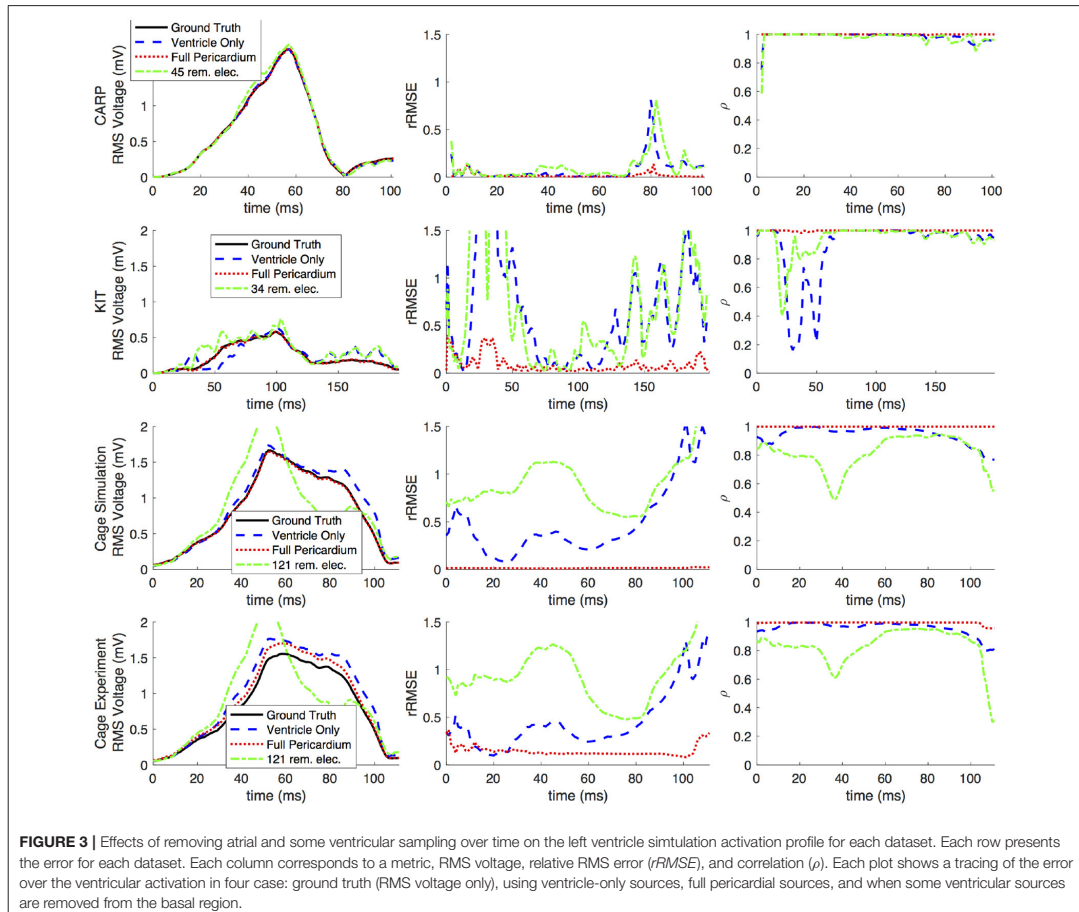


Figure 5 shows the mean peak $rRMSE$ for each dataset. An increase in the number of samples resulted in a near asymptotic reduction in error, so that adding even a few recording locations to the atrial surface provided a significant reduction in error. Every sampling strategy we employed reduced the mean peak $rRMSE$ in a similarly asymptotic relationship, but some strategies approached the minimum error with fewer added electrodes. In general, the single-direction strategies, i.e., applying electrodes only to the atrial roof or the AV plane, were less efficient than the more distributed approaches, i.e., the uniform and random distributions. The approach that combined adding electrodes to both the atrial roof and the AV plane was usually more efficient in reducing the mean peak $rRMSE$ than the single-direction strategies. However, for the CARP dataset, the combined approach was only more efficient than adding electrodes to the atrial roof first. The specific order of most efficient strategies varied based on the dataset and activation

profile. For example, the random distribution showed the greatest reduction of mean peak $rRMSE$ after one iteration for all but the CARP dataset.

Figures 6,7 show how the peak $rRMSE$ and the mean $rRMSE$, respectively, were affected by the different activation profiles when adding a limited number of recording electrodes to the atria with various sampling strategies. In general, the uniform, random, and combined distributions produced lower error for each of the activation profiles than the remaining two strategies. The uniform distribution produced the lowest error of any of the strategies for most of the tested activation profiles. The random distribution had the second lowest error for most activation profiles and the combined approach was third lowest for most activation profiles. Adding recording electrodes to the atrial roof first generally had the highest error of any of sampling strategy, both in terms of the mean and peak $rRMSE$. Though there are some overall trends, there are noticeable anomalies in the



responses to sampling. For instance, the apical stimulation of the CARP dataset had a noticeably higher mean and peak $rRMSE$ for all sampling strategies than the other activation profiles in the same dataset. There are also cases with the CARP dataset in which the AV plane or atrial roof strategies produced lower or similar errors compared to the distributed strategies.

Simulated BSPM results from ventricular epicardial sources with potentials from an additional simulated plaque array placed in various locations showed a consistent reduction in error when compared to the simulations with ventricle-only sources. The mean $rRMSE$ from all the plaque placements was 0.28 and the mean ρ was 0.97, compared to 0.40 and 0.95 with the ventricle-only sampling. The peak \bar{E} was reduced by a mean of 0.45 mV. The placement that resulted in the lowest error was at the roof of the atria, yet there was no other trend to predict the plaque location with lower error.

When source samples were removed from the ventricular sock, there was a general increase in error for most of the QRS complex, as shown in **Figure 2**. By reducing the number of ventricular leads by approximately 45% of the total added on the atria (45, 34, and 121 for the CARP, KIT, and cage datasets, respectively), the mean ρ dropped from 0.94 to 0.84, the mean $rRMSE$ increased from 0.16 to 0.28, and the peak \bar{E} increased by a mean of 0.40 mV.

Progressively reducing the number of ventricular samples also generally increased the error, but not consistently. As shown in **Figure 8**, using the KIT dataset, the mean peak $rRMSE$ decreased initially, but then increased continuously as samples were removed. The CARP dataset showed a increased continuously as samples were removed, with the exception of the final step. Results from the cage datasets showed a similar trend: an increase in mean peak $rRMSE$ with the first set of removed sources, a reduction with the second, and then a fairly consistent mean

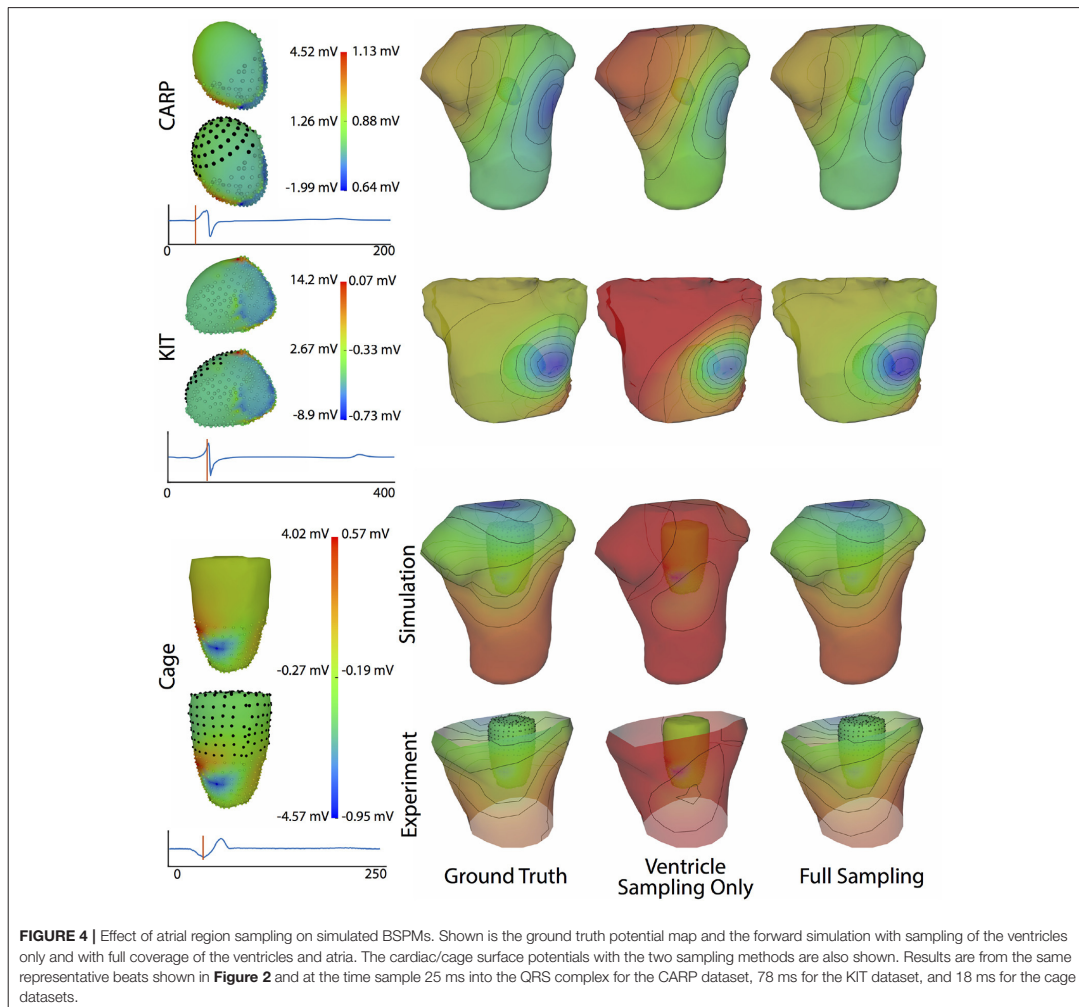


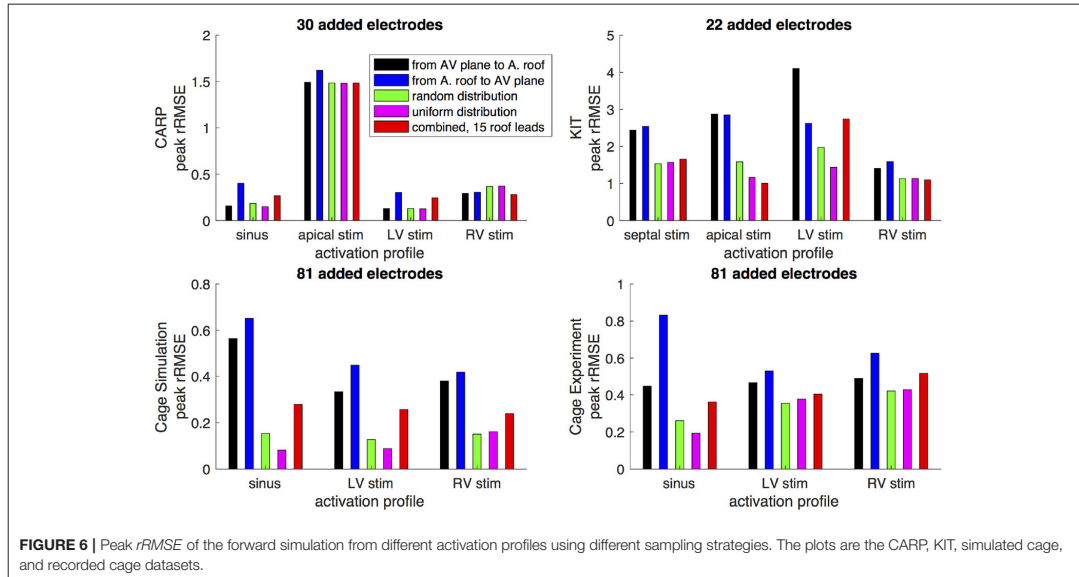
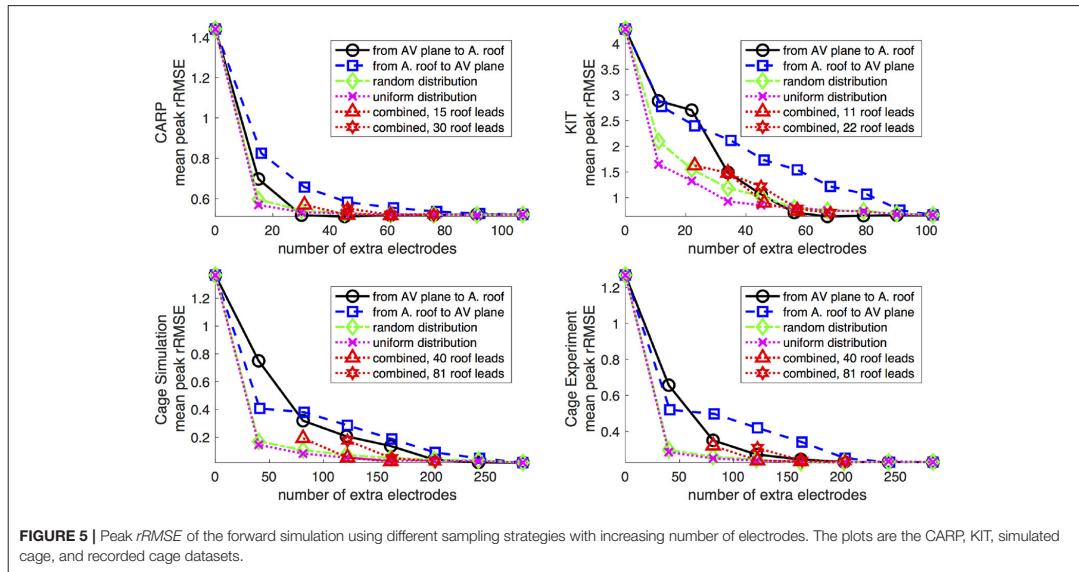
FIGURE 4 | Effect of atrial region sampling on simulated BSPMs. Shown is the ground truth potential map and the forward simulation with sampling of the ventricles only and with full coverage of the ventricles and atria. The cardiac/cage surface potentials with the two sampling methods are also shown. Results are from the same representative beats shown in **Figure 2** and at the time sample 25 ms into the QRS complex for the CARP dataset, 78 ms for the KIT dataset, and 18 ms for the cage datasets.

peak $rRMSE$ for the remaining steps. The plateau mean peak $rRMSE$ remained higher than for the full ventricular sampling for the cage experiment dataset, yet it was slightly lower for the cage simulation dataset. The mean $rRMSE$ gradually increased for the CARP and cage datasets as ventricle samples were removed. However, for the KIT dataset, the mean $rRMSE$ decreased slightly for the first four iterations before dramatically increasing for the final stages. The mean ρ consistently dropped as samples were removed for the CARP dataset and for all but one step in the cage datasets. For the KIT dataset, the mean ρ increased slightly for three iterations, then decreased for the remaining steps.

Figure 9 illustrates representative cases of changes in the predicted BSPMs as ventricle samples were reduced.

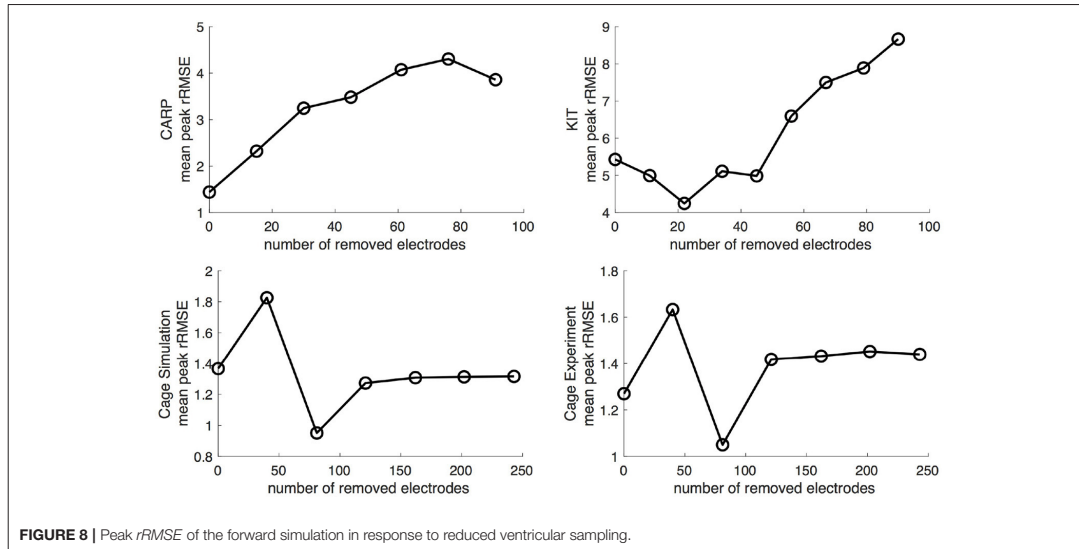
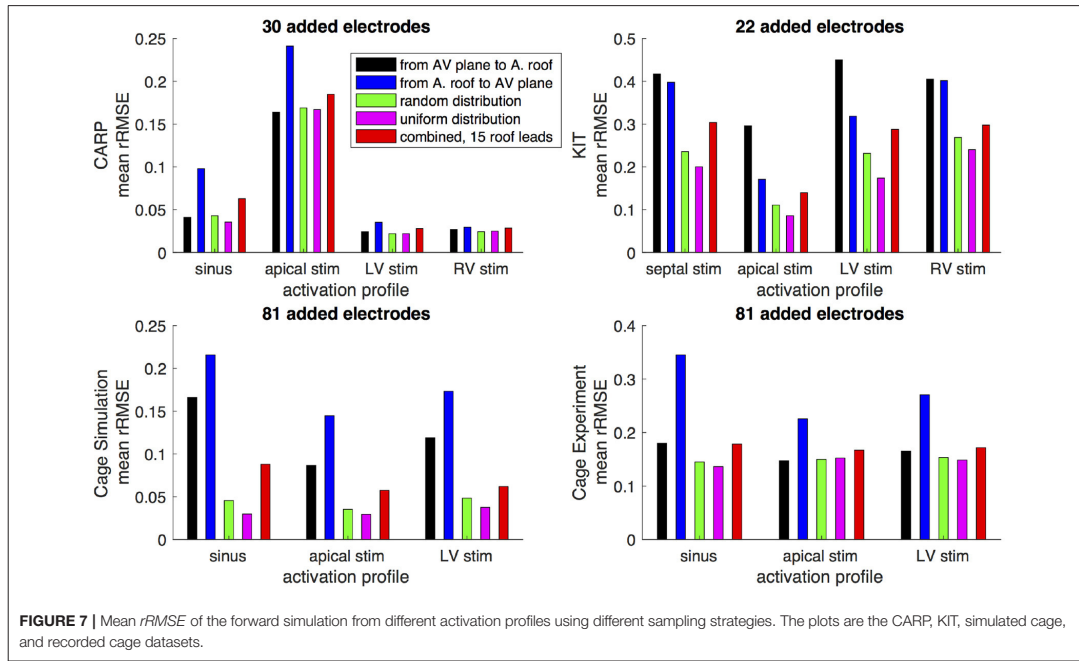
Most notably, removing ventricular sources produced greater qualitative differences than could be generated by removing the atrial sources (**Figure 4**). In each dataset, removing the ventricular sources produced changes in the apparent location of the extrema on the BSPM, or, as in the case of the simulated cage dataset, removed an extremum. Interestingly, although an extremum remained missing from the BSPMs, reducing the sampling further actually otherwise improved the qualitative and quantitative accuracy of the BSPM (**Figures 8, 9**). This result was likely due to removing a more balanced distribution of potentials in the more extreme sampling reduction.

Comparing forward simulations using experimentally recorded cardiac sock potentials, with and without additional



atrial plaque recordings, showed that the using a plaque electrode could alter the accuracy of the forward simulation. The comparison showed a mean $rRMSE$ of 0.21 and a mean ρ of 0.98 across all experiments. **Figure 10** shows a representative comparison over time for each of the experiments. The RMS values of the potential maps showed only minor variations,

and the $rRMSE$ showed some time frames with high error, most notably near the beginning of the QRS complex. The ρ remained high throughout ventricular activation, except at the beginning time instants (**Figure 10**, panels 1 & 2) Repeating the same experiment with simulated results yielded similar results.



Repeating the same experiment with simulated data, i.e., comparing forward simulation using cardiac sock potentials with and without an additional plaque, yielded similar results (**Figure 10**). The mean *rRMSE* and ρ were 0.26 and 0.98,

respectively. The comparison of the BSPM over the time showed different *rRMSE* and ρ profiles compared to the experimental data, in that there peaks or dips near the middle of ventricular activation in addition to near the beginning or the end

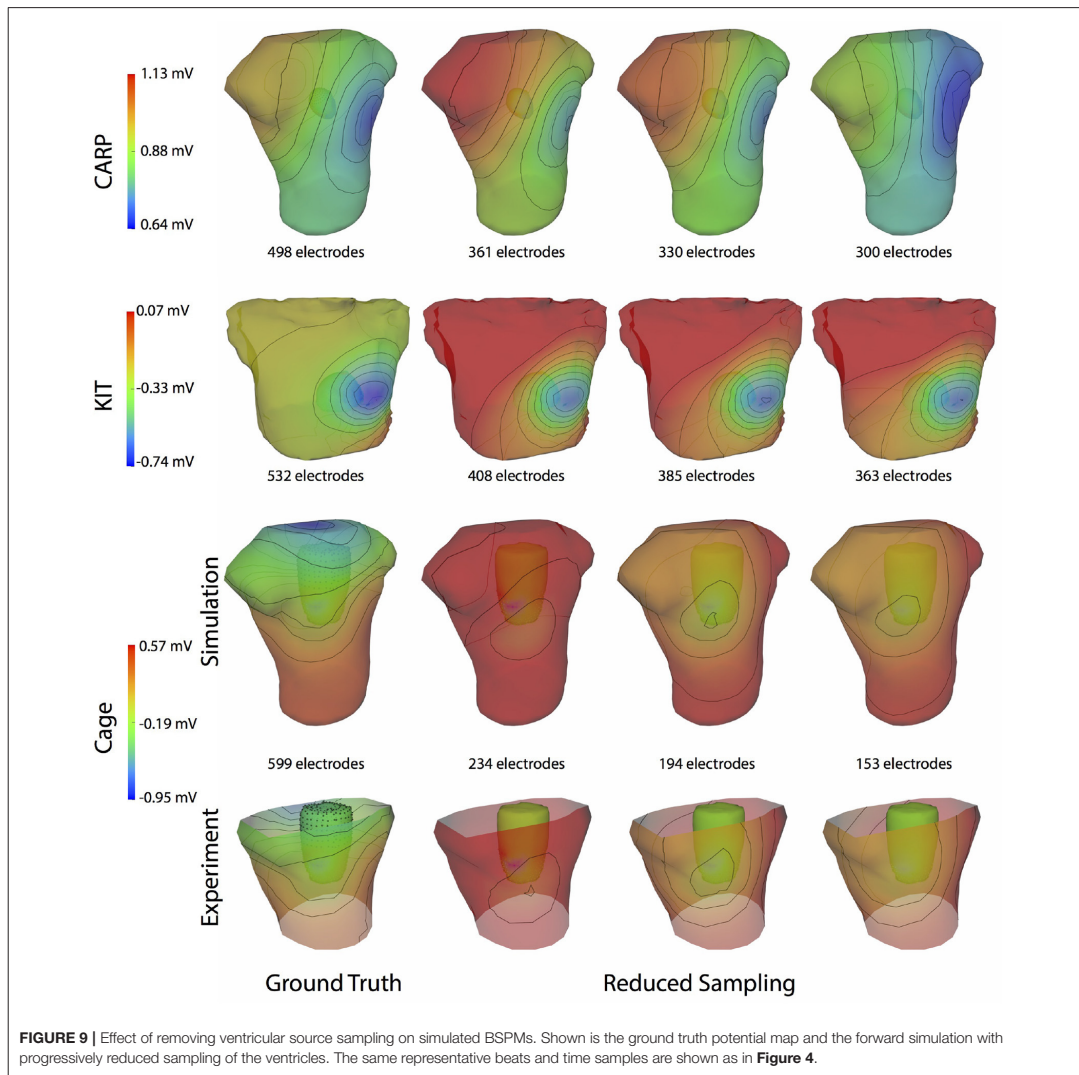


FIGURE 9 | Effect of removing ventricular source sampling on simulated BSPMs. Shown is the ground truth potential map and the forward simulation with progressively reduced sampling of the ventricles. The same representative beats and time samples are shown as in **Figure 4**.

(Figure 10). However, these profiles were similar, yet with a lower amplitude, to the corresponding profiles in Figure 2 comparing the ventricle-only recordings to the ground truth data.

Figure 11 shows the potential maps generated with and without additional recorded electrograms from a plaque based over the roof of the atria. The difference between BSPMs was relatively minor overall, but the region of greatest difference was in the right anterior region. The right posterior region also showed observable differences.

4. DISCUSSION

The goal of this study was to evaluate the hypothesis that complete sampling of the cardiac surface is needed to accurately perform forward simulations of body surface potentials based on pericardial potentials, a hypothesis our results support. Moreover, our findings indicate that the accuracy of the forward simulation depends in subtle ways on the specific atrial sampling strategies. Surprisingly, some strategies are more effective than others even though they contain fewer points, indicating that sampling *location* is as important as sampling *number*. The

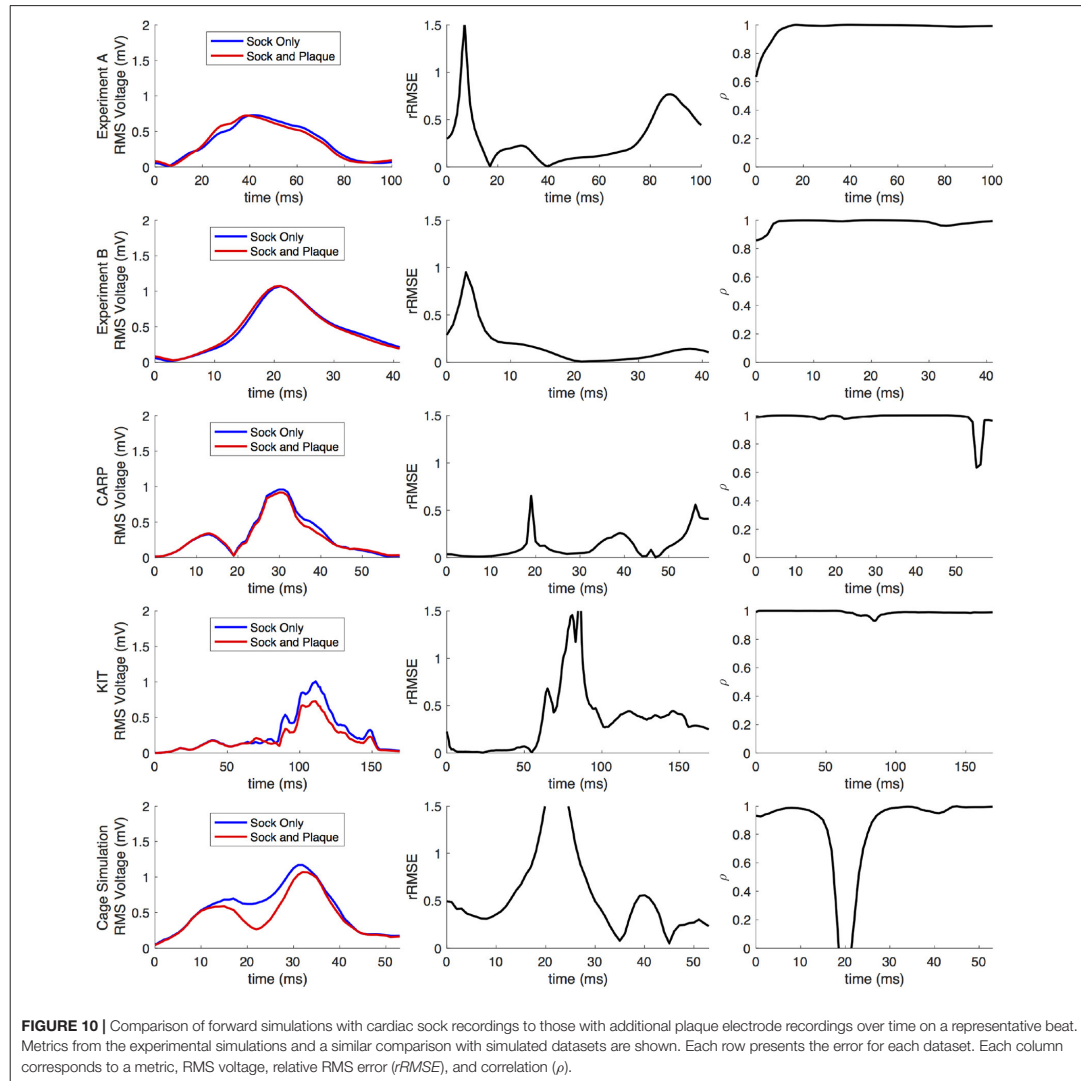


FIGURE 10 | Comparison of forward simulations with cardiac sock recordings to those with additional plaque electrode recordings over time on a representative beat. Metrics from the experimental simulations and a similar comparison with simulated datasets are shown. Each row presents the error for each dataset. Each column corresponds to a metric, RMS voltage, relative RMS error ($rRMSE$), and correlation (ρ).

results of this study could serve as guidance when carrying out simulations or animal and human experiments to validate electrocardiographic imaging approaches and may even impact the ECGI strategy for dealing with missing samples.

The motivation for the study came from reports and our own observations that forward simulations with ventricular pericardial sources often produced errors that exceed anticipated levels based on the relatively well-posed nature of the electrocardiographic forward problem (Ramsey et al., 1977; Bear et al., 2015). Previous, unreported results

from our group based on studies with torso-tank phantoms (Shome and MacLeod, 2007) also produced a similar level of error.

The results of this study indicate that, in general, any source sampling added to the atrial region will reduce the error between the measured potentials and computed forward simulation. Even a relatively small number, e.g., 11–40, of additional source samples produced a reduction in the overall error (Figures 5–7) across every dataset and with every sampling strategy. Similarly, simulations that included measurements from atrial plaque

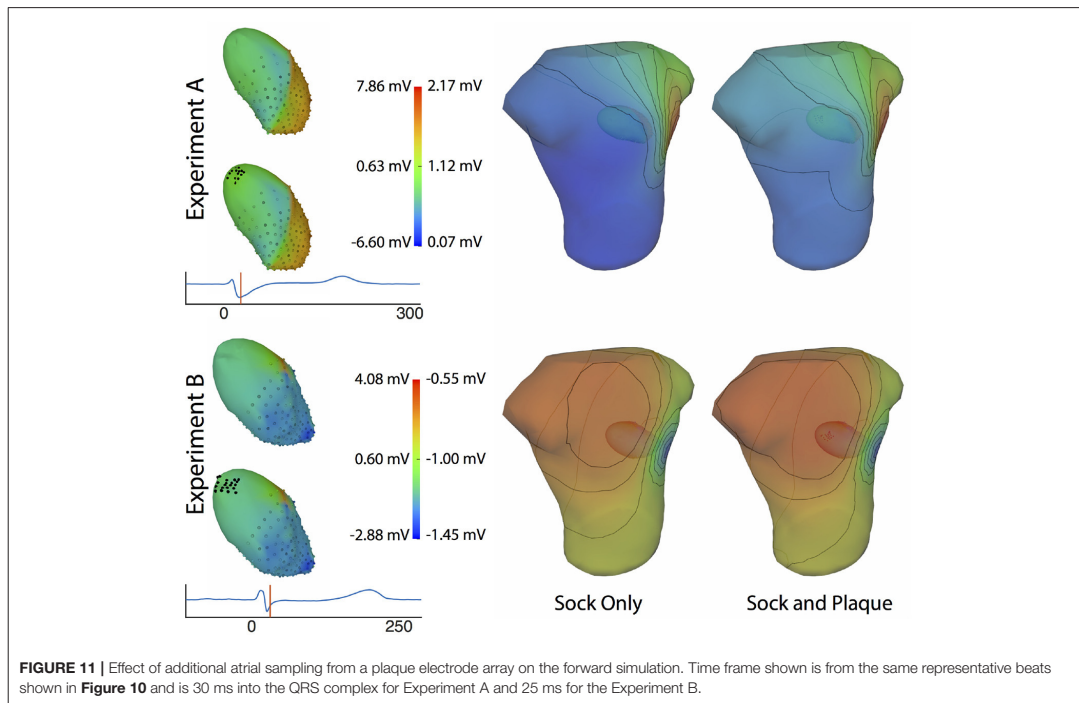


FIGURE 11 | Effect of additional atrial sampling from a plaque electrode array on the forward simulation. Time frame shown is from the same representative beats shown in **Figure 10** and is 30 ms into the QRS complex for Experiment A and 25 ms for the Experiment B.

electrodes also improved the agreement between ground truth torso potentials and simulations.

Although all strategies for additional atrial sampling improved the errors, we also sought specific strategies for picking the sample locations in future validation experiments. Analysis of the approaches we tested reveals that selecting evenly distributed points, such as the random and uniform strategies, are likely to produce greater accuracy with fewer added samples than other strategies (**Figure 5**). The combined strategy (i.e., basal plus atrial roof locations) also performed well, although not with the CARP dataset. The distributed nature of these strategies is likely a reason for their efficiency, because they reduce the need for interpolation over large distances that is an either explicit or implicit component of solving the forward problem.

Our analysis of the effect of various atrial plaque configurations on the simulated torso potentials revealed that the most valuable location may be at the roof of the atria, but placements even slightly away from the roof had lower accuracy. Therefore, it is difficult to identify and achieve the best location of additional measurement sites, typically in the form of a plaque electrode, in an experimental setting. Nevertheless, every plaque placement reduced the overall error of the simulated BSPMs, so it is likely that any plaque electrode placed on the atria will improve the overall accuracy of the forward simulation.

In comparing our results to similar studies, we found that eliminating the atrial sampling produced $rRMSE$ and \bar{E} values

in the simulated torso potentials similar to those reported as early as the mid 1970s by Ramsey et al. (1977) and as recently as by Bear et al. (2015). We eliminated or dramatically reduced these errors by including sampling over the atria, which suggests that the absence of atrial sampling contributed to the errors in their studies. However, both these studies showed higher qualitative differences in simulated BSPMs, e.g., differences in extrema location, than we could account for by removing atrial sampling locations, which suggests additional causes of error, possibly from registration, segmentation, or addition missing sampling.

One potentially significant additional source of error is in missing ventricular sampling locations. Such undersampling of the ventricle is possible even when using a ventricular sock because parts of the epicardium may not be sufficiently sampled, for example, because of poor electrode contact around the base of the heart or a lack of electrode density in regions of high spatial complexity of the potentials. Our results indicate that eliminating sampling locations from the ventricle can produce shifts in extrema locations, or remove them entirely, (**Figure 9**), and, in general, will decrease the overall accuracy of the forward simulations (**Figures 2, 8**). Removing ventricular samples can increase the $rRMSE$ even beyond that reported by Bear et al. (2015). All these results suggest that adequate sampling of both ventricles and atria is required to achieve the expected match between measured and predicted torso potentials.

The strategy of using more distributed sampling over the atria did not always produce the lowest error in the forward simulations (**Figures 6, 7**). The spatial variability of cardiac potentials means that there are likely sampling configurations that could reduce error more efficiently for specific geometries and activation profiles, for example, those that combined AV plane and atrial roof strategy produced the lowest error for apical stimulation in the KIT dataset, but in no other example (**Figures 6, 7**). Moreover, reducing error during different times of the cardiac cycle could also motivate different sampling strategies. There can be dramatic changes in the error and correlation through the cardiac cycle, as seen in the late stages of the CARP dataset sinus beat and cage datasets following left ventricular stimulation (**Figures 2, 3**). In a similar vein, the dramatic shift in error and correlation when the atria and basal region of the ventricles were undersampled could be attributed to incorrectly interpolating late activity near the AV plane over the atrial surface. The reduction in sampling either removes local potential extrema in this region, or could possibly remove transition regions to cause the extrema to become larger with the interpolation. In both these examples, we found that adding samples near the AV plane of the atria reduced error more than adding samples to the atrial roof (**Figures 6, 7**), which indicates that strategies that sample the AV plane would be important for late sinus activation or left ventricular activation. Therefore, with some *a priori* knowledge about activation profile and the regions of interest within the cardiac cycle, researchers could design specific strategies to correctly record them.

Implementing many of the strategies we tested in an experimental setting has many practical and logistical obstacles. For example, placing uniformly distributed recording electrodes on the epicardial surfaces of the atria is virtually impossible, due to limited access to the active myocardium. A combined approach including sampling near the atrial roof and near the AV plane would be feasible using multiple plaque electrodes and/or a ventricle sock that extended over the base to the atrial surface. Such sampling would likely be feasible in an *in situ* animal preparations, although placement of the plaque would remain a challenge due to the many vessels attached to the atria. The isolated, perfused heart suspended in a torso-shaped tank phantom (MacLeod et al., 1995; Shome and MacLeod, 2007; Milanic et al., 2014), similar to the one used to acquire the cage dataset, could provide the best option for recording full coverage cardiac source potentials because the vessels supplying the heart are gathered and fed through a small opening, and the rest of the surrounding surface can be instrumented with electrodes. A limitation of this approach is that the atria are not filled with blood and so collapse to lie on the base of the ventricles and lack both realistic shape and a stable surface for attaching electrodes.

Limitations to the study generally involved compromises in capturing cardiac sources and the associated torso potentials. By using fully simulated potentials, we could achieve levels of coverage and resolution not possible with experiments but with the caveat that these are simulations and reflect certain assumptions and conditions. For example, we ignored any electrical activation of the atria, assumed that the conductivity of the atria was the same as for the torso, and greatly simplified

the atrial epicardial surface by replacing it with a parameterized and smooth epicardial cap. Additionally, we did not account for possible scar or fibrosis formation which would occur in many disease states, possibly affecting any attempt to use these strategies in patients. Another source of validation data was a set of potentials from an isolated, perfused heart, captured with an instrumented rigid cage surrounding the heart. This arrangement provides full coverage of the heart and thus a complete source model, but the distance between heart and cage electrodes causes the signals to be smoother than on the epicardium and does not reflect perfectly the ECGI application. Finally, we assumed in this study that the only error would be due to insufficient source sampling of the atrial region, and thus we ignored other possible causes of error in source sampling, such as sampling density, uncertainty in individual electrode locations, or any other possible errors in capturing and representing the geometric model. These additional sources of error may compound those due to incomplete sampling over the atria.

This study focused specifically on the sampling of the atrial region and how it generally affected the forward simulation, but there are several additional, related questions that could be addressed in future studies. For example, of great interest would be a more direct spatial sensitivity analysis of the relationship between the potentials on the cardiac surface and the torso, or from the endocardial surface to the atria. Such results could suggest sampling strategies that would be specialized for specific regions of tissue, or types of activation. Other questions that could be similarly explored relate to the shape, location, and orientation of the heart, and how they might influence the forward simulation. Inclusion of torso heterogeneity due to other organs would affect the flow of current through the torso and may therefore affect the sampling strategies needed to more accurately predict BSPM. These questions and others could be the focus of future studies to help fully understand the effect of discretizing the cardiac electrical source with potential recordings.

This study illustrates the need to acquire adequate cardiac source sampling in ECG forward simulations, as well as the challenges in doing so. These findings also have implications for solving and validating the inverse solutions required for ECGI. Most mathematical formulations of ECGI solve for a subset of the cardiac sources without any cost to accuracy, but they are based on the assumption of a robust forward solution, i.e., that the relationship between the cardiac sources and the torso potentials is represented accurately (Barr et al., 1977; Plonsey and Barr, 1987; Plonsey and van Oosterom, 1991; Gulrajani, 1998). Our results suggest that coverage of the atrial surface with at least a schematic multielectrode cap could improve the resulting ECGI solutions. Additionally, our results have implications for how researchers validate ECGI methods using forward simulated BSPM data (Erem et al., 2011; Wang et al., 2011). Our findings suggest that the computed BSPMs used as inputs in these ECGI pipelines may contain errors due to inadequate cardiac sampling. Using BSPMs with such errors may bias the tuning of the constraints in the ECGI inverse problem and even alter the levels of accuracy achieved.

We conclude that complete sampling of the cardiac surface potentials is required to create realistic source descriptions for

validation experiments and simulations of ECGI. Ignoring or crudely interpolating over sources on the atrial surfaces or even parts of the ventricular surface will also reduce the accuracy of simulations. Researchers can mitigate these effects by ensuring that both the full ventricular epicardium and at least some locations on the atria are sampled. Even modest coverage of the atria can increase the accuracy of the resulting simulations dramatically. Distributed sampling over the atria will likely produce the lowest error, yet may be a challenge to implement experimentally. These efforts to improve source sampling will also improve the accuracy of the ECG forward simulations, which will further clarify the aspects of ECGI that need more research and development.

AUTHOR CONTRIBUTIONS

JT and RM originated the study idea and developed the hypothesis. JT, KG, BB, WG, BZ, JC-F, DB, and RM contributed

to the study design. JT, KG, BB, WG, and BZ contributed to data collection, organization, and processing. JT, KG, and JC-F contributed to developing the simulation pipelines used in the study. JT wrote the first draft of the manuscript. JT, KG, BB, WG, BZ, JC-F, DB, and RM contributed to manuscript revision and approved the submission of the manuscript.

ACKNOWLEDGMENTS

The research presented in this paper was made possible with help from the Cardiovascular Research and Training Institute (CVRTI) and the Nora Eccles Treadwell Foundation. This project was also supported by the National Institute of General Medical Sciences of the National Institutes of Health under grant number P41 GM103545-18. Some data used in this study was made available by a joint research project between the First Department of Medicine (Cardiology), University Medical Centre Mannheim, and the Karlsruhe Institute of Technology (KIT).

REFERENCES

- Aras, K. (2015). *Bioelectric Source Characterization of Acute Myocardial Ischemia*. Ph.D. thesis, University of Utah.
- Aras, K., Burton, B., Swenson, D., and MacLeod, R. (2016). Spatial organization of acute myocardial ischemia. *J. Electrocardiol.* 49, 689–692. doi: 10.1016/j.jelectrocard.2016.02.014
- Aras, K., Good, W., Tate, J., Burton, B., Brooks, D., Coll-Font, J., et al. (2015). Experimental data and geometric analysis repository: EDGAR. *J. Electrocardiol.* 48, 975–981. doi: 10.1016/j.jelectrocard.2015.08.008
- Barr, R., Ramsey, M., and Spach, M. (1977). Relating epicardial to body surface potential distributions by means of transfer coefficients based on geometry measurements. *IEEE Trans. Biomed. Eng.* 24, 1–11. doi: 10.1109/TBME.1977.326201
- Bear, L. R., Cheng, L. K., LeGrice, I. J., Sands, G. B., Lever, N. A., Paterson, D. J., et al. (2015). The forward problem of electrocardiography: is it solved? *Circ. Arrhythm. Electrophysiol.* 8, 677–684. doi: 10.1161/CIRCEP.114.001573
- Besl, P., and McKay, N. (1992). A method for registration of 3-D shapes. *IEEE Trans. Pat. Anal. Mach. Intell.* 14, 239–256. doi: 10.1109/34.121791
- Bishop, M. J., and Plank, G. (2011). Representing cardiac bidomain bath-loading effects by an augmented monodomain approach: application to complex ventricular models. *IEEE Trans. Biomed. Eng.* 58, 1066–1075. doi: 10.1109/TBME.2010.2096425
- Burton, B., Tate, J., Erem, B., Swenson, D., Wang, D., Brooks, D., et al. (2011). “A toolkit for forward/inverse problems in electrocardiography within the scirun problem solving environment,” in *Proceedings of the IEEE Engineering in Medicine and Biology Society 33rd Annual International Conference*. Boston, MA: IEEE, 1–4.
- Deo, M., Boyle, P., Plank, G., and Vigmond, E. (2009). Arrhythmogenic mechanisms of the purkinje system during electric shocks: a modeling study. *Heart Rhythm.* 6, 1782–1789. doi: 10.1016/j.hrtm.2009.08.023
- Erem, B., Ghodrati, A., Tadmor, G., MacLeod, R., and Brooks, D. (2011). Combining initialization and solution inverse methods for inverse electrocardiography. *J. Electrocardiol.* 44:e21. doi: 10.1016/j.jelectrocard.2010.12.059
- Fischler, M. A. and Bolles, R. C. (1981). Random sample consensus: a paradigm for model fitting with applications to image analysis and automated cartography. *Commun. ACM* 24, 381–395. doi: 10.1145/358669.358692
- Gulrajani, R. (1998). The forward and inverse problems of electrocardiography. *EMBS Mag.* 17, 84–101. doi: 10.1109/51.715491
- Johnson, C. (1997). Computational and numerical methods for bioelectric field problems. *Crit. Rev. Biomed. Eng.* 25, 1–81. doi: 10.1615/CritRevBiomedEng.v25.i1.10
- Johnson, C. (2015). *Chapter 43: Computational Methods and Software for Bioelectric Field Problems*, Vol. 1, 4th Edn. Boca Raton, FL: CRC Press, 1–28.
- Johnson, C., MacLeod, R., and Matheson, M. (1993). Computational medicine: Bioelectric field problems. *IEEE Comput.* 26, 59–67. doi: 10.1109/2.237454
- Loewe, A., Schulze, W. H. W., Jiang, Y., Wilhelms, M., Luik, A., Dössel, O., et al. (2015). ECG-based detection of early myocardial ischemia in a computational model: impact of additional electrodes, optimal placement, and a new feature for ST deviation. *BioMed Res. Int.* 2015:530352. doi: 10.1155/2015/530352
- MacLeod, R., and Buist, M. (2010). “The forward problem of electrocardiography,” in *Comprehensive Electrocardiology*, eds P. Macfarlane, A. van Oosterom, O. Pahlm, P. Kligfield, M. Janse, and J. Camm (London, UK: Springer Verlag), 247–298.
- MacLeod, R., Taccardi, B., and Lux, R. (1995). “Electrocardiographic mapping in a realistic torso tank preparation,” in *Proceedings of the IEEE Engineering in Medicine and Biology Society 17th Annual International Conference* (Montreal, QC: IEEE Press), 1–3.
- MacLeod, R., Weinstein, D., de St. Germain, J. D., Brooks, D., Johnson, C., and Parker, S. (2004). “SCIRun/BioPSE: integrated problem solving environment for bioelectric field problems and visualization,” in *IEEE International Symposium on Biomedical Imaging (ISBI)*, Arlington, VA: IEEE Press, 1–3.
- Messinger-Rappaport, B., and Rudy, Y. (1986). The inverse problem in electrocardiography: a model study of the effects of geometry and conductivity parameters on the reconstruction of epicardial potentials. *IEEE Trans. Biomed. Eng.* 33, 667–676. doi: 10.1109/TBME.1986.325756
- Milanic, M., Jazbinsek, V., Maclead, R., Brooks, D., and Hren, R. (2014). Assessment of regularization techniques for electrocardiographic imaging. *J. Electrocardiol.* 47, 20–28. doi: 10.1016/j.jelectrocard.2013.10.004
- Oostendorp, T., van Oosterom, A., and Huiskamp, G. (1989). Interpolation on a triangulated 3D surface. *J. Comp. Phys.* 80, 331–343. doi: 10.1016/0021-9991(89)90103-4
- Parker, S., Weinstein, D., and Johnson, C. (1997). “The SCIRun computational steering software system,” in *Modern Software Tools in Scientific Computing*, eds E. Arge, A. Brusset, and H. Langtangen, Boston, MA: Birkhauser Press, 1–40.
- Plonsey, R., and Barr, R. (1987). Mathematical modeling of electrical activity of the heart. *J. Electrocardiol.* 20, 219–226. doi: 10.1016/S0022-0736(87)80019-5
- Plonsey, R., and van Oosterom, A. (1991). Implications of macroscopic source strength on cardiac cellular activation models. *J. Electrocardiol.* 24, 99–112. doi: 10.1016/0022-0736(91)90001-3
- Pullan, A., Cheng, L. K., Nash, M., Brooks, D., Ghodrati, A., and MacLeod, R. (2010). “The inverse problem of electrocardiography,” in *Comprehensive*

- Electrocardiology*, eds P. Macfarlane, A. van Oosterom, O. Pahlm, P. Kligfield, M. Janse, and J. Camm (London, UK: Springer Verlag), 299–344.
- Ramsey, M., Barr, R. C., and Spach, M. S. (1977). Comparison of measured torso potentials with those simulated from epicardial potentials for ventricular depolarization and repolarization in the intact dog. *Circulation* 41, 660–672. doi: 10.1161/01.RES.41.5.660
- Rodenhauser, A., Good, W., Zenger, B., Tate, J., Aras, K., Burton, B., et al. (2018). Pfeifer: Preprocessing framework for electrograms intermittently fiducialized from experimental recordings. *J. Open Source Softw.* 3, 472. doi: 10.21105/joss.00472
- Rudy, Y., and Lindsay, B. (2015). Electrocardiographic imaging of heart rhythm disorders: from bench to bedside. *Card Electrophysiol. Clin.* 7, 17–35. doi: 10.1016/j.ccep.2014.11.013
- Schulze, W. H. W., Potyagaylo, D., Schimpf, R., Papavassiliu, T., Tülinnen, E., Rudic, B., et al. (2015). “A simulation dataset for ECG imaging of paced beats with models for transmural, endo-and epicardial and pericardial source imaging,” in *First Meeting of the Consortium for EGI Imaging* (Bad Herrenalb), 1.
- Shome, S., and MacLeod, R. (2007). “Simultaneous high-resolution electrical imaging of endocardial, epicardial and torso-tank surfaces under varying cardiac metabolic load and coronary flow,” in *Functional Imaging and Modeling of the Heart*, Lecture Notes in Computer Science 4466 (Berlin: Springer-Verlag), 320–329.
- Stanley, P., Pilkington, T., and Morrow, M. (1986). The effects of thoracic inhomogeneities on the relationship between epicardial and torso potentials. *IEEE Trans. Biomed. Eng.* 33, 273–284. doi: 10.1109/TBME.1986.325711
- ten Tusscher, K. H. W. J., and Panfilov, A. V. (2006). Alternans and spiral breakup in a human ventricular tissue model. *Am. J. Physiol. Heart Circ. Physiol.* 291, H1088–H100. doi: 10.1152/ajpheart.00109.2006
- Vigmond, E., Hughes, M., Plank, G., and Leon, L. (2003). Computational tools for modeling electrical activity in cardiac tissue. *J. Electrocardiol.* 36(Suppl.), 69–74. doi: 10.1016/j.jelectrocard.2003.09.017
- Vigmond, E. J., Weber dos Santos, R., Prassl, A. J., Deo, M., and Plank, G. (2008). Solvers for the cardiac bidomain equations. *Prog. Biophys. Mol. Biol.* 96, 3–18. doi: 10.1016/j.pbiomolbio.2007.07.012
- Wang, D., Kirby, R., and Johnson, C. (2011). Finite-element-based discretization and regularization strategies for 3-D inverse electrocardiography. *IEEE Trans. Biomed. Eng.* 58, 1827–1838. doi: 10.1109/TBME.2011.2122305

Conflict of Interest Statement: The authors declare that the research was conducted in the absence of any commercial or financial relationships that could be construed as a potential conflict of interest.

Copyright © 2018 Tate, Gillette, Burton, Good, Zenger, Coll-Font, Brooks and MacLeod. This is an open-access article distributed under the terms of the Creative Commons Attribution License (CC BY). The use, distribution or reproduction in other forums is permitted, provided the original author(s) and the copyright owner(s) are credited and that the original publication in this journal is cited, in accordance with accepted academic practice. No use, distribution or reproduction is permitted which does not comply with these terms.

CHAPTER 4

VALIDATING DEFIBRILLATION SIMULATION IN A HUMAN- SHAPED PHANTOM

4.1 Abstract

We previously developed a computational model to aid clinicians in positioning implantable cardioverter defibrillators (ICD), especially in the case of abnormal anatomies, such as in pediatric cases. However, high spatial resolution validation of the simulation is still needed to improve its use in clinical settings. The goal of this study is to record the ICD potential field within the heart and on the torso to validate the simulation.

We recorded defibrillator shock potentials from an ICD suspended with an animal heart in a human-shaped torso tank and compared them to simulated values. We also compared the critical mass threshold (CMT), an analogue to the defibrillation threshold, from the measured and simulated electric fields within the myocardium.

ICD potentials recorded on the tank and cardiac surface and within the myocardium agreed well with those predicted by the simulation. A quantitative comparison of the recorded and simulated potentials yielded a mean correlation of 0.94, relative error of 19.1 %, and normalized root-mean-squared error of 6.0 %. Comparisons of CMTs calculated from the measured and simulated electric fields also showed that the simulation can predict similar electric field and CMT values.

The agreement of the potential recordings within the torso tank with simulated values shows that the simulation can predict accurate potential fields within the heart as well as on the torso tank surface. These results support the use of this model for optimization of ICD placements.

4.2 Introduction

Defibrillation is a mature technology used in hundreds of thousands of patients to treat fibrillation and other life-threatening arrhythmias [1]–[3], but it is not without significant risks, including tissue damage from overshock [4] and the morbidity of implantation surgery for implantable cardioverter-defibrillators (ICDs) [2]. Device manufacturers, physicians, and researchers have proposed improvements to reduce the energy needed to defibrillate a patient, called the defibrillation threshold (DFT), and to minimize the invasiveness of the devices while maintaining patient safety. These improvements include new configurations such as subcutaneous ICDs [5]–[7] and wearable cardio-defibrillators [8], [9]. Testing the effectiveness of new device developments is essential, yet conducting such tests in animal or clinical experiments can be cost prohibitive or unethical.

Mathematical and computational modeling can facilitate defibrillator development, test new technologies, and guide their use. Such modeling may also reduce the number of patient and animal trials needed to test device configurations. We have developed a patient-specific pipeline for just such modeling, which has been used to allow researchers and physicians to test new or modified device configurations in subject-specific anatomies [10], [11]. The pipeline predicts the potential distribution throughout the torso and calculates the DFT based on the critical mass hypothesis to determine device safety and effectiveness. This pipeline has been shown to be generally accurate in predicting DFT and body-surface potential maps (BSPMs) in patients [12], [13]; however, to our knowledge, no such validations published by any group have included comprehensive measurements of potentials *within the volume of the heart*.

Previous studies have compared measured and simulated defibrillation potentials within the heart, but only with vary sparse sampling and often over limited regions of the heart. [14], [15]. Other groups have used electrolytic phantoms to measure cellular potentials during defibrillation using optical techniques [16], yet these studies measured tissue activity before and after defibrillation, i.e., the impact of defibrillation and are fundamentally unable to record the potentials generated by the device. We have carried out many studies in electrolytic, densely instrumented phantoms shaped like a human torso with an isolated, perfused heart suspended inside [17]–[19]. Such a configuration offers a unique opportunity to record multichannel signals of defibrillation pulses simultaneously in the

myocardium and on the heart and torso surfaces to compare with simulated potential distributions.

In this study, we recorded defibrillator potentials in a human-shaped torso tank phantom containing an isolated animal heart. We could capture up to 1024 channels of signals recorded from within the heart using intramural multielectrode needles and on the epicardial and torso surfaces with the goal of validating our defibrillation simulation pipeline. We compared the measured potential fields to those predicted by the simulation pipeline to establish its accuracy. We also computed the electric field strength from the recorded and simulation potentials and evaluated its similarity based on the critical mass threshold (CMT), an analogue to the DFT, computed using the assumptions of the critical mass hypothesis [20].

The results of this study establish the torso-tank setup as a method to record potentials at high spatial resolution within the heart with accompanying cardiac and torso measurements. The comparisons of simulated and measured potentials demonstrated good overall agreement and indicated that simulation was generally accurate and that the potential field was captured effectively enough to enable validation of the simulation. We also found that using needle electrodes in the myocardium could effectively capture the electric field in the tissue, and when compared to the simulated values, showed that simulation predict comparable electric fields.

4.3 Methods

We recorded potentials generated by an ICD implanted in an isolated animal heart within a torso-shaped electrolytic tank and compared them with simulated potentials. To record ICD potentials, we modified a previous setup designed to record potential distributions in and around a heart as it was suspended in a tank filled with electrolyte solution [17]–[19], but instead of recording cardiac potentials, we recorded potentials generated by an ICD. We simulated the potential field generated by the device using the same geometries and conductivities to predict the potentials at the measurement locations and compared them to the recorded values.

4.3.1 Tank Experiments

Each torso tank experiment ($N=4$) consisted of an explanted porcine ($N=3$) or dog ($N=1$) heart and an ICD (Medtronic Virtuoso II DR or Medtronic Maximo II VR) suspended in an instrumented tank filled with isotonic electrolytic solution of known conductivity. The hearts were excised, postmortem canine or porcine hearts that were electrically inactive. The three pig hearts were not perfused while submerged, but the dog heart was retrograde perfused with blood via a support animal. An epicardial sock was applied, and between 20 and 31 plunge needles were inserted into the walls of both ventricles. A 5 cm defibrillator coil was placed either in the right ventricle ($N=3$) or on the epicardium, held in place near the left anterior descending artery (LAD) with the cardiac sock (for the single case of the perfused heart). The electrolytic solution consisted of glucose and NaCl balanced to achieve a resistivity of $200 \Omega\text{m}$.

With the heart, ICD, and electrodes in place, we manually induced biphasic shocks and recorded the potentials within the torso tank. The shocks were generated by the ICDs or by an external cardioverter defibrillator (ECD) (VENTAK model 2815, Boston Scientific Corp.) while using the ICD casing and coil as the defibrillation electrodes. The defibrillator devices were attenuated by a factor of $\sim 1,300$ to allow recording with the recording system. Potentials were recorded with a 256-channel acquisition system developed at the Cardiovascular Research and Training Institute (CVRTI) on the tank surface (192 electrodes), epicardial sock (247 electrodes), and 20 to 34 plunge needles (200 to 340 electrodes). Electrode sets were recorded sequentially in three or four separate shocks at a sampling rate of 8 kHz and time aligned during postexperiment signal processing. For one of the experiments, an observable shift in the reference state of the recording system between the sequential recordings caused a dramatic shift in potential distribution between neighboring electrodes. We corrected this shift by comparing neighboring electrodes from different sets, i.e., adjacent needles or epicardial needles and the sock electrodes, to readjust the reference of the signals.

The recording system used in the experiment was designed to record cardiac potentials and so required attenuation of the ICD potentials to protect the instrumentation and keep signals within measurable range. The ICD was attenuated without changing the lead impedance outside the physiological range by adding a high wattage resistor ($R_1=68 \Omega$,

50 W) in parallel with a voltage divider, as shown in Fig. 4.1. Using high resistance for the second resistor ($R_2 = 100\text{K}\Omega$) reduced the amplitude of the signal by a factor of $\sim 1,300$, low enough to record with the cardiac mapping system. The scaling factor was dependent on the total resistance between the ICD coil and generator. We used the shock impedance calculated by the device (without attenuation) as this resistance value.

At the end of the experiment, corresponding landmark points were acquired using an electromechanical digitizer (Microscribe) to register the heart and recording locations (see Section 4.3.3). The correspondence points were acquired on the torso tank (16 points), the epicardial sock (20-40 points), the entry locations of each of the needles (20-31 points), the ICD can (10-20 points) and coil (5-10 points), and several points on the heart surface (~ 50), including the LAD (~ 10).

The heart was then imaged in a 7 T small animal MRI scanner with FISP and FLASH sequences. Preparation for imaging involved replacing the recording needles with spacers that marked the needle positions in the MRI scan, filling the chambers with alginate, and fixing the heart with formalin.

4.3.2 Signal Processing

The recorded ICD pulses were extracted, time aligned, and processed to enable comparison to the simulated values. All signals were scaled by the device attenuation factor.

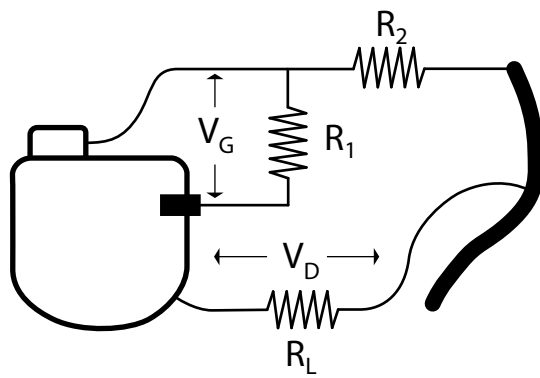


Fig. 4.1. Schematic of the ICD attenuation used to reduce the amplitude of the generated signal to allow for recording with a cardiac mapping system. V_G is the voltage generated by the device, V_D is the voltage delivered through the torso tank, R_1 and R_2 are resistors added to the device, and R_L is the total resistance through the torso between the ICD lead and the generator.

The pulse windows were calculated from a root mean squared (RMS) curve for all channels by identifying deviations from the baseline, with manual correction. The ICD pulse peak was identified as the mode of the time of the first maximum or minimum for all channels in a recording instance. Separately recorded time signals were time aligned with the pulse peak of each recording instance. Leads of unacceptable technical quality were identified as those with a low correlation to all other channels and were removed from the comparison calculations. Such missing leads were replaced with a Laplacian interpolation on the torso and heart surfaces and by thin-plate spline radial basis function for the cardiac tissue volume. Each channel was also baseline corrected and median filtered (window of five time steps). These steps were implemented using customized code written in MATLAB (The Mathworks, Inc) and our simulation environment SCIRun [21] (<http://scirun.org>).

4.3.3 Geometric Registration

The registration of the geometries used in these experiments requires aligning geometries from three sources: the points digitized during the experiment, the imaging of the heart, and the precomputed geometries of the equipment used in the experiment, i.e., the sock, heart images, needles, ICD geometries, and torso tank measurement nodes. We used a series of registration steps, illustrated in Fig. 4.2, that utilized the RANSAC [22], modified iterative closest point (ICP) [23], and thin-plate spline techniques, implemented in MATLAB or SCIRun [21] (<http://scirun.org>). The result was a co-registered geometric model that included all input elements combined in the same simulation space coordinate system, as shown in the lower right panel of Fig. 4.2.

4.3.4 Simulation Pipeline

The defibrillation simulation pipeline used in this paper is well established and described elsewhere [11], [13]. For this study, however, the pipeline was modified to use experimental signals and geometric models instead of patient data. Hence, the differences we summarize here deal with geometry and mesh generation.

The geometric models used in the simulation were generated from the registered image and electrode locations described in Section 4.3.3 using a combination of open-source software tools: Seg3D (<http://seg3d.org>), BioMesh3D [24] (<http://scirun.org>), SCIRun [21] (<http://scirun.org>), and Tetgen [25] (<http://tetgen.org>). Seg3D was used to segment the

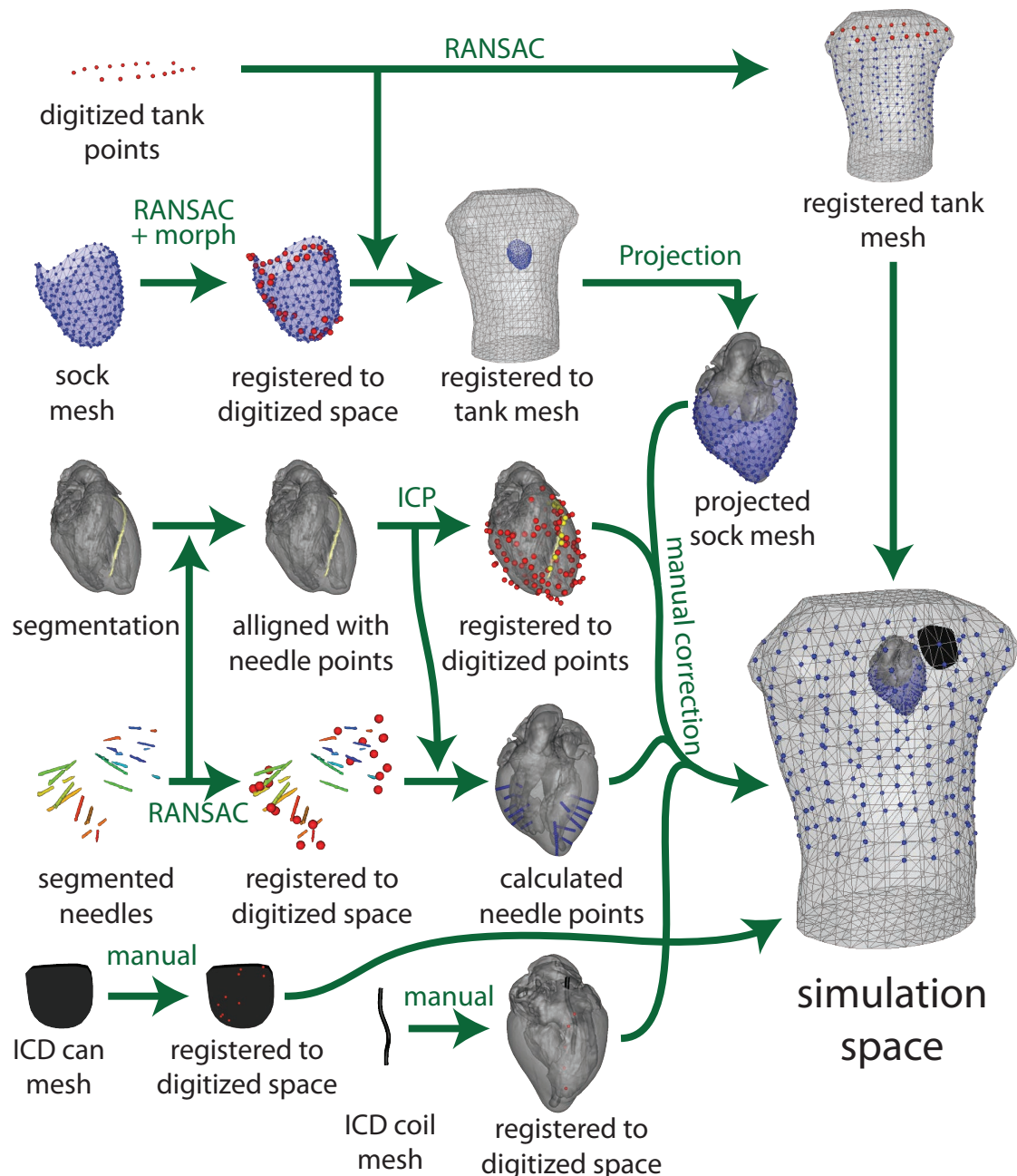


Fig. 4.2. Schematic of the registration pipeline used to merge the experimental and simulation space for comparison. On the left side are the recorded geometric information, which then had to be aligned and registered into a common coordinate system ("simulation space") to enable analysis of the defibrillation simulations.

MRI images of the excised hearts, from which a high-quality mesh of the ventricles was then generated using BioMesh3D. SCIRun and Tetgen were used to generate a conforming (i.e., a mesh that maintains the node locations at boundaries between regions of different conductivities [26]) tetrahedral mesh that included the tank, heart, and ICD geometries. This mesh was then used as the simulation domain to calculate the ICD potentials through the volume.

The potentials generated by the defibrillators were simulated using the finite element method implemented in SCIRun. The conductivities used were 0.3 S/m in the heart and 0.5 S/m in the tank. The ICD generator and coil potentials were set as the Dirichlet boundary conditions of the simulation, and the torso surface was set as the Neumann boundary condition. After the potentials were calculated, the values at the three tank reference electrode locations corresponding to the locations used to construct the Wilson's Central Terminal were averaged and subtracted from the volumetric potentials. Measured potential values were extracted at the electrode locations for the tank, sock, and needles for comparison with the simulations. A similar example of this calculation is included in the open-source SCIRun-Exchange repository (<https://github.com/SCIIInstitute/SCIRun-Exchange>).

4.3.5 Potential Comparisons

To validate the accuracy of our defibrillation pipeline, we compared simulated potential fields to those recorded at the same locations in our torso tank study. Each simulated potential field was compared to the recorded potential field at the first peak of each biphasic pulse at the corresponding locations. The differences in the field were quantified with three standard metrics: normalized root mean square error (\bar{E}), relative error (RE), and correlation (ρ), defined as follows:

$$\bar{E} = \frac{||\Phi_r - \Phi_s||}{\sqrt{n} \cdot (\max(\Phi_r) - \min(\Phi_r))} \quad (4.1)$$

$$RE = \frac{||\Phi_r - \Phi_s||^2}{||\Phi_r||^2} \quad (4.2)$$

$$\rho = \frac{\Phi_r^T \Phi_s}{||\Phi_r|| ||\Phi_s||}, \quad (4.3)$$

where Φ_r is a vector of the recorded potential values, Φ_s is a vector of the associated simulated potentials, and n is the number of electrodes in the set.

We also compared the computed electric field strength through the cardiac tissue near the plunge needles (within 10 mm). The electric field strength from the simulations was determined by calculating the gradient magnitude of the potential field through the myocardial tissue region. The equivalent measured electric field was computed from potentials interpolated through the region of the needles with a thin-plate spline radial basis function. We compared the measured and simulated electric field strength in the context of the critical mass threshold (CMT), which we defined as the shock energy needed to ensure that the electric field strength within tissue region was greater than 5 V/cm for 95% of the tissue; therefore, it is similar and analogous to the DFT as it is calculated via the critical mass hypothesis [10], [20]. We also calculated and compared the probability density functions of the electric field strength, i.e., the amount of myocardial tissue experiencing an electric field over any given value, for recorded and simulated data.

4.3.6 Ethics

All experiments were performed with approval from the Institutional Animal Care and Use Committee at the University of Utah and conform to the Guide for the Care and Use of Laboratory Animals (National Institutes of Health publication No. 85-23).

4.4 Results

The results presented in this section demonstrate the feasibility of using the torso-tank experimental preparation as a method to validate the simulation pipeline. Comparing potential fields measured with the torso tank setup and those predicted by the simulation pipeline showed high overall agreement, both qualitatively and quantitatively, for all experiments and recorded shocks. The same agreement was supported by a comparison of the electric field cumulative density functions between measurements and simulations. The critical mass thresholds (CMTs) from recorded and simulated electric fields agreed in some experiments but not in others.

4.4.1 Potential Field Comparison

Comparing the measured peak ICD potentials to values predicted by the simulation pipeline showed high ρ , low \bar{E} , and moderate RE (Table 4.1). The ρ ranged from 0.91 to 0.95 with a mean value of 0.94, the \bar{E} ranged from 4.9 to 7.4 % with a mean of 6.0 %, and

xTable 4.1. Statistical comparisons of the simulated and measured peak potential fields. Each row contains the results from a single test shock, with variable numbers of test shocks from each of the four experiments. ${}^{\dagger}\rho$ is the correlation, ${}^{\ddagger}RE$ is the relative error, and ${}^{\S}\bar{E}$ is the normalized RMS error.

experiment & species	lead impedance	shock energy	ρ^{\dagger}	RE^{\ddagger}	\bar{E}^{\S}
Exp A Pig	79 Ω	10 J	0.92	30.9 %	7.2 %
		15 J	0.91	33.4 %	7.4 %
Exp B Pig	77 Ω	5 J	0.94	19.3 %	5.1 %
		15 J	0.95	17.9 %	4.9 %
		25 J	0.95	19.0 %	5.1 %
Exp C Pig	73 Ω	0.6 J	0.94	20.4 %	6.7 %
		1 J	0.94	20.8 %	6.8 %
Exp D Dog	60 Ω	1 J	0.95	5.3 %	5.8 %
		10 J	0.95	4.5 %	5.2 %
mean	73 Ω	9.2 J	0.94	19.1 %	6.0 %

the RE ranged from 4.5 to 33.4 %. Experiment A showed the biggest differences with the highest error (RE and \bar{E}) and lowest ρ . Conversely, experiment D was the most accurate, with the highest ρ , lowest RE by a factor of ~ 4 , and near lowest \bar{E} (Table 4.1). Each experiment demonstrated relatively consistent accuracy across shocks based on comparing all measured potentials within each experiment.

Comparing each of the recorded subsets, i.e., the cardiac surface (sock), tank surface, and cardiac volume (needles), to the corresponding simulated potentials yielded results at finer spatial resolution than comparing all recordings. There was variability across the lead subsets; for example, ρ ranged from 0.77 to 0.98, the RE ranged from 2.7 % to 103 %, and \bar{E} ranged from 5.5 % to 22.6 %. As shown in Fig. 4.3, the accuracy of the predicted potentials varied by recordings surface as well as by experiment. The needle potentials showed lower correlation than the other recording subsets for three of the four experiments, but had the highest RE in one experiment and the highest \bar{E} in two experiments. The tank surface showed the highest correlation for all experiments, the lowest RE for two experiments, and the lowest \bar{E} for two experiments. Also, the tank surface recordings for experiment D showed the highest RE and \bar{E} for all surfaces over all experiments, despite the high correlation, likely because they also showed the highest noise levels. The standard deviation of the metrics for all recording subsets and experiments was also relatively low, except for the RE and \bar{E} with the tank recordings.

Figs. 4.4, 4.5, and 4.6 show the measured potential distributions at the peak of a defibrillator pulse along with the corresponding simulated potentials. The measured and predicted potential distributions show a high degree of qualitative agreement in the pattern of

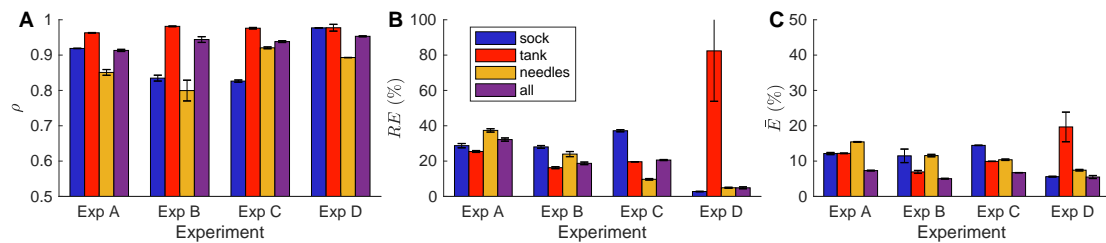


Fig. 4.3. Mean comparison of the simulated and measured potential fields by measurement domain, i.e., the sock, tank, needles, or all recordings. The metrics shown are the a) correlation (ρ), b) relative error (RE), and c) normalized RMS error (\bar{E}). Error bars represent the standard deviation.

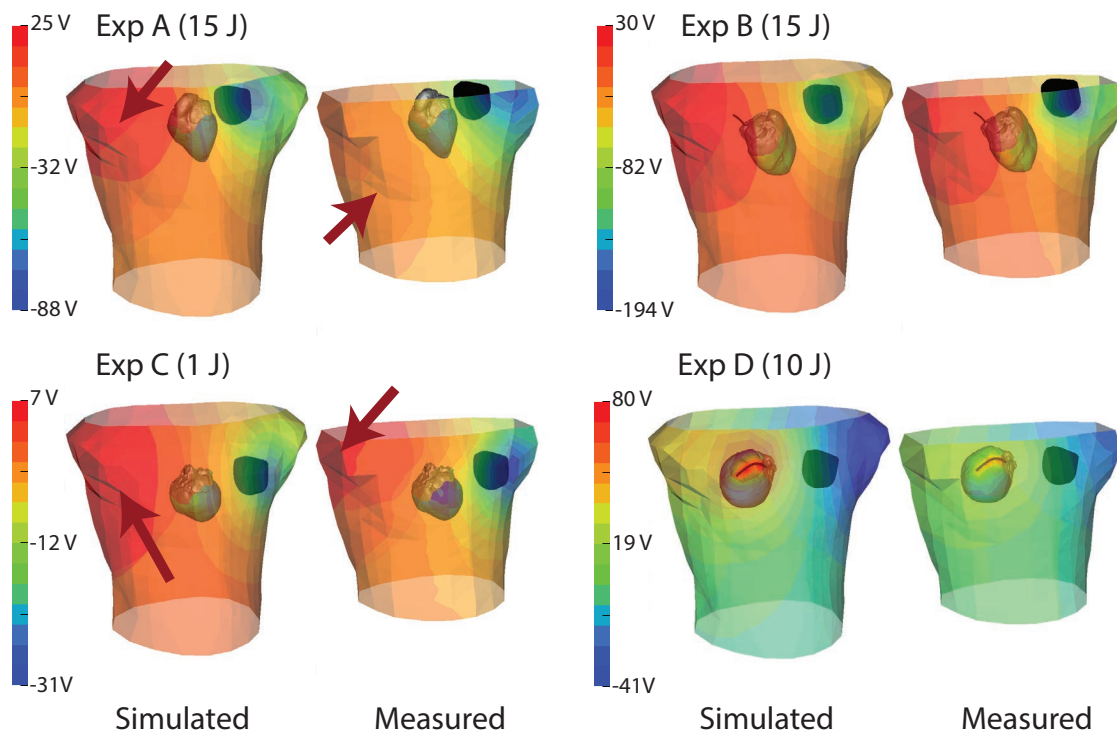


Fig. 4.4. Spatial comparison of the peak potential fields recorded on the torso tank and the simulated values. ICD generator and coil positions are included (black).

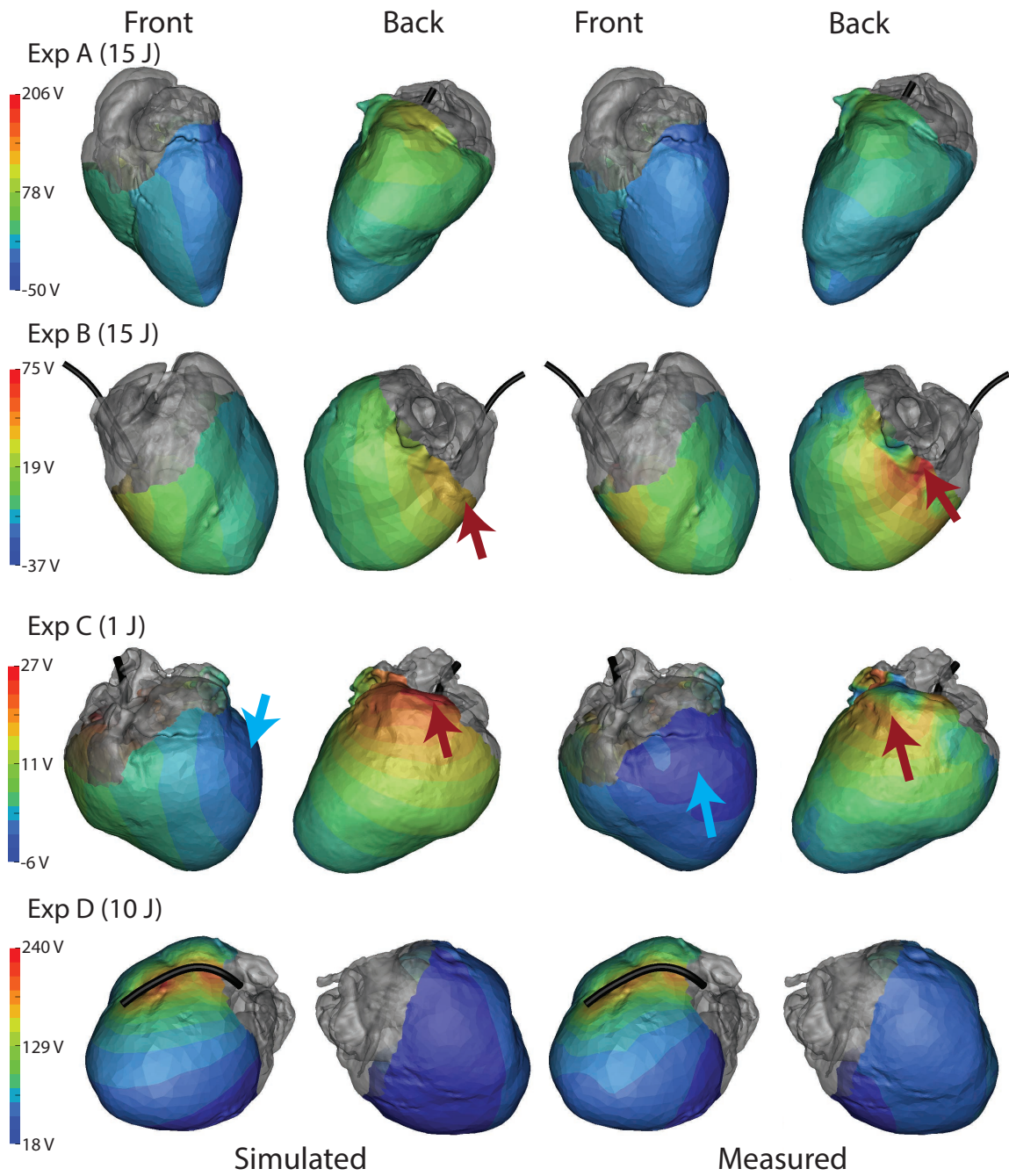


Fig. 4.5. Spatial comparison of the peak potential fields recorded on the epicardial sock and the simulated values. ICD coil position is included (black).

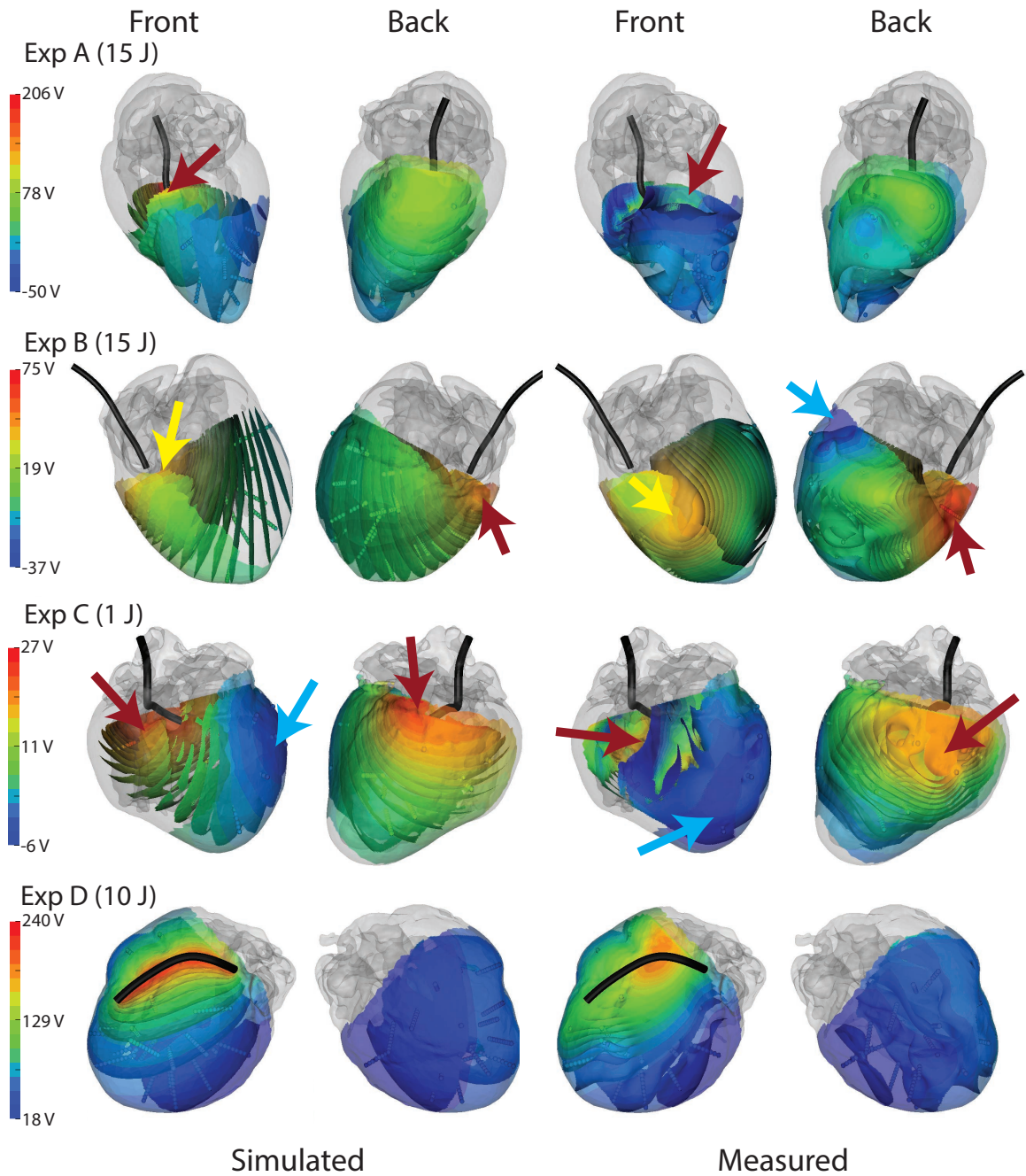


Fig. 4.6. Spatial comparison of the peak potential fields recorded within the myocardium with plunge needles and the simulated values. ICD coil position is included (black).

the potentials (a finding supported by the strong correlations). Amplitude variations were visible, largely accountable as scaling differences between simulations and measurements. However, some shifts in extrema were seen on the tank surface in experiments A and C (Fig. 4.4), the heart surface in experiments A, B, and C (Fig. 4.5), and in the myocardium in experiments A, B, and C (Fig. 4.6). Experiment D showed a difference in the maximum area shape observed in the myocardium (Fig. 4.6), which could be caused by undersampling of the region. The measured epicardial surface and myocardial volume potentials in experiments A, B, and C contained local extrema that were not predicted by the simulation (Figs. 4.5 and 4.6). Some of the local extrema on the epicardial surface, e.g., near the base of the heart, could be attributed to poor electrode contact.

Qualitative comparison of the simulated and measured potential gradients through the myocardium showed general agreement for most of the heart, yet not in some areas (Fig. 4.6). In one example in experiment D, the potential gradient was high near the coil but decreased quickly with distance from the coil in the simulated case, yet the transition was smoother in the recorded data. The areas of maximum gradient, which correlated to the areas maximum potential, were also shifted in experiments A, B, and C, with a superficial area of high gradient on the posterior wall of the heart in experiment B in the recorded data that were not present in the simulation.

4.4.2 Electric Field Comparison

Comparing the CMT calculated from the recorded and simulated electric field strength through the myocardial tissue showed some agreement with two of the experiments (experiments A and C) but not the other two (experiments B and D). The CMTs derived from the measured potentials ranged from 4.3 to 12.9 J, whereas values from simulation ranged from 5.2 to 18.5 J. As shown in Fig. 4.7, the CMT varied within an experiment, with the greatest range occurring in experiment D (10.5 to 12.9 J) and the lowest range in with experiment A (4.25 to 4.33 J). Experiment C showed the closest simulated CMT to the mean CMT from recordings with a difference of 1.6 J. Experiment A was the next closest with a difference of 2.7 J, followed by experiment D with 6.5 J, and finally experiment B with a difference of 7.8 J. The CMT from simulated data overpredicted the CMT from recorded data in experiments A and B and underpredicted in experiments C and D.

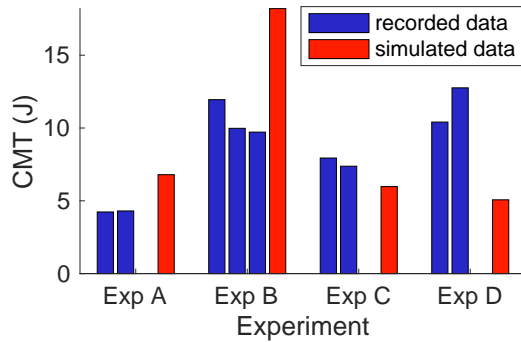


Fig. 4.7. Predicted CMTs based on recorded and simulated electric fields using the critical mass hypothesis (95 % over 5 V/cm). The CMT from each shock is shown compared to the simulated value from each experiment.

Fig. 4.8 shows the probability distribution of the electric field strength through the region of the tissue near the needles scaled to fit the critical mass hypothesis (95 % over 5 V/cm). The probability distributions of different shock recordings of the same experiment were nearly identical. Observable differences between the probability distributions corresponded to differences in the CMT calculation (Fig. 4.7). The distributions from the recorded fields had profiles similar to those for the simulated fields.

4.5 Discussion

The goal of this paper was to compare recordings from an ICD in a torso tank experiment to those predicted by our defibrillation simulation pipeline. The findings showed agreement, both qualitatively and quantitatively. We also found that the simulation could predict CMTs and cumulative density functions similar to those calculated from recorded potentials. The combination of accurate potential field comparison and similar electric field measures, although in a limited number of experiments, provides a proof of concept that the torso-tank experimental preparation can be used to validate the defibrillation simulation, including in the myocardium.

The high-density spatial sampling of the potential field within the torso tank and heart provides a unique validation of the defibrillation pipeline to predict potential distributions. Other studies have performed similar recordings and comparisons [13]–[15], i.e., recordings within the heart or on the body surface, yet none have recorded defibrillator potentials at this resolution within the heart and on the body surface. This study showed a

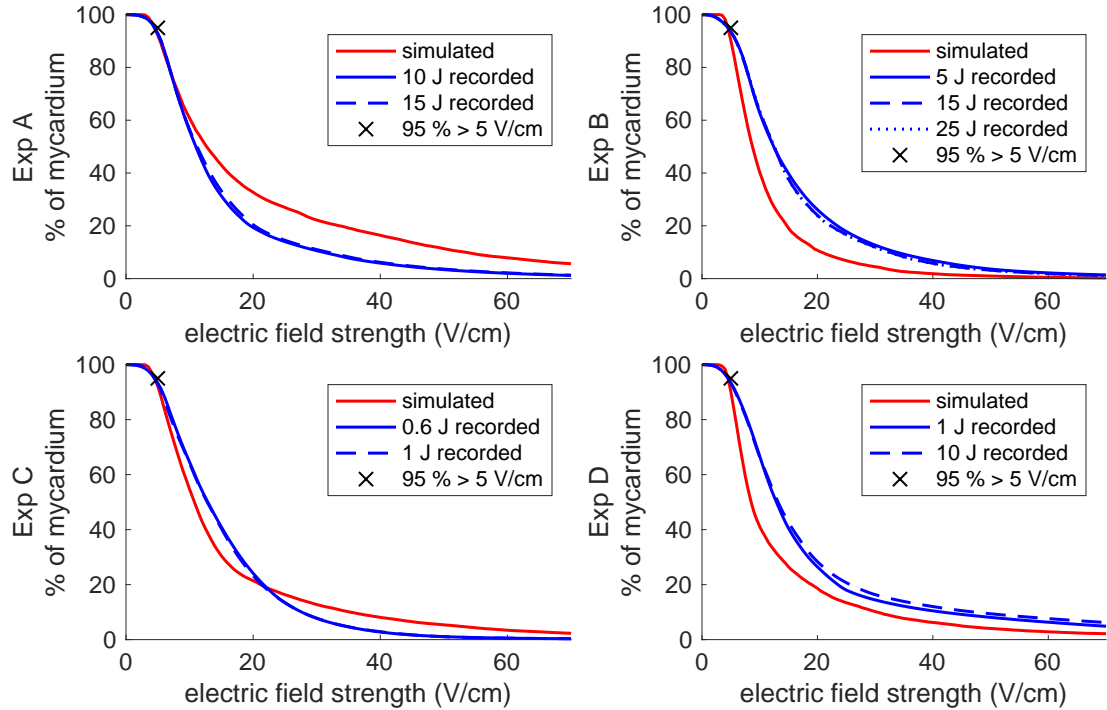


Fig. 4.8. Cumulative probability density plot showing the percentage of the myocardial tissue region above each electric field value. The electric fields were scaled to satisfy the critical mass hypothesis (95 % over 5 V/cm), which is marked as a X.

higher correlation and lower relative RMS error than those shown in an in situ study based on recorded epicardial potentials [15]. We also showed a correlation and relative error similar to those shown in another in situ animal study based on sparse torso recordings [14]. Our findings also showed ρ , RE , and \bar{E} similar to those reported in our previous study based on recorded body-surface maps during ICD testing [13].

The presented comparison of the CMTs calculated from the recorded and simulated electric fields provides some insight into the general accuracy of the simulation and the ability of the experimental preparation to capture the electric field (Fig. 4.7). Although the measured and simulated CMTs did not agree in every case, they did show generally comparable values. The comparable results indicate that the electric field captured by the needles was dense enough to provide a high spatial resolution comparison within the myocardium. The CMTs calculated in the study provide a metric to evaluate the electric field in a way that relates to the DFT as calculated using the critical mass hypothesis [12]. The CMT and DFT metrics used in this study are not designed to support the critical mass

hypothesis as an underlying explanation of the mechanism of defibrillation, yet the metrics are useful in comparing the electric field generated by a defibrillator.

The qualitative differences found in the potential fields (Figs. 4.4, 4.5, and 4.6) suggest improvements for future experiments. For instance, since the only electrical sources are the ICD generator and coil, changes in the absolute maximum and minimum in the potential field could easily be due to registration errors, particularly with the ICD coil (Fig. 4.6). This registration error may also be the cause of the difference in calculated CMTs from measured and simulated fields. However, experiment D also had a different calculated CMT, yet agreement with regard to the location of the maximum in the potential fields, so other factors may also be involved. Experiment D also displayed a difference in the shape of the maximum region as recorded with the needle data (Fig. 4.6). This maximum region is more fully sampled by the epicardial sock, which indicates that the difference in shape is likely due to incomplete needle sampling of the region near the ICD coil. Placing more plunge needles near the ICD may provide more effective measurements of the potential field through the myocardium.

Other experimental design components may have affected the recorded potential field in ways that we could not observe with the data recorded in the study. One potential cause of error is the attenuation of the defibrillators used in the torso-tank experiment. Tissue under large electric fields can produce nonlinear effects, such as electroporation [27], that would not be present in these attenuated shocks. However, previous studies have not shown these nonlinear effects to be significant [13]–[15]. Similarly, the effect of perfusing the tissue on the resulting recordings was not clear from the study. Although the recordings from the one experiment that was perfused were different from those for the other three, the data are inadequate to determine whether these differences are due to perfusion, species, or device placement.

In addition to experimental considerations, some of the assumptions made about the simulation pipeline could produce differences in the measured and simulated potential field. One previously discussed possible source of error is the isotropic conductivity values used in the simulation [13]. Past studies have shown anisotropic conductivities are needed to accurately predict [15], [28] defibrillation potentials; however, high spatial sampling of the myocardial tissue during ICD shock shows local extrema, indicating that heteroge-

neous conduction may be occurring. More intricate modeling of the tissue heterogeneity in the myocardium, such as the vasculature or the conduction system, may be needed to accurately predict the potential field generated by defibrillators. Another possible source of simulation error includes the quasi-static assumption, which simplifies the computation of the potential field. The frequencies generated by the device are high enough that frequency responses from the tissue are expected [29].

The overall accuracy of the predicted potential fields compared to the measured values in these torso tank experiments provides important validation of the ability of our simulation pipeline to predict potentials fields and DFTs. Combined with past validation studies, [10], [13] these findings provide further support that the simulation of defibrillation can be effective as a patient-specific tool to facilitate defibrillator use or design, such as guiding new placements of ICDs in patients with abnormal or developing anatomies [10]. The accuracy and computational efficiency of the pipeline also provides a possibility for an immediate impact as a ICD implantation planning tool. The pipeline can also be used to test new device configurations, such as subcutaneous ICD implantations [11], or to identify trends in defibrillator behavior based on many varied parameters, such as patient size, structural variability, tissue conductivity, and many others. With this simulation tool, which is demonstrably accurate, clinicians and researchers can better understand defibrillators for both individual and general applications.

4.6 Conclusions

In this study, we found that our simulation pipeline can consistently predict accurate potential fields through the torso volume, including on the epicardial surface and through the myocardial volume, and can generate reasonable electric field probability distributions. We also found that the simulation can predict CMT metrics that are comparable to measured values. An expanded validation study using the torso-tank experimental preparation would provide further insight into the accuracy of the simulation, especially in predicting potential fields through the myocardium. The demonstrated accuracy of the simulation pipeline supports findings that show the feasibility of using the torso-tank experimental preparation to validate the defibrillation simulation in the myocardium and provides further general confidence in the simulation's usefulness in improving defibrilla-

tion therapy.

4.7 Acknowledgements

The research presented in this paper was made possible with help from Philip Ershler, Bruce Steadman, Alicja Booth, Nancy Allen, and Jayne Davis from the Cardiovascular Research and Training Institute (CVRTI) and the Nora Eccles Treadwell Foundation. Technical editing was provided by Christine Pickett. Defibrillator equipment used in this study was provided by Medtronic plc and Boston Scientific Corp. This project was supported by the National Institute of General Medical Sciences of the National Institutes of Health under grant number P41GM103545.

4.8 References

- [1] E. J. Benjamin, M. J. Blaha, S. E. Chiuve, M. Cushman, S. R. Das, R. Deo, S. D. de Ferranti, J. Floyd, M. Fornage, C. Gillespie, C. R. Isasi, M. C. Jimenez, L. C. Jordan, S. E. Judd, D. Lackland, J. H. Lichtman, L. Lisabeth, S. Liu, C. T. Longenecker, R. H. Mackey, K. Matsushita, D. Mozaffarian, M. E. Mussolino, K. Nasir, R. W. Neumar, L. Palaniappan, D. K. Pandey, R. R. Thiagarajan, M. J. Reeves, M. Ritchey, C. J. Rodriguez, G. A. Roth, W. D. Rosamond, C. Sasson, A. Towfighi, C. W. Tsao, M. B. Turner, S. S. Virani, J. H. Voeks, J. Z. Willey, J. T. Wilkins, J. H. Wu, H. M. Alger, S. S. Wong, and P. Muntner, "Heart disease and stroke statistics-2017 update: A report from the American Heart Association," *Circ.*, vol. 135, no. 10, pp. e146–e603, Mar. 2017.
- [2] M. Alexander, F. Cecchin, E. Walsh, J. Triedman, L. Bevilacqua, and C. Berul, "Implications of implantable cardioverter defibrillator therapy in congenital heart disease and pediatrics," *J. Cardiovasc. Electrophysiol.*, vol. 15, pp. 72–76, Jan. 2004.
- [3] F. Bokhari, D. Newman, M. Greene, V. Korley, I. Mangat, and P. Dorian, "Long-term comparison of the implantable cardioverter defibrillator versus amiodarone: Eleven-year follow-up of a subset of patients in the canadian implantable defibrillator study (CIDS)," *Circ.*, vol. 110, pp. 112–116, Jul. 2004.
- [4] G. Ristagno, T. Wang, W. Tang, S. Sun, C. Castillo, and M. H. Weil, "High-energy defibrillation impairs myocyte contractility and intracellular calcium dynamics," *Crit. Care Med.*, vol. 36, no. 11, pp. S422–S427, Nov. 2008.
- [5] C. Berul, J. Triedman, J. Forbess, L. Bevilacqua, M. Alexander, D. Dahlby, J. Gilkerson, and E. Walsh, "Minimally invasive cardioverter defibrillator implantation for children: an animal model and pediatric case report," *Pacing Clin. Electrophysiol.*, vol. 24, no. 12, pp. 1789–1794, Dec. 2001.
- [6] R. Lieberman, W. Havel, E. Rashba, P. DeGroot, K. Stromberg, and S. Shorofsky, "Acute defibrillation performance of a novel, non-transvenous shock pathway in adult ICD indicated patients," *Heart Rhythm J.*, vol. 5, no. 1, pp. 28–34, Jan. 2008.

- [7] G. H. Bardy, W. M. Smith, M. A. Hood, I. G. Crozier, I. C. Melton, L. Jordaeans, D. Theuns, R. E. Park, D. J. Wright, D. T. Connelly, S. P. Flynn, F. D. Murgatroyd, J. Sperzel, J. Neuzner, S. G. Spitzer, A. V. Ardashev, A. Oduro, L. Boersma, A. H. Maass, I. C. V. Gelder, A. A. Wilde, P. F. van Dessel, R. E. Knops, C. S. Barr, P. Lupo, R. Cappato, and A. A. Grace, "An entirely subcutaneous implantable cardioverter defibrillator," *New Eng. J. Med.*, vol. 363, no. 1, pp. 36–44, Jul. 2010.
- [8] A. Auricchio, H. Klein, C. Geller, S. Reek, M. Heilman, and S. Szymkiewicz, "Clinical efficacy of the wearable cardioverter-defibrillator in acutely terminating episodes of ventricular fibrillation," *Am J Cardiol*, vol. 81, no. 10, pp. 1253–1256, May 1998.
- [9] N. K. Wassnig, M. Gunther, S. Quick, C. Pfluecke, F. Rottstadt, S. J. Szymkiewicz, S. Ringquist, R. H. Strasser, and U. Speiser, "Experience with the wearable cardioverter-defibrillator in patients at high risk for sudden cardiac death," *Circ.*, vol. 134, no. 9, pp. 635–643, Aug. 2016.
- [10] M. Jolley, J. Stinstra, S. Pieper, R. MacLeod, D. H. Brooks, F. Cecchin, and J. K. Triedman, "A computer modeling tool for comparing novel ICD electrode orientations in children and adults," *Heart Rhythm J.*, vol. 5, no. 4, pp. 565–572, 2008.
- [11] M. Jolley, J. Stinstra, J. Tate, S. Pieper, R. MacLeod, L. Chu, P. Wang, and J. Triedman, "Finite element modeling of subcutaneous implantable defibrillator electrodes in an adult torso," *Heart Rhythm J.*, vol. 7, no. 5, pp. 692–698, May 2010.
- [12] M. Jolley, J. Stinstra, S. Pieper, R. MacLeod, D. Brooks, F. Cecchin, and J. Triedman, "A computer modeling tool for comparing novel ICD electrode orientations in children and adults," *Heart Rhythm J.*, vol. 5, no. 4, pp. 565–572, Apr. 2008.
- [13] J. Tate, J. Stinstra, T. Pilcher, A. Poursaid, M. A. Jolley, E. Saarel, J. Triedman, and R. S. MacLeod, "Measuring defibrillator surface potentials: The validation of a predictive defibrillation computer model," *Comp. in Biol. & Med.*, vol. 102, pp. 402 – 410, 2018.
- [14] D. B. Jorgenson, P. H. Schimpf, I. Shen, G. Johnson, G. H. Bardy, D. R. Haynor, and Y. Kim, "Predicting cardiothoracic voltages during high energy shocks: Methodology and comparison of experimental to finite element model data," *IEEE Trans. Biomed. Eng.*, vol. 42, no. 6, p. 559, Jun. 1995.
- [15] F. Claydon, T. Pilkington, A. Tang, M. Morrow, and R. Ideker, "Comparison of measured and calculated epicardial potentials during transthoracic stimulation," in *IEEE EMBS 10th Ann. Intl. Conf.* New Orleans, Louisiana, USA: IEEE Press, 1988, pp. 206–207.
- [16] B. Rodriguez, L. Li, J. Eason, I. Efimov, and N. Trayanova, "Differences between left and right ventricular chamber geometry affect cardiac vulnerability to electric shocks," *Circ. Res.*, vol. 97, no. 2, pp. 168–175, Jul. 2005.
- [17] S. Shome and R. MacLeod, "Simultaneous high-resolution electrical imaging of endocardial, epicardial and torso-tank surfaces under varying cardiac metabolic load and coronary flow," in *Functional Imaging and Modeling of the Heart*, ser. Lecture Notes in Computer Science 4466. Berlin, Heidelberg, Germany: Springer-Verlag, 2007, pp. 320–329.

- [18] M. Milanic, V. Jazbinsek, R. Macleod, D. Brooks, and R. Hren, "Assessment of regularization techniques for electrocardiographic imaging," *J. Electrocardiol.*, vol. 47, no. 1, pp. 20–28, Jan.-Feb. 2014.
- [19] R. MacLeod, B. Taccardi, and R. Lux, "Electrocardiographic mapping in a realistic torso tank preparation," in *Proc. IEEE EMBS 17th Ann. Intl. Conf.* IEEE Press, 1995, pp. 245–246.
- [20] R. E. Ideker, P. D. Wolf, C. Alferness, W. Krassowska, and W. M. Smith, "Current concepts for selecting the location, size and shape of defibrillation electrodes," *PACE*, vol. 14, no. 2 Pt 1, p. 227, Feb. 1991.
- [21] R. MacLeod, D. Weinstein, J. D. de St. Germain, D. Brooks, C. Johnson, and S. Parker, "SCIRun/BioPSE: Integrated problem solving environment for bioelectric field problems and visualization," in *IEEE Intl. Symp. Biomed. Imag. (ISBI)*, IEEE. Arlington, VA, USA: IEEE Press, 2004, pp. 1–3.
- [22] P. Torr and A. Zisserman, "MLESAC: A new robust estimator with application to estimating image geometry," *J. Comp. Vision and Image Understanding*, vol. 78, no. 1, pp. 138–156, Jul. 2000.
- [23] P. Besl and N. McKay, "A method for registration of 3-D shapes," *IEEE Trans. Pat. Anal. & Mach. Intellig.*, vol. 14, no. 2, pp. 239–256, Feb. 1992.
- [24] M. Callahan, M. Cole, J. Shepherd, J. Stinstra, and C. Johnson, "BioMesh3D: A meshing pipeline for biomedical models," University of Utah, SCI Institute Technical Report UUSCI-2007-009, 2007. [Online]. Available: <http://www.sci.utah.edu/publications/SCITechReports/UUSCI-2007-009.pdf>
- [25] H. Si, "Tetgen, a delaunay-based quality tetrahedral mesh generator," *ACM Trans. Math. Softw.*, vol. 41, no. 2, pp. 11:1–11:36, Feb. 2015. [Online]. Available: <http://doi.acm.org/10.1145/2629697>
- [26] D. Swenson, J. Levine, R. Whitaker, and R. MacLeod, "Impacts of conformal meshing on electrical cardiac simulation," in *21st International Meshing Round Table*, San Jose, CA, USA, 2012.
- [27] J. L. Jones, R. E. Jones, and G. Balasky, "Microlesion formation in myocardial cells by high-intensity electric field stimulation," *Am. J. Physiol.*, vol. 253, no. 2 Pt 2, pp. H480–6, Aug. 1987.
- [28] N. Trayanova, K. Skouibine, and F. Aguel, "The role of cardiac tissue structure in defibrillation," *Chaos*, vol. 8, no. 1, pp. 221–233, Mar. 1998.
- [29] T. Ashihara and N. A. Trayanova, "Asymmetry in membrane responses to electric shocks: insights from bidomain simulations," *Biophys. J.*, vol. 87, no. 4, pp. 2271–2282, Oct. 2004.

CHAPTER 5

MEASURING DEFIBRILLATOR SURFACE POTENTIALS: THE VALIDATION OF A PREDICTIVE DEFIBRILLATION COMPUTER MODEL

In response to the lack of clinical validation of defibrillation simulation, this chapter presents research performed as described in the third aim: record human body-surface shock potentials during clinical procedures to validate a defibrillation simulation pipeline. The following paper was accepted for publication in *Computers in Biology and Medicine* journal in August 2018 as part of the 2018 Symposium on Quantitative Cardiology (DOI link: <https://doi.org/10.1016/j.combiomed.2018.08.025>). The typeset version is included here with permission.

ARTICLE IN PRESS

Computers in Biology and Medicine xxx (xxxx) xxx-xxx



Contents lists available at ScienceDirect

Computers in Biology and Medicine

journal homepage: www.elsevier.com/locate/compbioemed

Measuring defibrillator surface potentials: The validation of a predictive defibrillation computer model

Jess Tate^{a,b,*}, Jeroen Stinstra^{a,b}, Thomas Pilcher^c, Ahrash Poursaid^{a,b}, Matthew A. Jolley^d, Elizabeth Saarel^c, John Triedman^e, Rob S. MacLeod^{a,b}

^a Department of Bioengineering, University of Utah, Salt Lake City, USA^b Scientific Computing and Imaging Institute, University of Utah, Salt Lake City, USA^c Division of Pediatric Cardiology, University of Utah, Salt Lake City, USA^d Department of Anesthesiology and Critical Care Medicine, Children's Hospital of Philadelphia, Philadelphia, USA^e Department of Cardiology, Children's Hospital Boston, Boston, Massachusetts, USA

ARTICLE INFO

ABSTRACT

Keywords:
 Defibrillation
 Patient-specific modeling
 Limited lead selection
 Body surface mapping
 Defibrillation threshold
 Defibrillation modeling

Implantable cardioverter defibrillators (ICDs) are commonly used to reduce the risk in patients with life-threatening arrhythmias, however, clinicians have little systematic guidance to place the device, especially in cases of unusual anatomy. We have previously developed a computational model that evaluates the efficacy of a delivered shock as a clinical and research aid to guide ICD placement on a patient specific basis. We report here on progress to validate this model with measured ICD surface potential maps from patients undergoing ICD implantation and testing for defibrillation threshold (DFT). We obtained body surface potential maps of the defibrillation pulses by adapting a limited lead selection and potential estimation algorithm to deal with the limited space for recording electrodes. Comparison of the simulated and measured potential maps of the defibrillation shock yielded similar patterns, a typical correlation greater than 0.9, and a relative error less than 15%. Comparison of defibrillation thresholds also showed accurate prediction of the simulations. The high agreement of the potential maps and DFTs suggests that the predictive simulation generates realistic potential values and can accurately predict DFTs in patients. These validation results pave the way for use of this model in optimization studies prior to device implantation.

1. Introduction

Implantable cardioverter defibrillators (ICDs) are used to prevent fatal arrhythmias [1–4], with approximately 100,000 implantations each year [5]. Typically, these devices are designed for use in adults and implantation follows standardized techniques; however, neither the device nor the placement has been optimized for children or persons with abnormal cardiac anatomies or other congenital defects [6]. As a result, there is a rise in alternate configurations, such as eliminating the lead placed in the subclavian vein or placing the ICD generator in the abdomen instead of the left upper chest. Each configuration seeks to maximize the efficiency of the device and ensure safety for the patient [7]. A further motivation for exploring alternative ICD placement strategies are studies that associate negative consequences to either unnecessary or over-strength shocks. One study has shown that the discharge of the ICD can alter the Ca^{++} dynamics of cardiac tissue, which may inhibit normal cell contraction, especially if the shock uses

more energy than necessary [8]. Such risks have motivated new implantation strategies for ICDs, including subcutaneous implantation [9–15] and wearable external defibrillation devices [16–19]. With each new approach comes the need for optimization and testing, which can impede development, especially when each step requires animal and/or human experiments.

Mathematical modeling and computer simulation can efficiently accelerate the process of optimizing and testing of ICDs; to this end, we have developed a computational simulation pipeline that generates a patient-specific defibrillation model. With this pipeline, we can predict the potential field throughout the torso during defibrillation and estimate the defibrillation threshold (DFT), *i.e.*, the lowest level of energy needed for defibrillation, for any given device design, implantation, and patient [20–23]. In previous studies, this simulation pipeline has shown accuracy in predicting the threshold energy required for successful defibrillation [22]. However, our previous validation studies have been limited in their level of detail and complexity. We were able to compare

* Corresponding author. Department of Bioengineering, University of Utah, Salt Lake City, USA.
 E-mail addresses: jess@sci.utah.edu, jess.tate@utah.edu (J. Tate).

<https://doi.org/10.1016/j.compbioemed.2018.08.025>

Received 28 June 2018; Received in revised form 24 August 2018; Accepted 24 August 2018
 0010-4825/ © 2018 Elsevier Ltd. All rights reserved.

ARTICLE IN PRESS

J. Tate et al.

Computers in Biology and Medicine xxx (xxxx) xxxx-xxxx

holistic values such as the DFT, but could not evaluate how well the model predicted the actual distribution of potential over the heart and thorax. A more comprehensive verification requires comparison of our simulation to empirical data, ideally from clinical tests. To acquire such data in clinical studies, we have developed a method of measuring the body surface potential maps (BSPMs) generated by ICDs in humans.

The standard testing process that follows each ICD implantation provided the natural setting in which to acquire BSPMs during defibrillation shocks. Following implantation, the ICD is tested by inducing fibrillation in the patient and allowing the device to sense the arrhythmia and deliver a defibrillation shock to restore sinus rhythm. These test shocks provide a rare opportunity to record the ICD potential maps in patients. Although BSPM is a well established technique [24–28], using it during defibrillation and in the catheterization laboratory environment requires additional consideration to allow space on the torso surface for the sterile implantation region, the external defibrillation pads, and other instruments for the safety of the patient. Consequently, there is a highly limited and variable area of the torso surface that is available for the placement of validation BSPM lead systems. Fortunately, there are algorithms that use the spatial redundancy of potential recordings to estimate full torso surface potentials from a small number of electrodes [29–31].

In this study, we applied what is known as a limited lead selection and body surface estimation algorithm developed by Lux et al. [31–33] to deal with the restricted access to the torso surface. We adapted this algorithm for use with ICD potentials by training it with 3870 sets of simulated defibrillation potentials that included different human torso geometries and also a wide range of realistic ICD placement locations. We also validated the resulting estimation technique on a small set of patient geometries.

With these novel techniques, we were able to gather BSPMs and DFT from patients receiving an ICD implantation and compare them to the results of patient-specific simulations. The results reported here establish the ability to accurately reconstruct ICD potential maps from both measurements and simulations, show a strong correlation between them, and demonstrate similar accuracy between simulated and actual DFTs.

2. Methods

In order to validate the defibrillation simulation pipeline, we measured body-surface potentials during ICD shocks and the DFTs of patients who underwent ICD implantation and compared these data to those predicted by the simulation. The validation, therefore, consisted of three stages: adapting a limited lead selection and body surface estimation algorithm for use with ICD potential maps, recording ICD potential maps and DFTs for each patient, and generating the patient-specific model for each patient to predict the potential field and DFT to compare them to the recorded values.

2.1. Body surface potential estimation of ICD shocks

We adapted a previously published limited lead selection and body-surface potential estimation algorithm [31] for measuring body surface potentials during ICD implantation surgery. Fig. 1 illustrates the application of the algorithm, which is composed of two processes. The first process is limited lead selection, which consists of finding the optimal lead set for estimation by finding the most statistically unique locations one at a time until the desired number of leads (32 in our case) are found [31]. We applied additional spatial constraints imposed by the implantation surgery, the sterile area, and the area covered by the external defibrillator pads (Fig. 2), by removing from consideration the locations covered by these areas. From the resulting limited lead set, we modified the locations to fit regular strips of four leads for easier fabrication and application (Fig. 2). The second process, body-surface potential estimation, determines the linear transform that predicts from

the potentials measured with the lead set the potentials on the rest of the torso (Fig. 1). This relationship is found from the covariance matrix of the training potential maps and is represented as a transformation matrix. This matrix is multiplied by the potential recordings from the 32 limited-lead locations to yield the full estimated potential map. While our modeling approach could generate potential maps at any time step, we used the relatively stable peak of the ICD pulse to allow for direct comparison with measurements. Implementing these two processes requires a database of potential maps to provide the statistical information needed to create a limited lead mapping system.

For both these first two processes, we used a database of simulated potential maps generated using our defibrillation simulation pipeline [22] from a combination of 9 patient geometries, 43 tissue conductivity schemes, and 10 ICD placement geometries. Each of the resulting 3870 simulated potential fields was sampled at the same 370 body-surface locations to meet the requirements of the algorithm. These three parameters, i.e., patient geometry, tissue conductivities, and ICD placement, were chosen to represent the range of such parameters expected in patients. Previous studies [6,23,34–37] and our own preliminary simulation results showed that these parameters could be expected to affect the BSPM and DFTs consistent with bioelectric principles of conduction through an isotropic volume conductor. We tested the ability of the limited leads and estimation algorithm to reconstruct potentials on a separate database of simulated potential maps. This test dataset was generated with same 9 geometries, but a different set of 20 conductivity schemes and 10 different ICD placement geometries for a total of 1800 potential maps representing the peak of the ICD pulse. The simulated potentials were sampled at the limited lead set locations, and the previously calculated transformation matrix was applied to generate the full estimated torso potentials. The quality of the estimation was evaluated with absolute error, correlation (ρ), relative error (RE), and normalized RMS error (\bar{E}). We first evaluated the result of the estimation algorithm using an increasing number of leads from 5 to 100 to determine the number of leads required for acceptable estimation error. We also tested the sensitivity of the algorithm to changes in electrode location by evaluating the level of error from a variety of lead sets chosen to represent the placement variation likely to occur in the catheterization laboratory setting.

2.2. Recording surface potentials

We recorded the body surface potential maps from test shocks during standard ICD implantation surgery and testing. Table 1 lists each of the subjects used in the study with their weight, the device which was implanted, and geometric abnormalities. Surface recording electrodes (32 plus 2 electrodes for ground and reference) were applied to each subject as closely as possible to the locations described in Fig. 2 after intubation but before surgery. The surface potentials during each biphasic test shock were recorded using a 32-channel customized recording system (CVRTI, University of Utah) at 1 kHz or 4 kHz sampling rates. Ag/AgCl electrodes were used to mitigate the effects of electrode polarization on the measured potentials. To accommodate the large shock voltages (up to ~ 750 V) in a system originally constructed for ECG acquisition, we added attenuation by a factor of 10^4 using a voltage divider on each channel. Faulty leads were identified by the signal-to-noise ratio or pulse morphology and eliminated. The potentials for reconstruction were identified as the value at the first peak of the ICD pulse. The potential map was estimated using the transformation matrix described in Section 2.1, and compared to the simulated maps for each patient. Quantitative evaluation was by the same metrics as described in Section 2.1. The measured potentials from the 32-lead set were also compared to the simulated surface potentials and evaluated with the same metrics. The resulting error metrics are presented as mean \pm standard deviation.

ARTICLE IN PRESS

J. Tate et al.

Computers in Biology and Medicine xxx (xxxx) xxxx-xxxx

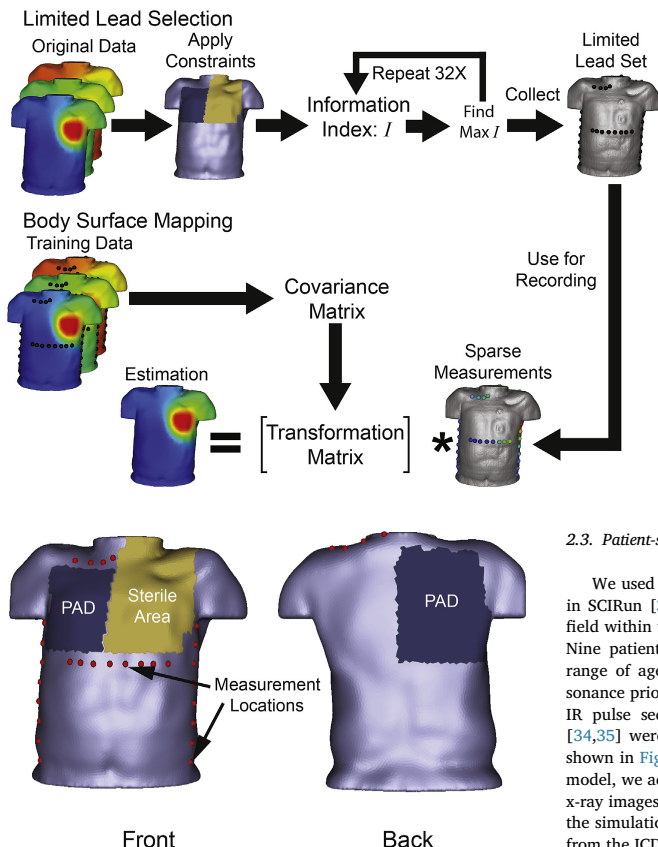


Fig. 2. The optimal locations for measuring and from which to estimate full body surface maps during implantation surgery (red dots). The dark gray areas are generally covered by the external defibrillator pads, and the tan area indicates the sterile field where the device is implanted. (For interpretation of the references to colour in this figure legend, the reader is referred to the Web version of this article.)

Table 1

List of patients in the study with the ICD device manufacturer and geometric information. Acronyms are: atrioventricular septal defect (AVSD), left ventricle (LV), ventricular septal defect (VSD), pulmonary valve (PV).

age	weight	device	geometric abnormalities
6 years	25 kg	Medtronic Virtuoso II DR	Normal Anatomy
8 years	36 kg	Medtronic Virtuoso II DR	Normal Anatomy, Long QT
9 years	35 kg	St. Jude Promote	Prosthetic MV, repaired AVSD, LV dilation
15 years	46 kg	Medtronic Virtuoso II DR	Repaired AVSD, Scoliosis, Spinal Rods
16 years	65 kg	St. Jude Current DR	Normal Anatomy
17 years	70 kg	St. Jude Current DR	Aortic Atresia, Repaired VSD, Cardiac Reconstruction
17 years	60 kg	Medtronic Virtuoso II DR	Cardiac Reconstruction, Scoliosis
29 years	85 kg	St. Jude Unify	Tetralogy of Fallot, PV Homograft
32 years	60 kg	Medtronic Virtuoso II DR	Tetralogy of Fallot

Fig. 1. Application of the limited lead selection and the body surface estimation algorithm from Lux et al. [31]. Original Data are body-surface potentials simulated from realistic ICD placements, and the Constraints are those imposed by the device implantation procedure. Lead selection follows iteratively to create reduced, constrained leadsets that we then used to create the estimation transform contained in the Transformation Matrix. Sparse Measurements are those signals acquired during each procedure.

2.3. Patient-specific simulation

We used the patient-specific simulation pipeline [22] implemented in SCIRun [38,39] (<http://www.scirun.org>) to simulate the potential field within the torso and predict the DFT of each patient in the study. Nine patients identified as candidates for ICD implantation, with a range of ages from 6 to 32 years, were imaged using magnetic resonance prior to implantation using a 1.5 T MRI scanner with a double IR pulse sequence. From these scans, segmentations of 11 tissues [34,35] were generated using Seg3D [40] (<http://www.seg3d.org>) as shown in Fig. 3, which provided torso geometries. Into this geometric model, we added the location of the implanted ICD from postoperative x-ray images. The torso and ICD geometries were then used as inputs in the simulation pipeline to predict the potential field through the body from the ICD for each shock level recorded for the patient. An example of how to run this simulation can be found on the SCIRun-Exchange (<https://github.com/SCIIInstitute/SCIRun-Exchange>). The calculated potentials were sampled at the same 370 points for which we measured/estimated the shock potentials (Section 2.2) and were compared

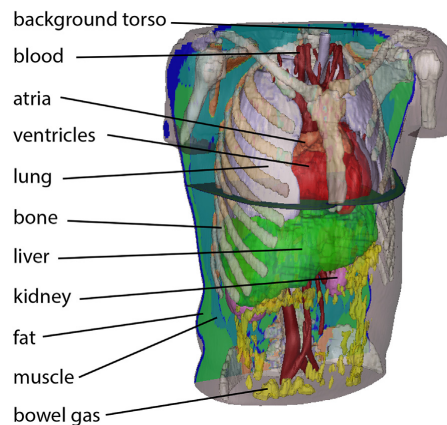


Fig. 3. 11 segmented tissue types included in the defibrillation simulation pipeline.

ARTICLE IN PRESS

J. Tate et al.

Computers in Biology and Medicine xxx (xxxx) xxxx-xxxx

using the same metrics as for the other map errors. The DFT corresponding to the ICD geometry was also calculated for each patient using the critical mass hypothesis, which holds that 95% of the ventricular myocardium must have an electric field above 5 V/cm for successful defibrillation [41]. The predicted DFTs were also compared with the clinically derived biphasic DFTs of each patient.

2.4. Collecting patient data

All patient data used in this study was collected with informed consent and under the direction of the local institutional review board of Primary Children's Medical Center at the University of Utah.

3. Results

The results presented in this section demonstrate the ability of the simulation pipeline to recreate ICD potential and DFT values measured in the clinical setting. We show the results of four comparisons: known simulated potential maps to those estimated using the limited lead set and training data, body-surface recordings at approximately 32 recording locations to simulated values at the same locations, potential maps estimated from the measured body-surface potentials to simulated surface potential maps, and predicted DFT to clinically measured DFT.

3.1. Reconstruction of simulated surface potentials

When tested against simulated body-surface shock potentials, the limited lead selection and estimation algorithm showed a low error and a high correlation. The limited lead sites preferred by the algorithm tended to be locations as close to the ICD device and active coils as possible. When unconstrained, the majority of the selected leads were on the left, anterior chest. With constraints there was a high concentration of leads on the shoulders, along the mid-axillary lines, and near the xiphoid process. The error of the estimations as a function of number of leads demonstrated a general exponential reduction as shown in Fig. 4. The minimum ρ for five or more leads was 0.993, the maximum RE was 1.8%, and the maximum \bar{E} was 4.6%. Although the correlation changed very little with the number of leads used, the improved values for RE and \bar{E} indicate substantial benefits are possible up to approximately 60 leads. The error did not significantly decrease when using more than 60 electrodes at which point the $\rho = 0.999$, $RE = 0.47\%$, and $\bar{E} = 2.2\%$. The error using 32 electrodes was acceptably low with a ρ of 0.997, RE of 0.88%, and \bar{E} of 3.1%.

The body surface estimation algorithm exhibited high accuracy when using a variety of lead sets when comparing estimated and simulated potential maps. The error was lowest using the unconstrained lead set, with a ρ of $0.99991 \pm 7 \times 10^{-5}$, a \bar{E} of $0.5 \pm 0.1\%$, RE of $0.02 \pm 0.02\%$, and a mean maximum error of $19 \pm 9\text{ V}$. Using the chosen clinical lead set reduced the accuracy, yet the metrics should very high accuracy with a high ρ ($0.999 \pm 2 \times 10^{-3}$), low \bar{E} ($1.6 \pm 0.7\%$), and low RE ($0.3 \pm 0.4\%$) between the estimated and simulated potential maps. The mean maximum error of the estimation

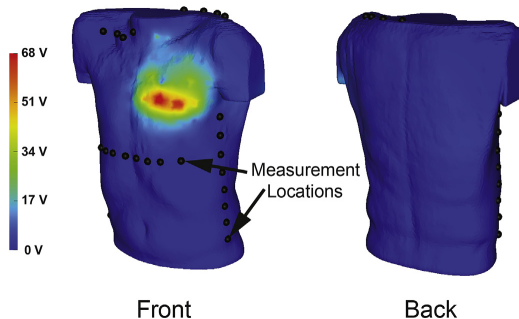


Fig. 5. Typical absolute error between actual and reconstructed potentials by location from a shock with 500 V magnitude.

was $68 \pm 39\text{ V}$ on shocks of 500 V. Comparing Fig. 5 shows the typical distribution of error, with highest values near the left upper chest, where the ICD was placed. The accuracy of estimated surface potentials was not sensitive to changes in the limited lead set, both in location and number of leads. The reconstruction of the lead set with the greatest error, based on the location and the number of the leads, did not change the mean \bar{E} more than 0.9%, the mean RE more than 0.3%, and the mean ρ more than 2×10^{-3} . These changes in the error metrics are within the standard deviation of the metrics from the limited lead set, with the exception of \bar{E} , which was slightly higher than the standard deviation.

3.2. Surface potential comparison

Comparison of the potentials measured at the lead locations against those from patient-specific simulation showed high correlation, with a varied RE and \bar{E} , which ranged from 5.8 to 47.3% and 8.1–23.1% respectively. As shown in Table 2, the mean ρ , RE , and \bar{E} were 0.97 ± 0.02 , $20 \pm 11\%$, and $15 \pm 4\%$, respectively. Comparing the potentials and the absolute error at the leads marked with black spheres in Fig. 6 also shows that the simulated potentials were generally lower in amplitude than the measured potentials.

The body surface estimation algorithm was effective in generating potential maps of ICD discharges that are qualitatively and quantitatively similar to the maps from the patient-specific simulation. Fig. 6 shows a comparison between the estimation from the ICD surface recordings and the patient-specific simulation. Qualitatively, the potential maps are similar, but there are regions of high error near the left, superior chest where the device was located. The quantitative comparison between the reconstruction and simulation also showed high accuracy, as listed in Table 3. The ρ for each shock was above 0.96, with a mean of 0.99 ± 0.01 from 29 shocks. Similarly, the RE was low for all shocks with a mean of $13 \pm 9\%$. The normalized \bar{E} demonstrated a similar level of accuracy of $6 \pm 2\%$.

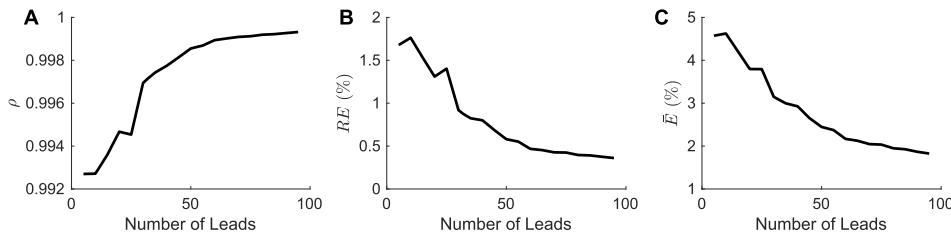


Fig. 4. Mean estimation accuracy as the number of leads used in estimation algorithm was increased. Error is expressed by A) correlation (ρ), B) relative error (RE), and C) normalized RMS error (\bar{E}).

Table 2

Metrics of comparison of the limited lead recordings and the simulated potentials at the corresponding location. Each row contains the results from a single test shock and there were variable numbers of test shocks from each subject.

Subject age	shock max	ρ	RE	\bar{E}
6 yo	216 V	0.96	37.9%	19.2%
	279 V	0.956	42.8%	20.5%
8 yo	279 V	0.959	12.3%	13.4%
	395 V	0.962	10.6%	12.4%
	483 V	0.977	5.83%	8.07%
9 yo	624 V	0.962	11.6%	13.1%
	405 V	0.974	27.9%	18.8%
	573 V	0.972	25.8%	18%
15 yo	216 V	0.991	10.4%	10.1%
	279 V	0.991	13.2%	11.5%
	395 V	0.991	10.8%	10.4%
16 yo	483 V	0.991	13.9%	11.7%
	395 V	0.938	26.7%	18%
	583 V	0.93	19%	14.2%
17 yo	286 V	0.976	32.2%	22.3%
	405 V	0.976	26.3%	20.2%
	496 V	0.976	35.4%	23.1%
17 yo	483 V	0.978	16.3%	13.6%
	624 V	0.975	15.9%	13.2%
	738 V	0.976	13.5%	12.4%
29 yo	405 V	0.948	11%	9.81%
	496 V	0.944	11.2%	10.1%
	573 V	0.949	10.7%	9.67%
32 yo	701 V	0.936	12.8%	10.9%
	279 V	0.983	25.8%	15.8%
	395 V	0.983	25.9%	16.2%
	432 V	0.982	47.3%	21.4%
	624 V	0.983	19.7%	14.4%
	738 V	0.983	19.8%	14.2%
mean	458 V	0.969	20.4%	14.7%

Fig. 7 shows the mean and standard deviation of the accuracy metrics for each patient as a condensed visualization of the information in Tables 2 and 3. This figure compares the accuracy of the simulation using both the full torso maps and the subsets for each patient form which we obtained measured signals. In general, the error is higher between the recorded potentials and the simulated potentials for the subset of the measured locations than in the full potential maps, however, the accuracy of the simulation varies among patients.

3.3. DFT comparison

Table 4 shows the comparison between the clinically determined DFTs and the predicted DFTs. The predictions for the 6-, 9-, 16-, and 29-year-old patients were within the range of the clinically determined DFTs, indicating a high predictive accuracy for these patients. The 8-, 15-, 17-, and the 32-year-old patients demonstrated predicted DFT outside the clinically determined DFT range but typically by less than 2 J, which is less than or equal to the range tested for each patient. The highest difference in predicted and observed DFTs was recorded for the first 17-year-old patient. This difference was nearly double the observed range (~ 10 J).

4. Discussion

The results presented in this paper demonstrate three major findings: a) that the limited lead selection and estimation algorithm can be applied with high accuracy to capture the shock potential over the entire torso, b) that patient-specific simulation of defibrillation can generate surface potentials that are qualitatively and quantitatively similar to those obtained in measurements, and c) that simulations can predict DFT values comparable to those found clinically. These findings support the effectiveness of our simulation pipeline in predicting

defibrillation in humans.

This study contains a new application of a well established approach, using limited lead selection and a body-surface potential reconstruction algorithm to estimate potential maps during ICD shocks. The lead selection algorithm suggested electrode placement locations that were as close as feasible to the electrical sources and sinks (the ICD and active leads), which is similar to findings using the same approach to identify limited leads to capture cardiac sources [31]. We found that the number of leads for which the error statistics became stable was approximately 60, compared to 30 found in Lux et al. [31,42]. However, the error using 30 leads to measure ICD shocks was still acceptably low (Fig. 4), supporting our decision to use existing 32-lead acquisition systems. Another important finding was that the estimation was insensitive to changes in the specific limited lead set identified by the algorithm, which allowed us to add clinically dictated constraints on electrode placement, constraints that varied from case to case. A final finding was that using simulations of defibrillation to create the training data to identify viable limited leadsets was successful. Our results are supported by a previous application of the limited lead and estimation approach in the setting of activation mapping on the epicardium of the heart from leads located in the coronary veins [43]. All these results support the utility and robustness of this approach and encourage further applications.

This study also provides unique and compelling validation of the utility of simulation to predict defibrillation potentials in a patient specific manner. The comparison between simulated and measured values exhibited a high correlation, demonstrating that the simulation predicted generally accurate spatial distributions of defibrillation potentials. The level of normalized \bar{E} and the correlation associated with the subset comparisons were similar to those from animal validation experiments in which an ICD was discharged *in situ* and potentials measured at several locations in the torso [41]. Also, the full potential maps estimated from recorded potentials were qualitatively and quantitatively similar to simulated potential maps (Section 3.2, Figs. 6 and 7). The errors in the comparison of the full maps were lower than those for the comparison of only the measured potentials, indicating that the estimation algorithm itself may contribute to reducing the error. A possible reason for this improvement is that the estimation algorithm captures features of the simulated defibrillation potentials, driving the estimation closer to the simulated distributions and improving the accuracy. Despite the possible bias, using estimated potential maps for evaluation allows for potential field comparison at locations on the torso that are likely impossible to directly record with contact electrodes, most notably near the ICD device, which is the location with the highest potentials amplitudes. However, Tables 2 and 3 show that high accuracy in comparisons with only the measured potentials generally correlates to high accuracy in the predicted full potential maps, indicating that the potential maps are driven by the recorded potentials.

A comparison of clinical and simulated DFTs further supports the accuracy of the simulation at the same time as it provides insight into the limitations of the model (Section 3.3). Generally, there was high agreement between the predicted and observed DFTs, which is similar to our previous findings [22]. However, there was a notable exception with one of the 17-year-old patients. This patient experienced the highest error in DFT comparison (Table 4), the highest potential map RE (Fig. 7), and a high \bar{E} . A possible explanation for this exceptional result is that the cardiac anatomy of this patient was vastly different from normal due to major cardiac reconstruction of the atria, which could have significantly altered both the myocardium and scar tissue near the heart to affect the DFT. We chose this case to explore (albeit superficially) the impact of heart conductivity on the DFT and found that by reducing conductivity by a factor of 10, the DFT dropped to a value of 9.1 J, within the measured range, indicating that there may also be underlying tissue conductivity changes, such as scar formation or fibrosis, in addition to geometric changes that may need to be included in the model. A further potential source of error in predicting

ARTICLE IN PRESS

J. Tate et al.

Computers in Biology and Medicine xxx (xxxx) xxxx–xxx

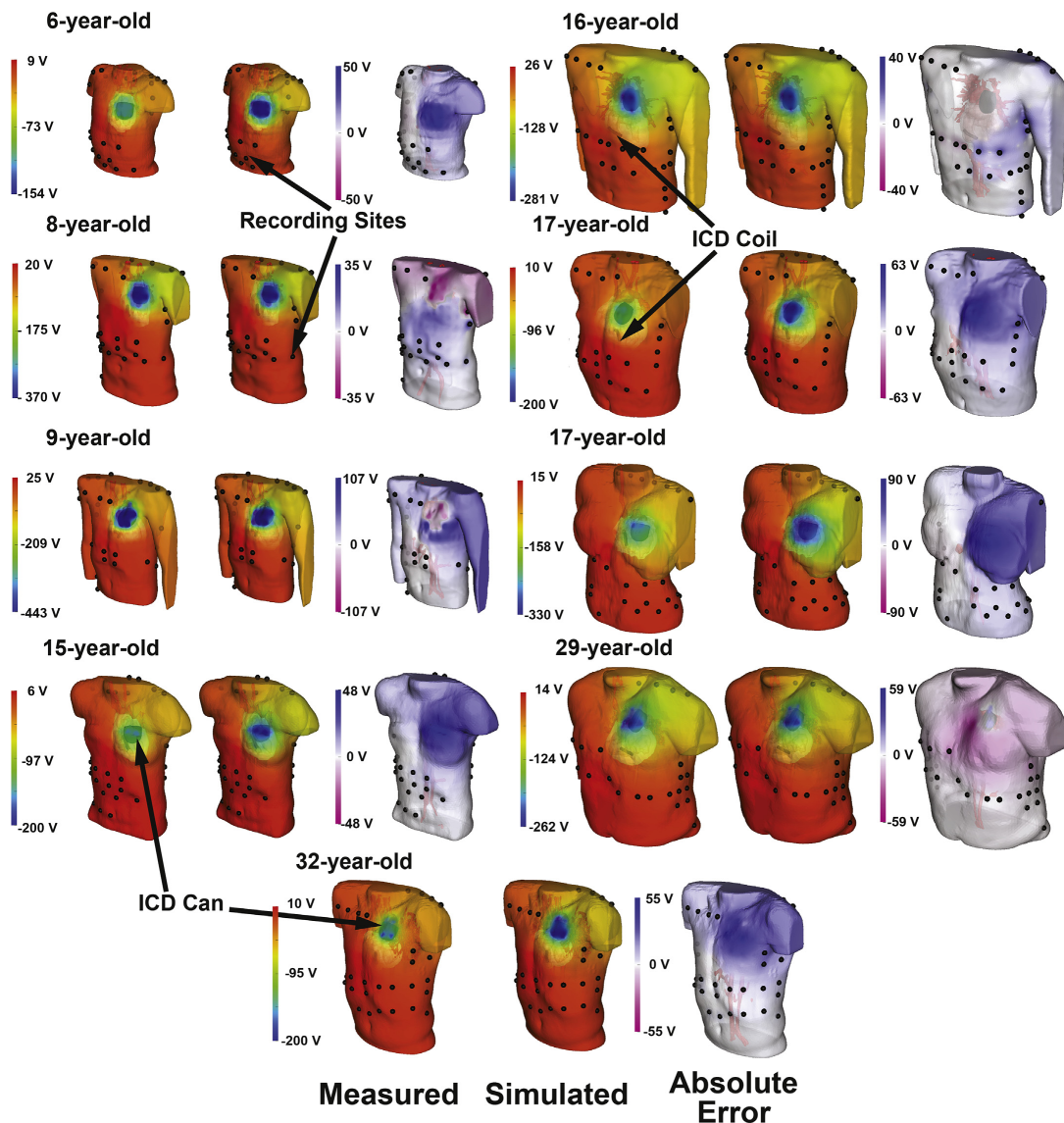


Fig. 6. Surface potential comparison between the reconstruction obtained from surface recordings and the original, patient specific simulation. The results show a single shock for all 9 subject and include the limited leads (black circles) selected during the ICD implantation for each subject. The absolute error is included for each patient.

DFTs comes from Rantner et al. [44], who questioned the ability of the critical mass hypothesis [45] to accurately predict defibrillation. Although they tested only one case, our single outlier case may provide further evidence that in some patients, the critical mass hypothesis may not be sufficient to predict the effect of defibrillation. This one case does not diminish the importance of the finding that the direct comparisons of DFTs predicted DFTs close to clinically observed values for all other patients (Table 4). With such high accuracy, we can show that in at least a substantial proportion of our cases, the critical mass hypothesis

used in our model could accurately predict DFT.

We do not claim that these results support the critical mass hypothesis as an underlying explanation of the mechanisms of defibrillation, but rather aimed to apply it as an efficient estimation tool to calculate DFTs and measure the effectiveness of defibrillation. There are other mechanistic explanations that more completely explain many of the more intricate tissue behaviors during defibrillation, such as the virtual electrode hypothesis [46]. Calculating the DFT with these other underlying assumptions often require computationally costly methods

ARTICLE IN PRESS

J. Tate et al.

Computers in Biology and Medicine xxx (xxxx) xxxx–xxx

Table 3

Metrics relating the simulated potential maps to the maps generated from the surface recordings. Each row contains the results from a single test shock and there were variable numbers of test shocks from each subject.

Subject age	shock max	ρ	RE	\bar{E}
6 yo	216 V	0.991	18.6%	9.0%
	279 V	0.982	26.9%	10.8%
8 yo	279 V	0.967	6.5%	5.1%
	395 V	0.97	6.0%	4.8%
9 yo	483 V	0.996	1.0%	2.0%
	624 V	0.967	7.0%	5.0%
15 yo	405 V	0.985	6.28%	4.16%
	573 V	0.976	6.19%	3.94%
16 yo	216 V	1.000	6.8%	5%
	279 V	0.999	10.9%	6.3%
17 yo	395 V	0.998	12.9%	6.9%
	483 V	0.998	16.8%	7.9%
17 yo	395 V	0.978	7.8%	5.0%
	583 V	0.964	7.3%	4.5%
29 yo	286 V	0.996	23.5%	7.7%
	405 V	0.996	22.9%	7.7%
29 yo	496 V	0.995	31.2%	8.8%
	483 V	0.997	15.2%	7.7%
29 yo	624 V	0.998	12.1%	6.7%
	738 V	0.994	13.5%	7.2%
32 yo	405 V	0.994	2.0%	2.5%
	496 V	0.99	2.2%	2.7%
32 yo	573 V	0.988	2.7%	2.9%
	701 V	0.978	4.6%	3.5%
mean	279 V	0.994	15.3%	5.2%
	395 V	0.992	18.4%	5.7%
mean	432 V	0.988	30.2%	7.0%
	624 V	0.99	19.3%	6.0%
mean	738 V	0.987	20.5%	6.1%
	458 V	0.990	12.9%	5.6%

such as bidomain simulation with active cell models to describe both the fibrillation and defibrillation wave-fronts and test multiple shock amplitudes for each ICD placement for success [44,47,48]. However, in the setting of guiding a clinical decision about ICD placement or settings it is necessary to be able to rapidly, ideally within seconds, evaluate many configurations, which, in turn, requires the efficiency of an approach like estimating DFTs based on the critical mass hypothesis. We welcome further progress in identifying new, efficient metrics of defibrillation and our computational pipeline is flexible enough to incorporate such improvements.

The occasional disparity of the error metrics in this study reveal the recurring challenge of comparing complex, three and four-dimensional results, of defining error metrics that capture the features that are most relevant to how the results will be used. For instance, there is an order of magnitude difference between the amplitudes of many of the measured potentials, differences not always reflected in the simulations and likely a product of controllable measurement error. Such amplitude

Table 4

Comparison of the DFTs found during clinical testing and predicted by simulation via the critical mass hypothesis. Biphasic pulses were used in clinical defibrillation testing and the peak electric field from both phases was used to satisfy the critical mass hypothesis for the prediction.

Subject age	Empirical DFT	Predicted DFT
6 years	0–3 J	2.7 J
8 years	10–15 J	8.31 J
9 years	10–15 J	14.5 J
15 years	3–5 J	5.2 J
16 years	14.6–20.7 J	20 J
17 years	5–10 J	19.9 J
17 years	20–25 J	26.8 J
29 years	15–20 J	18 J
32 years	10–12 J	12.9 J

fluctuations can combine with the mathematics of error metrics to result in distortions of the error metrics. In the calculation of RE , for example, simply swapping the nominally *correct* values between the measured and the simulated values can change the resulting error metrics by as much as a factor of two. Metrics that are less sensitive to these types of ambiguities, such as correlation and DFT, can provide less sensitive measures of the accuracy of simulations and comparisons, but come with their own bias and distortion.

The results of this study show that the simulation pipeline we have developed is generally accurate, but some areas can be improved specifically in the patient-specific model. Many assumptions and sources of error contribute to the discrepancies apparent in the computation of both potentials and DFTs, e.g., patient geometry and conductivity values. Previous studies suggest that the model is highly sensitive to changes in the myocardium and blood conductivity, i.e., that these factors can most affect the potential distribution on the torso surface [34]. However, animal studies also suggest only a modest change in error when such conductivities are modified, even when a voltage drop is applied to the interface of the defibrillator [41]. Therefore, scalar changes in conductivity values may not provide a sufficient improvement in the simulation to significantly reduce error.

One additional source of error is the anisotropy of conductivity in the heart. In the current model, the myocardium was modeled as an electrically isotropic tissue. Previous studies of propagation of excitation have shown a marked increase in accuracy in the predicted electric field by including the anisotropy of the heart [36,37]. It is also evident from other studies that the myocardial fiber direction significantly affects the electric field around and through the myocardium [49]. Adding anisotropy to the myocardium based on fiber direction will likely change the electric field around the heart and may provide a significant change in the surface potentials, thereby increasing the accuracy of our model to predict the electric field in the torso.

The subjects used in this study were cases following corrective surgery for congenital cardiac defects, and therefore much younger

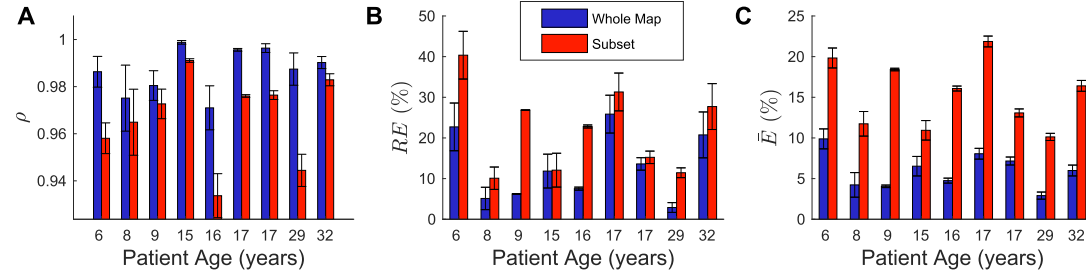


Fig. 7. Mean accuracy for each subject expressed by A) correlation (ρ), B) relative error (RE), and C) normalized RMS error (\bar{E}). Error bars indicate standard deviation.

ARTICLE IN PRESS

J. Tate et al.

than typical ICD recipients. They also differed from typical ICD recipients in that the causes of their arrhythmias were rooted in their congenital defects and the subsequent corrective surgery and not, for example, myocardial infarcts suffered in adulthood. While their diseases were pediatric, many of the subjects were at least teenagers and two were mature adults (29 and 32 years of age) so that factors of torso size and organ development were similar to patients in the aging population. Our results also showed that patient-specific applications of this modeling approach were accurate across a range of patient sizes and cardiac anatomical abnormalities. Clinical experience also suggests that these types of patients would likely benefit most from the patient-specific modeling of their ICD placement [20,35]. Placement of ICDs in adults with arrhythmias originating from other structural or non-structural causes have become largely standardized and successful so that such patient-specific modeling is less justified. Finally, our approach modeling the patient geometry and function is highly adaptable and so could be easily modified for more typical adult cases.

Another use of the simulation pipeline would be to test the affects of variations in patient geometry, tissue conductivity [34], and ICD position and type [23,35] on the expected DFT and the resulting BSPMs. The simulation framework we describe could be used to vary any number of patient geometry parameters, including: heart size, wall thickness, torso size, and any other change in the geometry of the patient and then to evaluate the changes in DFTs and BSPMs. By testing a wide range of geometric parameters in a rigorous and systematic fashion, some general trends could emerge that may provide guidance to physicians placing ICDs in patients with abnormal geometries. We have previously carried out similar studies using our model to derive general clinical guidelines for ICD placement [23].

The accuracy demonstrated in this study provides important validation of our simulation approach and of the application of estimation of potentials to this new domain. High agreement in potential field recordings and DFT comparisons shows that such simulations can accurately predict the electric potentials on the surface of the body and likely throughout the torso. The main application of this model is to improve ICD use in a patient-specific case, for example, patients with abnormal cardiac anatomy. More generally, there is a pressing need for optimization of ICD placement for pediatric cases or subcutaneous ICD configurations [23]. The accuracy of our simulation compared to recorded potentials demonstrated in this study provides confidence in our simulation pipeline, which could further the usefulness of ICD for many patients. We also note that all elements of the software described in this study are part of an open-source software suite created for bioelectric field simulations. The software is available completely freely at <http://www.sci.utah.edu/cibc-software.html>.

Conflicts of interest

None Declared.

Acknowledgements

The research presented in this paper was made possible with help from Philip Ershler and Bruce Steadman from the Cardiovascular Research and Training Institute (CVRTI). This project was supported by the National Institute of General Medical Sciences of the National Institutes of Health under grant number P41GM103545 and the University of Utah Research SEED Award, award number 10008039.

References

- [1] M. Alexander, F. Cecchin, E. Walsh, J. Friedman, L. Bevilacqua, C. Berul, Implications of implantable cardioverter defibrillator therapy in congenital heart disease and pediatrics, *J. Cardiovasc. Electrophysiol.* 15 (2004) 72–76.
- [2] F. Bokhari, D. Newman, M. Greene, V. Korley, I. Mangat, P. Dorian, Long-term comparison of the implantable cardioverter defibrillator versus amiodarone: eleven-year follow-up of a subset of patients in the canadian implantable defibrillator study (CIDS), *Circulation* 110 (2004) 112–116.
- [3] A. Buxton, K. Lee, J. Fisher, M. Josephson, E. Prystowsky, G. Hailey, A randomized study of the prevention of sudden death in patients with coronary artery disease, *N. Engl. J. Med.* 314 (1991) 1882–1890.
- [4] A. Moss, W. Hall, D. Cannom, J. Daubert, S. Higgins, H. Klein, J. Levine, S. Saksena, A. Waldo, D. Wilber, M. Brown, M. Heo, Improved survival with an implanted defibrillator in patients with coronary disease at high risk for ventricular arrhythmia, *N. Engl. J. Med.* 335 (1996) 1933–1940.
- [5] E.J. Benjamin, M.J. Blaha, S.E. Chiue, M. Cushman, S.R. Das, R. Deo, S.D. de Ferranti, J. Floyd, M. Fornage, C. Gillespie, C.R. Isasi, M.C. Jimenez, L.C. Jordan, S.E. Judd, D. Lackland, J.H. Lichtman, L. Lisabeth, S. Liu, C.T. Longenecker, R.H. Mackey, K. Matsushita, D. Mozaffarian, M.E. Mussolini, K. Nasir, R.W. Neumar, L. Palaniappan, D.K. Pandey, R.R. Thiagarajan, M.J. Reeves, M. Ritchey, C.J. Rodriguez, G.A. Roth, W.D. Rosamond, C. Sasson, A. Towfighi, C.W. Tsao, M.B. Turner, S.S. Virani, J.H. Voeks, J.Z. Willey, J.T. Wilkins, J.H. Wu, H.M. Alger, S.S. Wong, P. Muntner, Heart disease and stroke statistics–2017 update: a report from the american heart association, *Circulation* 135 (10) (2017), <https://doi.org/10.1161/CIR.000000000000485> e146–e603.
- [6] J.D. Kugler, C.C. Erickson, Nontransvenous implantable cardioverter defibrillator systems: not just for small pediatric patients, *J. Cardiovasc. Electrophysiol.* 17 (1) (2006) 47 ID: 1020756; ppublish 1045–3873 Journal.
- [7] B. Cannon, R. Friedman, A. Fenrich, C. Fraser, E. McKenzie, N. Kertesz, Innovative techniques for placement of implantable cardioverter-defibrillator leads in patients with limited venous access to the heart, *PACE (Pacing Clin. Electrophysiol.)* 29 (2006) 181–187.
- [8] G. Ristagno, T. Wang, W. Tang, S. Sun, C. Castillo, M.H. Weil, High-energy defibrillation impairs myocyte contractility and intracellular calcium dynamics, *Crit. Care Med.* 36 (11) (2008) S422–S427.
- [9] C. Berul, J. Friedman, J. Forbes, L. Bevilacqua, M. Alexander, D. Dahlby, J. Gilkerson, E. Walsh, Minimally invasive cardioverter defibrillator implantation for children: an animal model and pediatric case report, *Pacing Clin. Electrophysiol.* 24 (12) (2001) 1789–1794.
- [10] M. Luedemann, K. Hund, W. Stertmann, I. Michel-Behnke, M. Gonzales, H. Akintuerk, D. Schranz, Implantable cardioverter defibrillator in a child using a single subcutaneous array lead and an abdominal active can, *Pacing Clin. Electrophysiol.* 27 (1) (2004) 117–119.
- [11] V. Jayanti, M. Zivman, S. Nazarian, H. Halperin, R. Berger, Novel electrode design for potentially painless internal defibrillation also allows for successful external defibrillation, *J. Cardiovasc. Electrophysiol.* 18 (10) (2007) 1095–1100.
- [12] R. Lieberman, W. Havel, E. Rasbla, P. DeGroot, K. Stromberg, S. Shorofsky, Acute defibrillation performance of a novel, non-transvenous shock pathway in adult ICD indicated patients, *Heart Rhythm* 5 (1) (2008) 28–34.
- [13] G.H. Bardy, W.M. Smith, M.A. Hood, I.G. Crozier, I.C. Melton, L. Jordaeans, D. Theuns, R.E. Park, D.J. Wright, D.T. Connolly, S.P. Flynn, F.D. Murgatroyd, J. Sperzel, J. Neuzaer, S.G. Spitzer, A.V. Ardashev, A. Oduro, L. Boersma, A.H. Maass, I.C.V. Gelder, A.A. Wilde, P.F. van Dessel, R.E. Knops, C.S. Barr, P. Lupo, R. Cappato, A.A. Grace, An entirely subcutaneous implantable cardioverter defibrillator, *N. Engl. J. Med.* 363 (1) (2010) 36–44.
- [14] S. Aziz, A. Leon, M. El-Chami, The subcutaneous defibrillator: a review of the literature, *J. Am. Coll. Cardiol.* 63 (15) (2014) 1473–1479.
- [15] E.K. Heist, W. Stahl, A. Belalcazar, Impact of generator location and sub-coil fat on subcutaneous-ICD defibrillation thresholds, *Proceedings of Heart Rhythm Society, Heart Rhythm Society*, 2016AB05–03.
- [16] A. Auricchio, H. Klein, C. Geller, S. Reek, M. Heilman, S. Szymkiewicz, Clinical efficacy of the wearable cardioverter-defibrillator for acutely terminating episodes of ventricular fibrillation, *Am. J. Cardiol.* 81 (10) (1998) 1253–1256.
- [17] A. Feldman, H. Klein, P. Tchou, S. Murrali, W. Hall, D. Mancini, J. Boehmer, M. Harvey, M. Heilman, S. Szymkiewicz, A. Moss, Use of a wearable defibrillator in terminating tachyarrhythmias in patients at high risk for sudden death: results of the WEARIT/BROAD, *Pacing Clin. Electrophysiol.* 27 (1) (2004) 4–9.
- [18] A. Epstein, W. Abraham, N. Bianco, K. Kern, M. Mirro, S. Rao, E. Rhee, S. Solomon, S. Szymkiewicz, Wearable cardioverter-defibrillator use in patients perceived to be at high risk early post-myocardial infarction, *J. Am. Coll. Cardiol.* 62 (21) (2013) 2000–2007.
- [19] N.K. Wassnig, M. Gunther, S. Quick, C. Pfluecke, F. Rottstadt, S.J. Szymkiewicz, S. Ringquist, R.H. Strasser, U. Speiser, Experience with the wearable cardioverter-defibrillator in patients at high risk for sudden cardiac death, *Circulation* 134 (9) (2016) 635–643.
- [20] M. Jolley, J. Friedman, C. Westin, D. Weinstein, R. Macleod, D. Brooks, Image based modeling of defibrillation in children, *Proceedings of the IEEE Engineering in Medicine and Biology Society 28th Annual International Conference, IEEE, IEEE Press*, 2006, pp. 2564–2567.
- [21] M. Jolley, J. Stinstra, D. Weinstein, S. Pieper, R.S.J. Estepar, F. Cecchin, D. Brooks, R. MacLeod, J. Friedman, Finite element modeling of novel defibrillation approaches in children and adults, *Proceedings of Heart Rhythm Society*, 2007.
- [22] M. Jolley, J. Stinstra, S. Pieper, R. MacLeod, D.H. Brooks, F. Cecchin, J.K. Friedman, A computer modeling tool for comparing novel ICD electrode orientations in children and adults, *Heart Rhythm* 5 (4) (2008) 565–572.
- [23] M. Jolley, J. Stinstra, J. Tate, S. Pieper, R. MacLeod, L. Chu, P. Wang, J. Friedman, Finite element modeling of subcutaneous implantable defibrillator electrodes in an adult torso, *Heart Rhythm* 7 (5) (2010) 692–698.
- [24] L.D. Ambroggi, E. Musso, B. Taccardi, Body surface potential mapping, in: P. Macfarlane, T. Veitch Lawrie (Eds.), *Comprehensive Electrocardiology*, 2 Springer Verlag, 2005, pp. 1375–1413 Ch. 32.
- [25] L.D. Ambroggi, B. Taccardi, E. Macchi, Body surface maps of heart potentials, tentative localization of pre-excited areas in forty-two wolfe-Parkinson-white

ARTICLE IN PRESS

J. Tate et al.

Computers in Biology and Medicine xxx (xxxx) xxxx-xxxx

- patients, *Circulation* 54 (Aug. 1976) (1976) 251–263.
- [26] G. Vincent, J. Abildskov, M. Burgess, K. Millar, R. Wyatt, R. Lux, New diagnostic evidence of myocardial infarction in body surface isopotential maps, *Am. J. Cardiol.* 35 (Feb. 1975) (1975) 174.
- [27] R. MacLeod, B. Hoyt, P. MacInnis, R. Potter, B. Horáček, A body surface potential mapping unit for recording during coronary angioplasty, *Proceedings of the IEEE Engineering in Medicine and Biology Society 10th Annual International Conference*, IEEE Press, 1988, pp. 97–98.
- [28] D. McPherson, B. Horacek, D. Sutherland, C. Armstrong, A. Spencer, T. Montague, Exercise electrocardiographic mapping in normal subjects, *J. Electrocardiol.* 18 (1985) 351–360.
- [29] R. Barr, M. Spach, G. Herman-Giddens, Selection of the number and position of measuring locations for electrocardiography, *IEEE Trans. Biomed. Eng.* 18 (2) (1971) 125–138.
- [30] F. Kornreich, P. Rautaharju, J. Warren, T. Montague, B. Horacek, Identification of best electrocardiographic leads for diagnosing myocardial infarction by statistical analysis of body surface potential maps, *Am. J. Cardiol.* 56 (1985) 852–856.
- [31] R.L. Lux, C.R. Smith, R.F. Wyatt, J.A. Abildskov, Limited lead selection for estimation of body surface potential maps in electrocardiography, *IEEE Trans Biomed Eng BME-* 25 (3) (1978) 270–276.
- [32] R. Lux, A. Evans, M. Burgess, R. Wyatt, J. Abildskov, Redundancy reduction for improved display and analysis of body surface potential maps. I. spatial compression, *Circ. Res.* 49 (No 1, July 1981) (1981) 186–194.
- [33] R.L. Lux, Electrocardiographic potential correlations: rationale and basis for lead selection and ECG estimation, *J. Electrocardiol.* 35 (Supplement) (2002) 1–5.
- [34] J. Stinstra, M. Jolley, J. Tate, D. Brooks, J. Friedman, R. MacLeod, The role of volume conductivities in simulation of implantable defibrillators, in: A. Murray (Ed.), *Computers in Cardiology*, 35 IEEE Press, 2008, pp. 481–484 Computers in Cardiology.
- [35] M. Jolley, J. Stinstra, S. Pieper, R. MacLeod, D. Brooks, F. Cecchin, J. Friedman, A computer modeling tool for comparing novel ICD electrode orientations in children and adults, *Heart Rhythm* 5 (4) (2008) 565–572.
- [36] F. Clayton, T. Pilkington, A. Tang, M. Morrow, R. Ideker, A volume conductor model of the thorax for the study of defibrillation fields, *IEEE Trans. Biomed. Eng.* 35 (1988) 981–992.
- [37] F. Clayton, T. Pilkington, A. Tang, M. Morrow, R. Ideker, Comparison of measured and calculated epicardial potentials during transthoracic stimulation, *IEEE Engineering in Medicine and Biology Society 10th Annual International Conference*, IEEE Press, 1988, pp. 206–207.
- [38] S. Parker, D. Weinstein, C. Johnson, The SCIRun computational steering software system, in: E. Arge, A. Brusaset, H. Langtangen (Eds.), *Modern Software Tools in Scientific Computing*, Birkhauser Press, Boston, 1997, pp. 1–40 URL http://www.sci.utah.edu/publications/Parl997a/Parker_SCIRun1997.pdf.
- [39] R. MacLeod, D. Weinstein, J. D. de St Germain, D. Brooks, C. Johnson, S. Parker, SCIRun/BioPSE: integrated problem solving environment for bioelectric field problems and visualization, *IEEE International Symposium on Biomedical Imaging (ISBI)*, IEEE, IEEE Press, 2004, pp. 1–3.
- [40] CIBC, Seg3D: volumetric image segmentation and visualization. Scientific computing and imaging Institute (SCI), [link]. URL <http://www.seg3d.org>, (2015) <http://www.seg3d.org>.
- [41] D.B. Jorgenson, P.H. Schimpf, I. Shen, G. Johnson, G.H. Bardy, D.R. Haynor, Y. Kim, Predicting cardiothoracic voltages during high energy shocks: methodology and comparison of experimental to finite element model data, *IEEE Trans. Biomed. Eng.* 42 (6) (1995) 559 ID: 14; LR: 20041117; PUBM: Print; JID: 0012737; ppublish 0018-9294 Journal.
- [42] R. Lux, R. MacLeod, M. Fuller, L. Green, F. Kornreich, Estimating ECG distributions from small numbers of leads, *J. Electrocardiol.* 28 (Supplement 1) (1995) 92–98, [https://doi.org/10.1016/S0022-0736\(95\)80032-8](https://doi.org/10.1016/S0022-0736(95)80032-8) research and Technology Transfer in Computerized Electrocardiology <http://www.sciencedirect.com/science/article/B6WJ4-4C4X16N-2F/2/ee0217b344a91d180183fa1794d24d6>.
- [43] B. Yilmaz, R. MacLeod, B. Puniske, B. Taccardi, D. Brooks, Venous catheter based mapping of ectopic epicardial activation: training data set selection for statistical estimation, *IEEE Trans. Biomed. Eng.* 52 (11) (2005) 1823–1831.
- [44] L. Rantner, F. Vadakkumpadan, P. Spevak, J. Crosson, N. Trayanova, Placement of implantable cardioverter-defibrillators in paediatric and congenital heart defect patients: a pipeline for model generation and simulation prediction of optimal configurations, *J. Physiol.* 591 (Pt 17) (2013) 4321–4334.
- [45] R.E. Ideker, P.D. Wolf, C. Alferness, W. Krassowska, W.M. Smith, Current concepts for selecting the location, size and shape of defibrillation electrodes, *PACE (Pacing Clin. Electrophysiol.)* 14 (2 Pt 1) (1991) 227 ID: 32; LR: 20051116; PUBM: Print; JID: 7803944; RF: 47; ppublish 0147-8389 Journal.
- [46] I. Efimov, C.M. Ripplinger, Virtual electrode hypothesis of defibrillation, *Heart Rhythm* 3 (9) (2006) 1100–1102, <https://doi.org/10.1016/j.hrthm.2006.03.005> URL <https://doi.org/10.1016/j.hrthm.2006.03.005>.
- [47] N. Trayanova, R. Gray, D. Bourne, J. Eason, Virtual electrode-induced positive and negative graded responses: new insights into fibrillation induction and defibrillation, *J. Cardiovasc. Electrophysiol.* 14 (7) (2003) 756–763.
- [48] N. Trayanova, Defibrillation of the heart: insights into mechanisms from modelling studies, *Exp. Physiol.* 91 (2) (2006) 323–337.
- [49] N. Trayanova, K. Skouibine, F. Aguel, The role of cardiac tissue structure in defibrillation, *Chaos* 8 (1) (1998) 221–233.

CHAPTER 6

CONCLUSIONS

Arrhythmias are a major individual and public health concern whose mechanistic understanding and treatment remain incomplete [1]. One can improve the understanding, detection, and treatment of arrhythmias with computer models, but these models must be robustly validated. The studies performed as part of this dissertation have developed and applied novel approaches to validation and also revealed insights into strategies for validating and improving computer models of arrhythmias, specifically simulations of defibrillation and ECG forward simulations.

We performed studies to validate two computational pipelines: the ECG forward problem and defibrillation simulation. For the ECG forward problem, our results provided some insights into methods that may improve future validation studies and suggest implications for the more clinically relevant ECG imaging (ECGI). Our studies to validate the defibrillation pipeline were completely novel and quantified the errors with the pipeline we have developed and used previously; the results support its use as a tool to guide defibrillation treatment in patient-specific cases.

6.1 ECG Forward Simulation

As outlined in specific aim 1 (Section 1.1), one of the goals of this dissertation was to evaluate and reduce the error in the ECG forward simulation from incomplete sampling of the atria. We tested various approaches to sampling the epicardial potentials on the atrial surface and evaluated the effect of these strategies on the computed BSPMs (Chapter 3). The results of this study led to three major findings: complete sampling of the epicardial potentials is needed to accurately predict the BSPM, some sampling strategies are more effective than others, and the possible error due to missing cardiac samples is great enough to account for the errors reported previously [2], [3] and observed in our own studies.

It is clear from the work shown in Chapter 3 that reducing the spatial coverage of

epicardial samples from the ECG forward simulation will produce errors in the body-surface potentials, regardless of geometry or activation profile (Figs. 3.2, 3.3, and 3.4). Therefore, sampling only the ventricular epicardium is insufficient for generating accurate ECG forward simulations, and we have yet to adequately predict the missing values. Adding a small number of sampling locations on the atria did, in general, reduce the error in the simulated BSPMs (Fig. 3.5), motivating our studies to identify better sampling strategies in experimental settings.

In our analysis of various sampling strategies, we identified several that effectively reduced error in the simulated BSPMs with fewer sampling locations. In general, the more distributed strategies, such as the uniform distribution, produced less error in the simulation BSPMs given the same number of sampling locations (Fig. 3.5). Another strategy that performed well much of the time consisted of adding additional sampling locations to both the atrial roof and the AV plane. These distributed strategies likely performed well because they facilitated approximating the missing potentials during subsequent interpolation in the forward simulation pipeline. The distributed strategies reduce the maximum distance between known potential values, so that interpolation is more likely to preserve local fluctuations. Even among the successful sampling strategies, each had several practical limitations. The several vessels attached to the atria prohibit the use of a sock to completely cover the epicardial surface in an *in situ* setting. These vessels also limit the possible locations for a plaque electrode array and preclude the use of a uniform or full pericardial sampling strategy. However, a combination of a plaque electrode and a larger ventricle sock could approximate the combined atrial roof and AV plane strategy. The torso-tank preparations offer more opportunities, especially by means of a cardiac cage, which could be used to sample potentials near the epicardium and completely surrounding the heart.

Comparing the errors we determined in the simulated BSPM caused by missing atrial sampling locations to previously published ECG forward simulation validation studies [2], [3] indicated that this single source of error may not fully account for the error previously reported. We had to remove at least a few ventricular samples in order to observe errors at the error level previously reported. Without more details from the investigators, we can only speculate that previous attempts to validate the ECG forward simulation pipeline were missing not only epicardial atrial sampling but also some ventricular sampling.

More fruitful than trying to diagnose past errors is the impact of the findings of Chapter 3 for future validation studies. Such studies should ensure that the ventricular epicardium is completely sampled with the cardiac sock or other electrode array and that some sampling occurs on the atrial epicardium. Strategies to sample the atrial surface include plaque electrodes or a cardiac cage.

These findings also have implications for how researchers validate ECGI methods using forward simulated BSPM data [4]–[7]. Our findings suggest that the computed BSPMs used as inputs in these ECGI pipelines may contain errors due to inadequate cardiac sampling, which biases the tuning of the constraints in the ECGI inverse problem and can possibly alter the levels of accuracy achieved. Using ECG forward simulation data to test ECGI implementations is just one example that shows how improving the validation of the ECG forward simulation will also help improve ECGI techniques. The data collected as part of this research will be valuable in ECGI tuning and validation studies that are already underway.

6.1.1 Future Work

This dissertation outlined new guidelines to source sampling for ECG forward simulation validation studies (Chapter 3). Natural next steps include implementing these guidelines in experiments with recorded torso surface potentials. We propose (and are carrying out) new animal studies with two experimental preparations: closed-chest and torso-tank.

The proposed closed-chest *in situ* animal experiments are designed to further evaluate the effect of source sampling on the ECG forward problem. The proposed protocol would involve recording epicardial potentials with cardiac sock and atrial plaque electrode arrays together with simultaneous body-surface potentials. Using systematically varied subsets of the epicardial recordings as sources, we hope to identify specific sensitivities on the location and density of epicardial sampling. Such experiments will be unique in their anatomical and physiological fidelity and provide new validation data for many questions related to both sampling of cardiac bioelectricity and the forward and inverse problems in electrocardiography.

The proposed torso-tank experiments are designed with similar goals to those using

the closed-chest animal experiments: to further evaluate the effect of source sampling within the ECG forward solution using unique ground truth measurements. The main difference in the torso-tank experiments is the lack of fidelity to the intact animal, which is traded off against the extensive access to the heart. The torso-tank protocol allows many forms of measurement, including cardiac sock, extracardiac cage, and torso-tank electrode arrays. The cardiac cage provides near full epicardial sampling of the heart (Fig. 6.1), which enables repeat analysis of any sampling strategy and would further test the findings in this dissertation. The addition of a cardiac sock within the cage will help quantify the effect of the spatial smoothing that occurs in the short distance from the epicardium to the cage and the subsequent effect on the ECG forward simulation and ECGI. These data will be especially important because they can help develop interpolation strategies to minimize error in the ECG forward simulation from missing cardiac source recordings.

With the cardiac sources more fully characterized, we can analyze other aspects of the ECG forward simulation pipeline to better quantify the origins of error. Previous reports

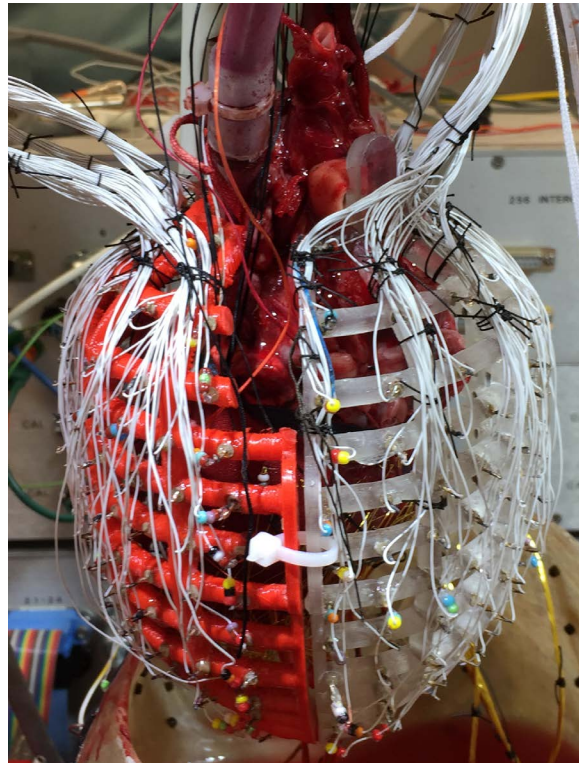


Fig. 6.1. Cardiac cage to record near epicardial potentials in a torso-tank filled with electrolyte.

from our group and others have described the effect of the position of the heart in the torso on the ECG forward simulation [8] and ECGI [9], [10], but these findings have been based only on ventricular epicardial source recordings. Using full pericardial sampling of sources in similar studies could provide better quantification of geometric errors because of the reduced residual error in the predicted body-surface potentials for ECG forward simulations.

Previous studies have tested ECGI methods on computed from sources only on the ventricle [4]–[7], and therefore a natural extension of the findings in the dissertation would be to quantify the difference between using BSPMs computed with full pericardial sampling and epicardial ventricle-only sampling in ECGI pipelines. This study would need similar data to those used in Chapter 3, simulated pericardial potentials, or potentials recorded from a cardiac cage. In addition to changes in recomputed cardiac sources, the optimized regularization parameters used in the ECGI methods may also change.

6.2 Defibrillation Simulation

Another goal of this dissertation was to validate the potential fields predicted by the defibrillation simulation using clinical and animal experiment recordings, as outlined in specific aims 2 and 3 (Section 1.1). We recorded potential fields generated by an ICD with two setups: a torso-tank preparation to record potentials within the heart and on the torso surface (Chapter 4) and with patients undergoing ICD implantation and testing to record surface potentials and DFTs (Chapter 5). The simulation showed high overall accuracy in predicting measured potential fields, including within the myocardium (Chapter 4) and with patient BSPM (Chapter 5). Additionally, the simulation was able to accurately predict the DFT in a majority of cases, suggesting that the critical mass hypothesis is sufficient to compute the DFT for a majority of patients (Table 5.4, Chapter 5). However, the outlier in this case combined with those of Rantner et al. [11] indicates that the critical mass hypothesis may not always sufficiently predict the DFT of a patient. In these cases, more complex modeling may be required [11]–[14]. Nevertheless, the accuracy of the simulation in predicting the potential field and the DFT shows that it can be used to effectively predict the behavior of defibrillators.

The findings of Chapter 4 and 5 suggest several ways to improve the simulations

to provide more agreement in validation studies and to improve accurate predictions to encourage its use as a clinical tool. The conductivity assumptions used in our pipeline can cause errors in the results [15], especially due to the assumption of isotropic conduction through the myocardium [16], [17]. Adding anisotropy is likely to alter the potential distributions through the torso. The inclusion of boundary conforming meshes in patient models may also increase the accuracy of the potential field and computed DFTs by producing more accurate electric field predictions [18].

The findings presented in this discussion support trends and predictions made in previous studies using simulation to predict ICD behavior in patients [19], [20]. These studies have evaluated several aspects of the ICD implantation strategy with the goal of establishing trends in ICD behavior. The findings have shown that, in most cases, the trend in predicted DFT matched what was clinically and experimentally observed (Chapters 4 and 5), which further supports the claims set forth in the previous reports, such as the effect of patient size on DFT with subcutaneous electrodes [19]. Furthermore, the findings in this study also showed that both predicted and observed DFTs are generally correlated with the size of the patient, which also agrees with experimental and clinical findings [21], [22]. The ability of the simulation to predict general trends in the relationship in size, and also the exceptions to the trend (Chapter 5), support the ability of the simulation to provide important patient-specific guidance while planning ICD implantation positions.

6.2.1 Future Work

Closed-chest animal experiments could provide complementary validation of the defibrillation simulation and would build upon the studies performed in this dissertation (Chapters 4 and 5). Although similar experiments have been conducted in the past [16], [17], [23], [24], our approach could provide a combination of subject-specific geometry and high spatial sampling. The protocol would involve recording in the myocardium with plunge needles, on the cardiac surface with a sock electrode array, and on the torso surface with contact electrodes to compare to predicted values. DFTs could also be measured and compared to predicted values using this preparation.

In addition to improving the validation of the defibrillation simulation, we could also improve the pipeline by including anisotropic conductivity throughout the heart. Adding

anisotropy could alter the potential distribution throughout the torso and on the body surface [15]. It might also produce potential distributions and predicted DFTs that match even more closely our experimentally recorded data. The fiber directions could be estimated using a rule-based approach [25], [26], and one could also test the response of the simulated potentials and DFTs to changes in the distribution of the fiber orientation. Such experiments could provide insight into the sensitivity of the defibrillation simulation to fiber orientation.

As discussed in Section 6.2, the critical mass hypothesis may not accurately predict the DFT for every patient, which suggests the need for more advanced biophysical models [12], [27], [28] in some instances. If we could identify patients who are likely to have inaccurate predictions based on the critical mass hypothesis, we could reduce computational cost by performing only the more complex models on the patients who need it (Fig. 6.2). To determine methods of categorizing these patients, we would need to collect medical imaging and DFTs after receiving an ICD, and use statistical shape analysis on segmented hearts to compare statistical trends of patients for whom the critical mass hypothesis is and is not accurate. Differences in the shape statistics could provide a basis for stratifying patients who need an ICD to determine which simulation pipeline would achieve the best predictions of the DFT.

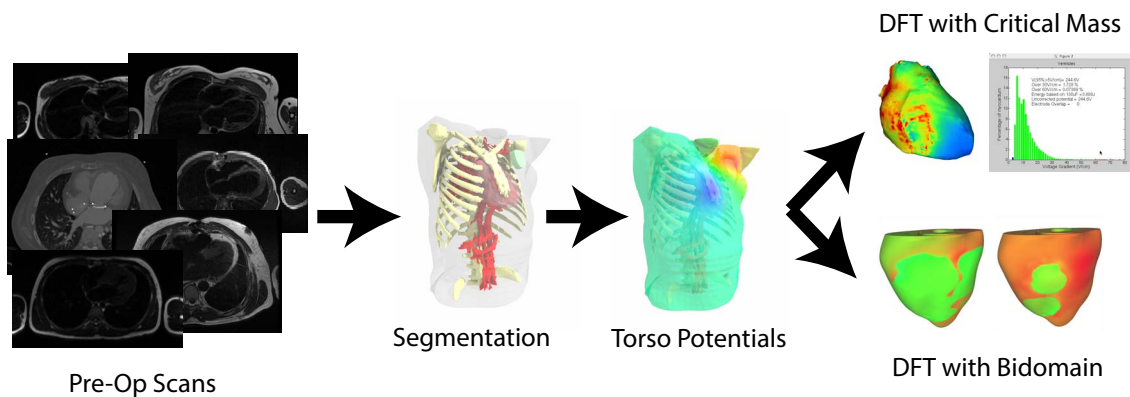


Fig. 6.2. Ideal pipeline for predicting defibrillation. The pipeline would use the critical mass hypothesis for most patients and a more computationally expensive bidomain simulation when needed.

6.3 References

- [1] E. J. Benjamin, S. S. Virani, C. W. Callaway, A. R. Chang, S. Cheng, S. E. Chiuve, M. Cushman, F. N. Delling, R. Deo, S. D. de Ferranti, J. F. Ferguson, M. Fornage, C. Gillespie, C. R. Isasi, M. C. Jiménez, L. C. Jordan, S. E. Judd, D. Lackland, J. H. Lichtman, L. Lisabeth, S. Liu, C. T. Longenecker, P. L. Lutsey, D. B. Matchar, K. Matsushita, M. E. Mussolini, K. Nasir, M. O'Flaherty, L. P. Palaniappan, D. K. Pandey, M. J. Reeves, M. D. Ritchey, C. J. Rodriguez, G. A. Roth, W. D. Rosamond, U. K. Sampson, G. M. Satou, S. H. Shah, N. L. Spartano, D. L. Tirschwell, C. W. Tsao, J. H. Voeks, J. Z. Willey, J. T. Wilkins, J. H. Wu, H. M. Alger, S. S. Wong, and P. Muntner, "Heart disease and stroke statistics—2018 update: A report from the American Heart Association," *Circ.*, 2018. [Online]. Available: <http://circ.ahajournals.org/content/early/2018/01/30/CIR.0000000000000558>
- [2] M. Ramsey, R. C. Barr, and M. S. Spach, "Comparison of measured torso potentials with those simulated from epicardial potentials for ventricular depolarization and repolarization in the intact dog," *Circ. Res.*, vol. 41, no. 5, pp. 660–672, Nov. 1977.
- [3] L. R. Bear, L. K. Cheng, I. J. LeGrice, G. B. Sands, N. A. Lever, D. J. Paterson, and B. H. Smaill, "The forward problem of electrocardiography: Is it solved?" *Circ. Arrhythm. Electrophysiol.*, vol. 8, no. 3, pp. 677–684, Jun. 2015. [Online]. Available: <https://www.ahajournals.org/doi/10.1161/CIRCEP.114.001573>
- [4] J. Burnes, B. Taccardi, R. MacLeod, and Y. Rudy, "Noninvasive electrocardiographic imaging of electrophysiologically abnormal substrates in infarcted hearts: A model study," *Circ.*, vol. 101, pp. 533–540, Feb. 2000.
- [5] J. Burnes, B. Taccardi, and Y. Rudy, "A noninvasive imaging modality for cardiac arrhythmias," *Circ.*, vol. 102, pp. 2152–2158, Oct. 2000.
- [6] B. Erem, A. Ghodrati, G. Tadmor, R. MacLeod, and D. Brooks, "Combining initialization and solution inverse methods for inverse electrocardiography," *J. Electrocardiol.*, vol. 44, no. 2, p. e21, Apr. 2011.
- [7] D. Wang, R. Kirby, and C. Johnson, "Finite-element-based discretization and regularization strategies for 3-D inverse electrocardiography," *IEEE Trans. Biomed. Eng.*, vol. 58, no. 6, pp. 1827–1838, Jun. 2011.
- [8] D. Swenson, S. Geneser, J. Stinstra, R. Kirby, and R. MacLeod, "Cardiac position sensitivity study in the electrocardiographic forward problem using stochastic collocation and BEM," *Annal. Biomed. Eng.*, vol. 30, no. 12, pp. 2900–2910, Dec. 2011.
- [9] J. Coll-Font, B. Roig-Solvas, P. van Dam, R. S. MacLeod, and D. H. Brooks, "Can we track respiratory movement of the heart from the ECG itself - and improve inverse solutions too?" *J. Electrocardiol.*, vol. 49, no. 6, p. 927, Jun. 2016.
- [10] J. Coll-Font, B. Roig-Solvas, P. van Dam, R. MacLeod, and D. Brooks., "Tracking the heart movement with the ECG; a way of improving the inverse problem in electrocardiography?" in *Proc. Internat. Soc. Comp. Electrocardiol.*, 2016.

- [11] L. Rantner, F. Vadakkumpadan, P. Spevak, J. Crosson, and N. Trayanova, "Placement of implantable cardioverter-defibrillators in paediatric and congenital heart defect patients: A pipeline for model generation and simulation prediction of optimal configurations," *J. Physiol.*, vol. 591, no. Pt 17, pp. 4321–4334, Sep. 2013.
- [12] N. Trayanova, R. Gray, D. Bourn, and J. Eason, "Virtual electrode-induced positive and negative graded responses: new insights into fibrillation induction and defibrillation," *J. Cardiovasc. Electrophysiol.*, vol. 14, no. 7, pp. 756–763, Jul. 2003.
- [13] N. Trayanova, "Defibrillation of the heart: insights into mechanisms from modelling studies," *Exp. Physiol.*, vol. 91, no. 2, pp. 323–337, Mar. 2006.
- [14] I. Efimov and C. M. Ripplinger, "Virtual electrode hypothesis of defibrillation," *Heart Rhythm J.*, vol. 3, no. 9, pp. 1100–1102, Aug. 2006. [Online]. Available: <https://doi.org/10.1016/j.hrthm.2006.03.005>
- [15] J. Stinstra, M. Jolley, J. Tate, D. Brooks, J. Triedman, and R. MacLeod, "The role of volume conductivities in simulation of implantable defibrillators," in *Computers in Cardiology*, A. Murray, Ed., vol. 35, Computers in Cardiology. Bologna, Italy: IEEE Press, 2008, pp. 481–484.
- [16] F. Claydon, T. Pilkington, A. Tang, M. Morrow, and R. Ideker, "A volume conductor model of the thorax for the study of defibrillation fields," *IEEE Trans. Biomed. Eng.*, vol. 35, pp. 981–992, Nov. 1988.
- [17] F. Claydon, T. Pilkington, A. Tang, M. Morrow, and R. Ideker, "Comparison of measured and calculated epicardial potentials during transthoracic stimulation," in *IEEE EMBS 10th Ann. Intl. Conf.* New Orleans, Louisiana, USA: IEEE Press, 1988, pp. 206–207.
- [18] D. Swenson, J. Levine, R. Whitaker, and R. MacLeod, "Impacts of conformal meshing on electrical cardiac simulation," in *21st International Meshing Round Table*, San Jose, CA, USA, 2012.
- [19] M. Jolley, J. Stinstra, S. Pieper, R. MacLeod, D. Brooks, F. Cecchin, and J. Triedman, "A computer modeling tool for comparing novel ICD electrode orientations in children and adults," *Heart Rhythm J.*, vol. 5, no. 4, pp. 565–572, Apr. 2008.
- [20] M. Jolley, J. Stinstra, J. Tate, S. Pieper, R. MacLeod, L. Chu, P. Wang, and J. Triedman, "Finite element modeling of subcutaneous implantable defibrillator electrodes in an adult torso," *Heart Rhythm J.*, vol. 7, no. 5, pp. 692–698, May 2010.
- [21] H. P. Gutgesell, W. A. Tacker, L. A. Geddes, J. S. Davis, J. T. Lie, and D. G. McNamara, "Energy dose for ventricular defibrillation of children," *Pediatrics*, vol. 58, no. 6, pp. 898–901, 1976. [Online]. Available: <http://pediatrics.aappublications.org/content/58/6/898>
- [22] C. R. Killingsworth, S. B. Melnick, F. W. Chapman, R. G. Walker, W. M. Smith, R. E. Ideker, and G. P. Walcott, "Defibrillation threshold and cardiac responses using an external biphasic defibrillator with pediatric and adult adhesive patches in pediatric-sized piglets," *Resuscitation*, vol. 55, no. 2, pp. 177 – 185, 2002. [Online]. Available: <http://www.sciencedirect.com/science/article/pii/S0300957202001570>

- [23] D. B. Jorgenson, P. H. Schimpf, I. Shen, G. Johnson, G. H. Bardy, D. R. Haynor, and Y. Kim, "Predicting cardiothoracic voltages during high energy shocks: Methodology and comparison of experimental to finite element model data," *IEEE Trans. Biomed. Eng.*, vol. 42, no. 6, p. 559, Jun. 1995.
- [24] J. P. Rosborough, D. C. Deno, R. G. Walker, and J. T. Niemann, "A percutaneous catheter-based system for the measurement of potential gradients applicable to the study of transthoracic defibrillation," *PACE*, vol. 30, no. 2, pp. 166–174, Feb. 2007. [Online]. Available: <http://dx.doi.org/10.1111/j.1540-8159.2007.00645.x>
- [25] J. Wong and E. Kuhl, "Generating fibre orientation maps in human heart models using poisson interpolation," *Comput. Methods Biomed. Eng.*, vol. 17, no. 11, pp. 1217–1226, Dec. 2014.
- [26] S. Merchant, A. Gomez, J. Morgan, and E. Hsu, "Parametric modeling of the mouse left ventricular myocardial fiber structure," *Ann. Biomed. Eng.*, vol. 44, no. 9, pp. 2661–2673, Sep. 2016.
- [27] N. Trayanova and J. Eason, "Shock-induced arrhythmogenesis in the myocardium." *Chaos*, vol. 12, no. 3, pp. 962–972, Sep. 2002.
- [28] M. Trew, I. L. Grice, B. Smaill, and A. Pullan, "A finite volume method for modeling discontinuous electrical activation in cardiac tissue," *Annal. Biomed. Eng.*, vol. 33, no. 5, pp. 590–602, May 2005.